Microfluidic technologies for genomic interrogation of *Mycobacterium tuberculosis* clinical isolates using the polymerase chain reaction (PCR) and high resolution melting analysis (HRMA)

By

TAWANDA MANDIZVO

Submitted in fulfilment of the requirements for the degree of Master of Science (Med) in the Discipline of Medical Microbiology, School of Laboratory Medicine and Medical Sciences College of Health Sciences,

University of KwaZulu-Natal

South Africa

November, 2015

KRITH KWAZULU-NATAL RESEARCH INSTITUTE FOR TUBERCULOSIS AND HIV

DECLARATION

I, **MANDIZVO TAWANDA**, declare that;

1. The research reported in this thesis is my original research, except where indicated otherwise.
2. This thesis has not been submitted for any degree or examination at any other university.
3. This thesis does not contain other persons' data, pictures, graphs or other information, unless specifically acknowledged and referenced as being sourced from other persons.
4. This thesis does not contain other persons' writing, unless specifically acknowledged as being sourced from other researchers. Where other written sources have been quoted, then:
    a) Their words have been re-written but the general information attributed to them has been referenced.
    b) Where their exact words have been used, then their writing has been placed in italics and inside quotation marks, and referenced.
5. This thesis does not contain text, graphics or tables copied and pasted from the Internet, unless specifically acknowledged, and the source being detailed in the thesis and in the References sections.

……

MANDIZVO TAWANDA (Candidate)

Dated this, 30th day of November 2015

As the candidate's Supervisor I agree to the submission of this thesis

……

DR FREDERICK BALAGADDÉ (Supervisor)

Dated this, 30th day of November 2015

-Chancellor William Gladstone on seeing Michael Faraday's experiment-

William Gladstone: "*But after all, what use is it?"*

Michael Faraday: "*Why sir, there is the probability that you will soon be able to tax it!"*

WITH LOVE FOR MY FAMILY AND TO LOVING PARENTS CHIRANGO & MILDRED MANDIZVO

CONFERENCE CONTRIBUTIONS

1. **Mandizvo T**, Mbano IM, Rogich J, Balagadde' FK (17/09/2015). ***The LightForge Real-Time PCR & HRMA System.*** 3rd International Workshop on Microsystems Technologies for African Health, Microsystems for African Health, Protea Hotel, Stellenbosch, South Africa. Oral and Poster Presentations.

2. **Mandizvo T**, Mbano IM, Rogich J, Balagadde' FK (24/07/2015) ***LightForge - a highly scalable microfluidic platform for interrogation of tuberculosis strains using Real-Time PCR and High Resolution Melt Analysis on a chip***. Canon Collins Scholars' Annual Conference 2015, Theories of Change, Webber Wentzel, Convention Tower, Heerengracht Street, Foreshore, Cape Town, South Africa. Oral Presentation

3. **Mandizvo T**, Mbano IM, Rogich J, Balagadde' FK (17/07/2015). ***The LightForge Real-Time PCR & HRMA System.*** KwaZulu-Natal Research Institute for TB & HIV Current Research (CURE) Seminar Series. K|RITH Tower Building, Level 1, Seminar K2, Durban, South Africa. Oral Presentations.

ACKNOWLEDGEMENTS

Most Importantly I would like to thank **The Lord God Almighty** for giving me strength that saw me through this process and for giving me at no price the people in my life who helped me through this Masters degree. All the credit rests in You Lord.

I would like to thank my supervisor, **Dr Frederick K Balagadde'**, I have learnt a lot from his patience, generosity, guidance, support, helpful suggestions and motivation. I also want to extend my gratefulness to him for providing me with the opportunity to work on this project. It expressed his confidence in my ability as a student, paving way for my development as a scientist in this chosen field.

Ian Maheti Mbano I am really so grateful for working with you. Your vast expertise in the off-chip Mtb genome interrogation and PCR master mix optimisation (using Roche LightCycler 96) as well as optimisation of PCR master mixes that were used on the LightForge Microfluidic platform was extremely instrumental in driving this project to success. Your support, friendship, prayers, criticism, helpful suggestions and motivation were just priceless as they forced this work into fruition.

The Financial Support from **KwaZulu-Natal Research Institute for TB/HIV (K|RITH)**, **NRF Innovation Masters and Doctoral Scholarship for 2014-2015** (Grant number: 92720) and **The Canon Collins Educational and Legal Assistance Trust** is gratefully acknowledged.

To **Dr Adrie Steyn, Dr Manormoney Pillay and Dr Koleka Mlisana;** I thank you for your gracious assistance with the Mtb clinical isolates.

Special thanks to **Jerome Rogich** for designing—during his tenure as a research specialist at KwaZulu-Natal Research Institute for TB and HIV (K|RITH)—the Spider Design bulk PCR microfluidic chip that we fabricated and optimised to work for PCR and HRMA on the LightForge platform.

Special thanks to **Yashveer Ramlakhan** and **Jerome Rogich** for providing me with initial training that was essential for the success of this project.

I would like to acknowledge the comments and constructive criticism given to this project by **KRITH Principal Investigators (PIs) and Students/Postdocs** during Current Research (CURE) research seminars.

Special thanks to **Ashmika Surujdeen, Jared Mackenzie, Sharon Khuzwayo** and **Dr Justen Manasa** for constructive criticism and words of encouragement. Thanks a lot for helping to proofread this document.

I would like to thank all the members of the **Balagadde' Research group at K|RITH**. Thank you for your company, you have been very supportive and encouraging.

I also wish to thank **my family members and friends** who have been very supportive and encouraging. Thank you all for the prayers.

To **Precious Mangena**, thanks a lot for the support, prayers and encouragement. **Tafara Takunda Remigio Kunota**, apart from being a colleague, you have been an unbelievably supportive friend from the start, thanks a lot.

ABSTRACT

Background: A number of *Mycobacterium tuberculosis* (Mtb) genes have been shown to be under positive selection pressure in the presence of anti-TB therapy. This results in the selection of drug resistant phenotypes associated with genetic changes—which can be point mutations, deletions and/or insertions. Some mutations from multiple genes have been documented to be associated with reduced susceptibility to anti-TB drugs such as rifampicin, ethambutol, carpreomycin and fluoroquinolones. The list is continuously updated as new mutations are discovered and validated. In principle therefore, there is an urgent need to design robust molecular diagnostics and more efficacious therapeutic strategies that are able to indicate diverse genetic mechanisms behind drug resistance in individual isolates

Materials and Methods: We used the LightForge system we developed at K-RITH. This LightForge system is a fluorescence detection based, highly scalable microfluidic platform. It interrogates *Mycobacterium tuberculosis* strains using Real-Time PCR and High Resolution Melt Analysis (HRMA) on a chip.

Results and Discussion: We have used this LightForge system to identify clinical Mtb strains resistant to rifampicin—a frontline drug used to treat tuberculosis, relative to a susceptible strain H37RV, based on mutations in the rpoB gene. This system has the potential to contribute towards a low-cost solution to diagnosis of multidrug resistant tuberculosis—a current critical global healthcare challenge. The interrogation of clinical Mtb isolates—including R35, KZN 605 and Tkk 01-062—using the LightForge system has detected mutations linked to rifampicin resistance including single nucleotide polymorphisms (SNPs) in a congruous manner with commercial systems.

Conclusions: In preparation for diagnosis of clinical samples, this LightForge approach is now being expanded to incorporate detection of genetic markers linked with resistance to other TB drugs that include fluoroquinolones and isoniazid based on mutations in *gyrA, katG* and *Mab-inhA* regions of the Mtb genome. The scalability of LightForge can also be harnessed to conduct digital PCR (dPCR), a critical tool for detecting genetic heterogeneity in Mtb.

ABBREVIATIONS

%	percentage
(DR)-TB	Drug Resistant Tuberculosis
(DS)-TB	Drug Susceptible Tuberculosis
°C	celcius
µg	micro gram
µl	micro liter
µM	microMolar
µm	micro-meter
2D	two- dimensional
AC	Alternating Current
Al	Aluminium
amol	attomols
BD	Becton. Dickinson
bp	Base pair
BSA	Bovine Serum Albumin
CCD	Charge Coupled Device
CFU	colony-forming unit
cm^2	Square centimetres
cm^3	cubic centimeters
CMOS	Complementary metal–oxide–semiconductor
DC	Direct Current
ddPCR	Droplet digital PCR
dL	Deci-litre

DNA	deoxyribonucleic acid
dNTPs	deoxynucleotide triphosphates
dPCR	Digital PCR
dpi	Dots per inch
E. coli	*Escherichia Coli*
ELISA	Enzyme-Linked-Immunosorbent Assay
erg	10^{-7} joules
FDA	Food and Drug Administration
fM	femtoMolar
H	hours
H_2O	Water
HBCs	High Burden Countries
HDMS	hexamethyldisilazane
HIV	Human Immunodeficiency Syndrome
HRMA	High Resolution Melting Analysis
HRP	horseradish peroxidase
INH	Isoniazid
ISFETs	Ion-Selective Field Effect Transistors
ISO	International Organization for Standardization
K	kelvin
kPa	kilo-pascal
K-RITH	KwaZulu-Natal Research Institute for TB and HIV
MDR	multi-drug resistant
mg	milli gram
MHz	Mega-Hertz

min	minutes
mL	milliliter
mM	milli molar
mm^2	square millimeter
Mtb	*Mycobacteria tuberculosis*
ng	nano gram
nL	nano litre
nM	nanoMolar
nM	nanoMolar
nm	Nano-meter
NTM	Non tuberculous mycobacteria
nW	Nano-watts
OFLX	Ofloxacin
PCR	polymerase chain reaction
PDMS	polydimethylsiloxane
pg	picogramm
PMT	Photomultiplier tube
POCs	Points of Care
ppb	Parts per billion
QCM	Quartz Crystal Microbalance
RDTs	Rapid Diagnostic Tests
RFU	Relative Fluorescence Unit
RIF	Rifampicin
RNA	ribonucleic acid
RNA	Ribonucleic Acid

rpm	Rounds per minute
RRDR	Rifampicin Resistance Determining Region
rRNA	Ribosomal ribonucleic acid
s	seconds
SAV	Surface Area to Volume Ratio
SDA	Strand Displacement Amplification
SiO_2	Silicon Dioxide
SiOH	Silicon Hydroxide
SNP	Single Nucleotide Polymorphism
SPR	Surface Plasmon Resonance
STP	Standard Temperature and Pressure
TB	Tuberculosis
T_m	Melting Temperature
TMA	Transcription-mediated amplification
TMCS	Trimethylchlorosilane
TPD	Thermal Particle Detection
tPSA	total prostate specific antigen
UK	United Kingdom
UKZN	University of Kwazulu-Natal
US	United States of America
USA	United States of America
UV	ultraviolet
Vm^{-1}	Volts per meter
W	watts
WHO	World health organization

XDR-TB	Extensively-drug-resistant tuberculosis

TABLE OF CONTENTS

Contents Page

LIST OF TABLES

Table **Page**

LIST OF FIGURES

Figure **Page**

DISSERTATION STRUCTURE

The dissertation is presented in the following order:

CHAPTER 1: Introduction

Presents a brief overview on the current dire status of TB/HIV globally followed by a review of the current challenges in fighting these infectious diseases. Finally, the current genomic approaches to TB diagnosis are outlined providing the rationale behind moving towards point of care diagnostic platforms.

CHAPTER 2: Microfluidics

Gives detailed information on the subject of microfluidics as a potential solution to the problems outlined in Chapter 1. The chapter provided a literature review on the application of microfluidics in diagnostics. It highlights the current knowledge gap that our research has potential to fill. The research aims and objectives are also outlined in this chapter.

CHAPTER 3: Materials and Methods

Provides a full account of the activities implemented in the research. This includes; aims & objectives; all consumables; chemical reagents; equipment; software; microfluidic chips' designing and fabrication protocols.

CHAPTER 4: Results

Describes in detail how the LightForge System (highly scalable microfluidic platform for real-time PCR and HRMA) works. A detailed description of how the system was used to detect rifampicin resistance conferring mutations in several Mycobacteria tuberculosis clinical isolates is given. The chip design optimization towards digital PCR (dPCR) and the potential of the LightForge system to conduct digital PCR for heteroresistance detection from the onset are also highlighted.

CHAPTER 5: Discussion

This chapter focusses on discussing the LightForge system's SNPs resolution ability in comparison to other systems on the market in reference to cost, selectivity, speed, user friendliness, scalability, sensitivity, specificity and simplicity. The demonstrated potential application of the LightForge system towards digital PCR as well as other applications is discussed.

CHAPTER 6: Conclusions

This chapter summarises the answers to the questions that this project sought to answer. It also gives an insight to the projected future research interest.

CHAPTER 1

1. Introduction

1.1. TB/HIV Global Situation

Tuberculosis (TB) is a highly contagious airborne disease that ranks as the second leading cause of death by an infectious agent after the Human Immunodeficiency Virus (HIV) [1]. The most recent annual global report on Tuberculosis by the World Health Organisation (WHO) indicates that an estimated 9 million clinical TB (inclusive of 550 000 children) cases were recorded in the year 2013. This number included about 1.1 million cases of TB/HIV co-infection [2]. Of these reported clinical cases, 1.5 million deaths were recorded, which included 360 000 cases of TB/HIV co-infection, 510 000 women and 80 000 children[3]. A recent TB epidemiological study conducted by the WHO identified a group of 22 countries with the greatest burden of the TB epidemic with HIV infection being a prominent accelerator of the epidemic[4]. The countries belonging to this group have been classified as high-burden countries (HBCs) and are responsible for 81% of all reported TB clinical cases globally. South Africa is among the HBCs with the third highest absolute number of TB incidence cases reported [5]. It is also ranked fifth in terms of estimated undiagnosed active TB cases. However, normalising these statistics by taking into account the countries' population sizes, South Africa has the highest incidence and prevalence of TB (per 100 000 people). Statistics further reveal that South Africa has the highest number of HIV-linked TB cases and the second highest number of diagnosed multidrug-resistant TB (MDR-TB) cases after India among the HBCs[6].

Based on this state of affairs, South Africa has an unmet need for effective strategies to minimise transmission of TB infection within its communities; as well as strategies for early diagnosis of both drug susceptible TB (DS-TB) and drug resistant TB (DR-TB). There is also a dire need for timely treatment initiation in diagnosed patients. The rate limiting step in the implementation of these strategies is the diagnosis step.

There are several factors affecting the diagnostics infrastructure in South Africa and other developing countries. For instance;

a) People often have to present themselves with TB symptoms at a healthcare providing facility. This means that they may never know of their status until it is too late to be treated effectively or when they become seriously ill.
b) In the majority of cases, people should first test positive for HIV in order to elicit suspicion of a possible TB opportunistic infection. Accordingly, patients may remain untested for TB until they test positive for HIV.

c) The proper TB diagnosis is largely dependent on the sensitivity, specificity and accuracy of the test employed. As a result, misdiagnosis still exist in resource limited settings where the lack of access to efficient diagnostic tools is the norm.
d) Often, the turnaround time before the test results become available to the patient is too long (8 weeks on average in resource limited settings), which is also crippling to the efforts in the fight against TB. This is because as long as patients are still unaware of their test results, they still remain in the community spreading the disease.
e) There is also a need for functional healthcare systems capable of tracing TB positive patients ensuring that their treatment is initiated promptly and that they respond appropriately to treatment. The absence of such systems is also hindering the efforts to ensure a TB free society because most developing countries lack the resources to retest individuals because of the high incidence numbers.
f) Comprehensive diagnosis of TB is also dependent on the healthcare delivery system's ability to track and test persons who made contact with recently diagnosed TB patients. All these factors can be addressed through development of large scale and inexpensive diagnostic platforms that are capable of screening all at-risk citizens at least once a year [7].

1.2. Genomic Approach to TB Diagnosis

Basing on the current genetic findings, spontaneous mutations—that include point mutations, deletions and insertions—emanate from the selective pressure due to treatment regimens used for TB. Studies have shown this to result in the positive selection of drug resistant phenotypes associated with genetic changes—which can be point mutations, deletions and/or insertions. Some mutations from multiple *Mycobacterium tuberculosis* (Mtb) genes have been documented to be associated with reduced susceptibility to anti-TB drugs such as rifampicin, ethambutol, carpreomycin and fluoroquinolones[8]. Conventional approaches to genomic studies (for instance studies using the GeneXpert machine) heavily depend on analysis of genomic material from populations of multiple cells as opposed to single cells [9]. The problem of diagnosing using this approach is that the resultant diagnostic indication is population averaged and the derived measurements may fail to detect minority events (e.g. mutations) occurring in a minority of the cell population [10].

Conventionally, a 1% subpopulation harbouring drug resistant mutations may not be detectable upon first appearance based on population averaged analysis. However, continued treatment may kill off the susceptible population allowing the drug resistant sub-population to become dominant, leading to treatment failure. In attempts to circumvent population averaged measurements and detect mixed infections—occurring at rates of 10-20% in high incident settings[11]—researchers have moved towards analyses of genomic material extracted from single cell derived culture isolates. Culture diagnostic technique is more sensitive than smear microscopy because it detects a higher proportion of

cases among patients with symptoms. It requires further interrogation of positive cultures to distinguish TB from Nontuberculous Mycobacteria (NTM). The time to positive results is dependent on bacillary load and usually positive by 4 weeks. However, a culture is only confirmed negative after 6 weeks incubation. Traditionally culture employs a solid medium for instance coagulated egg (e.g. Löwenstein-Jensen) or agar (e.g. Middlebrook 7H10) as a base. The drawbacks of solid medium approach are; slow bacterial growth (3-4 weeks); and errors due to manual reading of results. Currently, mycobacterial culture methods are gold the standard diagnostic tools in cases of paucibacillary tuberculosis (with low Mtb bacilli load), such as in HIV positive patients with smear negative pulmonary tuberculosis and children. More sensitive liquid medium culture techniques have been developed for shortening the detection of TB bacilli to 2 weeks[12]. Automated systems such as the MGIT 960 detect bacterial growth in liquid media using a fluorescence-quenching based oxygen sensor within specialised vials/tubes which are inoculated with patients' specimens[13]. The major limitation of culture methods is that they increase the turnaround time for diagnosis by weeks and subsequently intensify the risk of other people in communities being exposed to infectious doses of Mtb. Recently research has shown that culturing decreases the microbiome diversity thereby causing measurements to deviate from true diversity *in vivo* [8, 14]. In principle therefore, there is an urgent need to design robust molecular diagnostic strategies that are able to indicate diverse genetic mechanisms behind drug resistance in individual isolates[11].

Some of the validated commercially available nucleic acid assays include those from: Roche (Amplicor, PCR, FDA-approved)[15], Becton Dickson (BD Probe Tec, strand displacement amplification [SDA])[16], Genprobe (Amplified Mycobacterium tuberculosis Direct [AMTD]--FDA-approved)[17], transcription mediated amplification [TMA])[18], Hain Lifescience[19], (GenoType Mycobacteria Direct, PCR)[20] and Cepheid GeneXpert® MTB/RIF assay[21]. However their impact is being limited by their high cost, reliance on skilled personnel and inapplicability at points of care. Furthermore, all these quantitative assays are analog in nature, meaning that the fluorescent readouts are an average of the total sample volume. This poses a problem in the analysis, as the minority events or the heterogeneity of the sample goes undetected.

To circumvent these problems a novel technique called digital PCR (dPCR) has been developed. Digital PCR (dPCR) is a refinement of conventional PCR where the PCR master mix containing minimally diluted DNA sample is partitioned into many chambers such that each chamber contains one genome or nothing[10]. This "divide and conquer" approach allows individual genomes to be interrogated in isolation thus offering more accuracy and less ambiguity than conventional PCR[22]. Corporations such as Fluidgm, Life technologies, Bio-Rad and RainDance have developed dPCR systems that are currently available on the market at exorbitant prices that are prohibitively expensive for diseases that principally affect poor people in poor social settings. The prices quoted in **Table 1.1** [23] for both machine purchase

and operational costs are difficult for affected governments to justify expenditure as they are likely to consume the entire healthcare budget.

Table 1.1|Commercial Digital PCR Systems Currently on the Market.

Manufacturer	**Machine & Price Range**	**Consumables Cost**
Fluidigm Corporation Headquarters	BioMark HD: US$200,000 - $250,000	$400 per chip
	EPI: US$100,000 - $150,000	$400 per chip
Life Technologies	Open Array RealTime PCR System US$140,000	$150 per plate
	QuantStudio 12K Flex US$90,000-$190,000	$150 per plate
Bio-Rad Laboratories	QX100 ddPCR System US$89,000	$3 per sample
RainDance	RainDrop Digital PCR US$100,000	$10 -$30 per sample

1.3. Evaluating the Cepheid GeneXpert® MTB/RIF Assay

Cepheid has developed the GeneXpert® desktop machine that, through the MTB/RIF assay it can simultaneously detect *Mycobacterium tuberculosis* and rifampicin resistance within 2 hours directly from sputum[24]. This enables the identification of patients needing second-line drug treatment[25]. It has also made it feasible for use in peripheral laboratories and clinics by minimally trained personnel. The machine has five versions namely; GeneXpert I; GeneXpert II, GeneXpert IV, GeneXpert XVI and GeneXpert Infinity-48 (for one, two, four, sixteen and 48-module configurations respectively)[26]. Recent studies have also demonstrated the MTB/RIF assay sensitivity by detecting 98% of smear-positive TB patients and 70% of smear-negative TB patients[25]. However, this machine has limitations that include; short diagnostic cartridge shelf-life; restricted operating environmental conditions; unestablished long-term robustness; detects only rifampicin resistance; low scalability; high cost and reliance on compulsory annual service maintenance as well as calibration[21]. With the tiered pricing for developing countries, each machine costs between US$17,000 and $62,000 while each of its single use disposable test-cartridges costs between US$17 and $120[27]. These prices translate to costing patients $26.54 per laboratory test and $38.91 per point-of-care test. In practical consideration, if each GeneXpert run takes 2 hours, when a GeneXpert I is used, only 12 patients can be diagnosed in a day. Therefore for a disease that affects millions of poor people, it is unsustainable to be charging them

US$26.54 - $38.91 at such a low service execution rate. In 2014, the South African government decided on GeneXpert roll-out to smear microscopy laboratories; the expected volumes were each for 274 laboratories or 4020 points of care. The idea was to test 2.6 million pulmonary TB suspects. The total cost for national placement of GeneXpert at laboratories was projected at US$71 million per year and US$107 million per year for point-of-care placement[28]. However, with the above stated shortcomings of the GeneXpert, there is no reason to substantially justify this additional expenditure to the national health budget.

1.4. Towards Point of Care (POC) TB Diagnosis

As far as TB diagnosis, treatment and management are concerned, the use of traditional "heavy" lab instrumentation for diagnostic tests has been essentially important for their accuracy[29]. However, with the current high demand for frugally sustainable alternatives with user friendly analytical platforms, there is an urgent need for simple rapid diagnostic tests (RDTs) for diagnosis at points of care (POCs). As per guidelines an ideal POC device should have its minimal strengths adhering to WHO's ASSURED (affordable, sensitive, specific, user-friendly, rapid, equipment free and be deliverable to the needing parties) criteria that condense specification goals for point of care testing [30]. **Figure 1.1** illustrates the goals towards the true POC diagnosis approach and the time it saves towards patient recovery. With technologies such as bioelectronics, microfabrication as well as nanofabrication hitting the strides, novel methods and tools for TB diagnosis are being developed. These emerging tools are showing great potential to provide efficient, low cost and miniaturized microfluidic diagnostic platforms for *Mycobacterium tuberculosis*.

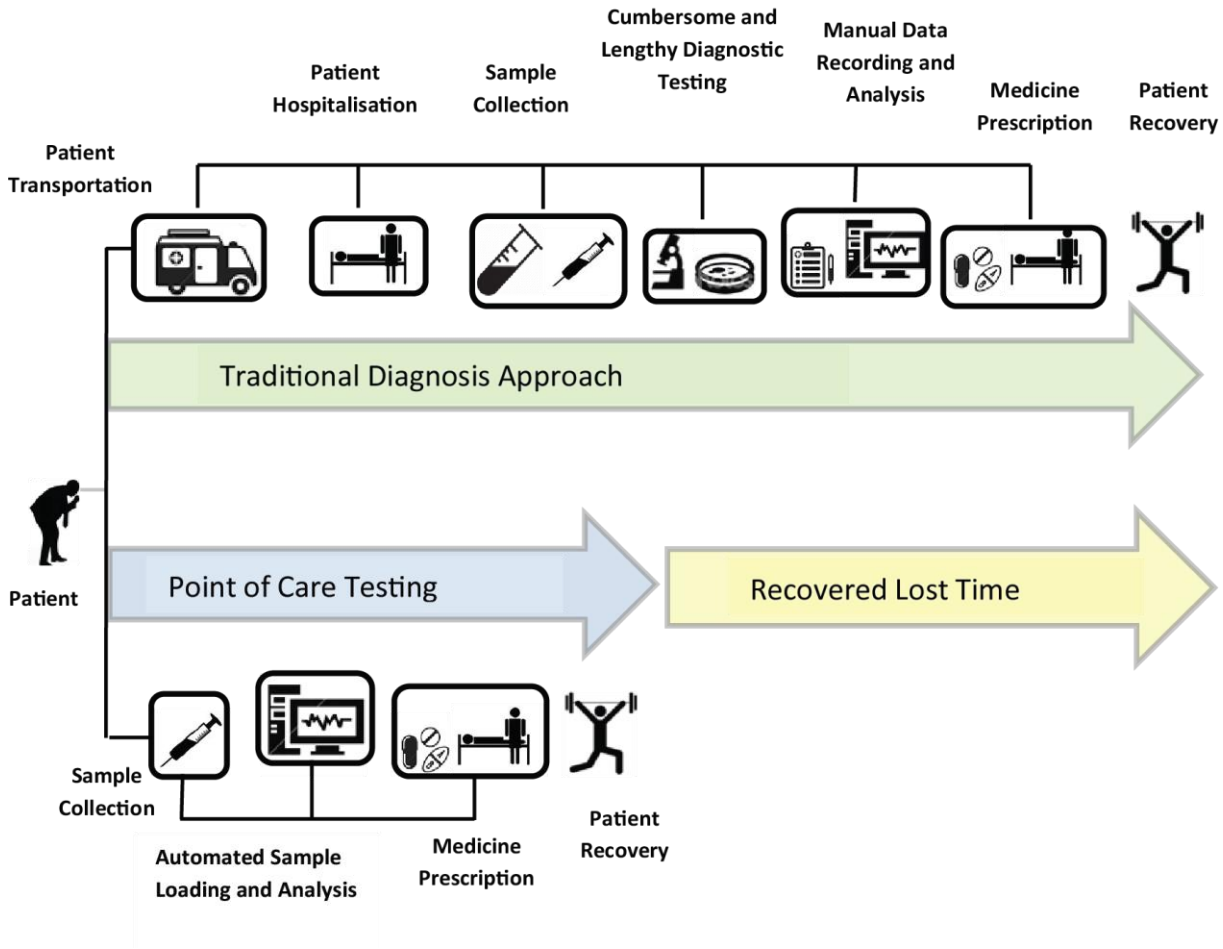

Figure 1.1|Schematic illustration of the vision towards an ideal point of care (POC) diagnosis. The figure is comparing point of care testing and the traditional testing approaches in parallel. It illustrates the goals towards a true POC diagnosis approach and the time it saves towards patient recovery. It can be seen that the projected POC allows patients to be tested and treated at bedside or in the community thus significantly simplifying the costly, laborious and long traditional approach. The traditional approach involves; patient transportation; patient hospitalisation; patient specimen collection; cumbersome lengthy diagnostic testing; manual data capturing and analysis; and finally medicine prescription and patient recovery if they are still alive. The highlighted recovered lost time can be crucial for: i) preventing loss of lives due to curable diseases such as TB or ii) minimising the development of drug resistance; iii) preventing the spread of the disease in communities.[a]

[a] Concept adapted from http://aetcnmc.org/curricula/promoting/mod5_1.html

CHAPTER 2

2. Microfluidics

2.1. Microfluidics Definition

Microfluidics is a science involving building devices that precisely manipulate and control minute volumes (10^{-9} – 10^{-18} litres) of fluids and particles through the use of channels with widths ranging from tens to hundreds of micrometres[31]. There are scenarios where reagents are very expensive, therefore microfluidics has become important as it preserves the functionality of the assay while saving time and reagents. Microfluidics has a rich history that dates back as early as the 1950s when it became the basis of inkjet printer technology[32]. Later the 1970s saw the compacted gas chromatographs being invented also based on this principle[33]. As the 1980s approached the first silicon micro-machining based micro-valves and micro-pumps were realized [34-36]. Then the three decades that approached to date, involved extensive research in the development of specialized microfluidic components designed to transport, meter, mix, valve, concentrate and separate fluids[37].

2.2. Underlying Principles of Microfluidics

In contrast to macrofluidics—which deals with the realm of millilitres to litres, there are several forces that dominate fluid flow within channels with microscale dimensions[38]. Studies have proven that the normal functional efficiency is not conserved when currently existing macroscale devices are shrunk to microscale. Miniaturization comes with domination of effects that include laminar flow, diffusion, fluidic resistance, surface area to volume ratio and surface tension[39]. However, an understanding of these parameters in the microscale allows us to manipulate them to our advantage.

2.2.1. Reynolds Number

A description of viscous fluidic motion (laminar or turbulent) is given by the dimensionless Reynolds number (Re) parameter which is calculated by:

$$Re = \frac{\rho v D_h}{\mu} \tag{1}$$

where ρ is the fluid density, v is the characteristic velocity of the fluid, D_h is the hydraulic diameter that is calculated based on the cross-section of the channel and μ is the fluid viscosity[40]. For a fluidic flow to be classified as laminar (See section **2.2.2.** for a more detailed explanation on laminar flow), the

Reynolds number as calculated by the above formula needs to be less than 2300. Signs of turbulence begin to manifest as the Re approaches 2300. When Re surpasses 2300, the motion is rendered turbulent by definition. This reason declares macroscale platforms challenging to work with because they are largely considered turbulent. Inversely, the laminar motions that exist in microscale systems make them more predictive and easier to work with[41].

2.2.2. Laminar Flow

Contrary to turbulent flow that is considered chaotic and difficult for predicting the location of a particle in a stream of fluid as a function of time, particles in laminar flow can have a well-defined function of time. Microfluidics guarantees this laminar flow of fluids[42, 43]. **Figure 2.1a** (below) shows an interesting laminar flow illustration of how multiple streams flowing in contact with one another will only mix by diffusion and not by any other mechanism. The non-uniformity of this multiple stream diffusive mixing within the same channel has been proven under certain conditions [44]. Researchers have capitalized on this phenomenon to predictively perform assays and size dependent sorting of particles. As also illustrated in **Figure 2.1b** (below), laminar flow has also been harnessed to compartmentalise fluids into droplet packets. The components of adjacent packets only mix by diffusive forces, other than that, the composition in each packet remain relatively maintained. These packets for instance can be manipulated to allow multiple reactions or cellular analysis [45].

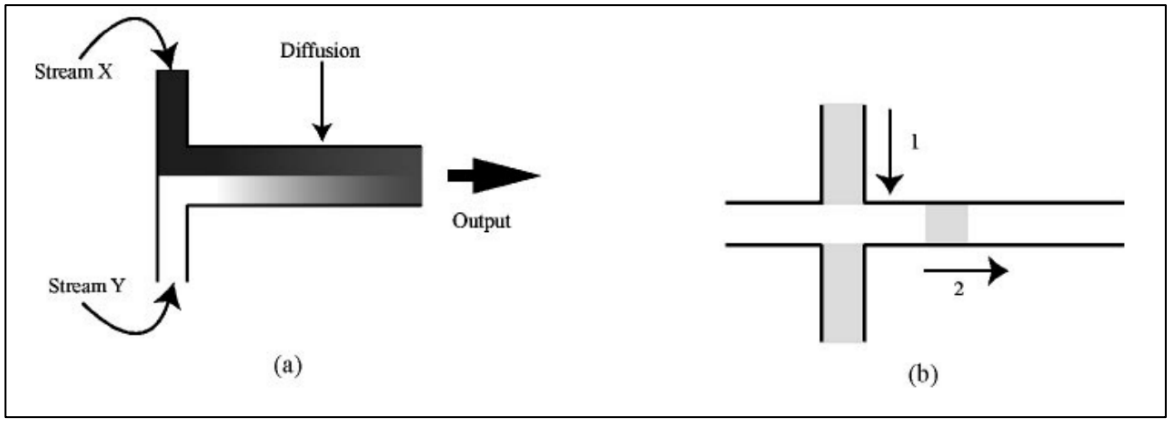

Figure 2.1|Microchannel fluid dynamics (a) Two adjacent flowing streams only mix by diffusion. As the duration of the streams' contact increases the degree of diffusion between the streams under study increases. (b) The fluid is initially flown vertically following direction 1 with minimal diffusion effects along the horizontal channel. When the fluid is subsequently flown along direction 2, a fluid packet is created from stream 1 and moves along the horizontal channel. (*Adapted from a 2002 Physics and applications of microfluidics in biology annual review of biomedical engineering*) [41].

2.2.3. Diffusion

Diffusion is a mechanism of Brownian motion by which a concentrated group of particles distributes out as a function of time and this ultimately leads to a uniform concentration of particles in a fixed volume container. The equation that models diffusion in one dimension is given by;

$$d^2 = 2Dt \tag{2}$$

where d is the distance travelled by a particle in time t, while D is the diffusion constant of the particle [46]. Diffusion effects become critically exacerbated in microsystems because according to the equation above distance varies to the square power. As an illustration, haemoglobin (D = 7× 10^{-7} cm^2s^{-1}) has been shown to take 10^6 sec to diffuse over 1 cm, but only 1 sec to diffuse 10μm distance [41]. This means that diffusion is a negligible parameter in macrosystems. However, in microsystems it becomes a critical effect to neglect. In fact, when dealing with microfluidic systems, diffusion can be relied on for mixing reagents, thus preventing the need for expensive and complex mixers often required in macrosystems. Researchers have harnessed these diffusion effects in microsystems to create concentration gradients with high complexity for various applications [47].

2.2.4. Resistance

The resistance in microfluidic systems' channels can be characterised to depend on the following equation;

$$Q = \frac{\Delta P}{R} \tag{3}$$

where Q is the flow rate, ΔP is the pressure drop across the microchannel, and R is the microchannel resistance [48]. An understanding of the geometry of microfluidic channels allows us to predictively harness resistance for microfluidic manipulation. If we consider the most common circular microchannel geometry, the resistance is given by the equation;

$$R = \frac{8\mu L}{\pi r^4} \tag{4}$$

Where μ is the fluid viscosity, L is the microchannel length, and r is the channel radius [49]. However, if we change the geometry to a low aspect ratio ($h \approx w$) rectangular the expression for resistance becomes much more complicated and follows the following equation;

$$R = \frac{12\mu L}{wh^3}\left[1 - \frac{h}{w}\left(\frac{192}{\pi^5}\sum_{n=1,3,5}^{\infty}\frac{1}{n^5}tanh\left(\frac{n\pi w}{2h}\right)\right)\right]^{-1} \quad (5)$$

where w is channel width while h is the channel height. However for rectangular microchannel geometry with high aspect ratio (either $h \ll w$ or $w \ll h$) the resistance can be computed using the following equation [50];

$$R = \frac{12\mu L}{wh^3} \quad (6)$$

2.2.5. Surface Area to Volume Ratio

With miniaturisation to microscale, surface area to volume ratio (SAV ratio) becomes an important factor. In microsystems, a small decrease in the microchannel dimensions is accompanied by an increase in the SAV ratio. With high SAV ratio in microfluidic systems, reaction rates and thermal transfer occur at faster rates. This high SAV ratio in contrast to macroscale vessels—including flasks, tubes and dishes—makes microfluidic systems ideal for close mimicry of *in vivo* conditions where the SAV ratio is typically very high. The high SAV ratio is however only disadvantageous for the reason that it allows particles to easily adsorb to the surface of the channels thus reducing the efficiency of fluid motion [51].

2.2.6. Surface Tension

The resulting force of cohesion between liquid molecules at the liquid/gas interface is called surface tension[52]. This force presents one of the most important differences between macroscale and microscale fluidic motions. Surface tension can assist in propelling fluid flow through exploitation of capillary action. This is a phenomenon that is commonly described as wicking. It occurs when intermolecular forces between the fluid and the narrow microchannel's surface overcome those within the fluid itself, such that it is drawn through the channel[53]. Researchers have found a way of inhibiting or inducing flow by altering the hydrophobicity of the channel's surface. Using various physicochemical modifications, scientists have created hydrophobic stops at locations of interest within microfluidic circuits so that aqueous solutions can be impeded upon reaching that location[41]. This principle based on surface tension has been applied to droplet-based digital microfluidics. Often employed are two immiscible phases where the continuous phase is a hydrophobic fluid such as oil or air. Since most biological samples are in aqueous solutions, they form the disperse phase of the system[54]. The mathematical description of the pressure that a liquid surface with perpendicular radii of curvature given by R_1 and R_2 generates can be computed using the Young-LaPlace equation;

$$\Delta P = \gamma \left(\frac{1}{R_1} + \frac{1}{R_2} \right) \tag{7}$$

where γ is the free energy of the liquid surface. If virtual walls are involved, the R defining the wall length approaches infinity such that the relation reduces to;

$$\Delta P = \frac{\gamma}{R} \tag{8}$$

This gives the pressure that is present at the liquid boundary existing between two infinitely large parallel plates that have a $2R$ distance apart. If we consider a spherical surface where $R_1 = R_2$ the relation reduces to;

$$\Delta P = \frac{2\gamma}{R} \tag{9}$$

This relation makes it easier to compute the pressure contained within a liquid spherical drop[55].

2.3. Microfabrication

2.3.1. Clean Rooms

To guarantee acceptable yields, the processes of microfabrication (manufacturing microfluidic devices) must be carried out within a microfluidic clean room[56]. This room is specially designed in such a way that the size and the quantity of particulates that are airborne are critically controlled. Other parameters that are also controlled with high specificity include temperature, air pressure, humidity, vibration and lighting (yellow is the standard to avoid activation of photo-reactive resist). Classification of microfluidic clean rooms is based on the quantity and size of particulates that they allow per unit volume of air. **Table 2.1**[57] summarises the guidelines used by the International Organisation for Standardisation (ISO) for classification of clean rooms.

Table 2.1|ISO 14644-1 Classification of Clean Rooms.

	Highest Particle Count per Cubic Meter					
Class	**≥ 0.1µm**	**≥ 0.2µm**	**≥ 0.3µm**	**≥ 0.5µm**	**≥ 1µm**	**≥ 5µm**
ISO 1	10	2				
ISO 2	100	24	10	4		
ISO 3	1,000	237	102	35	8	
ISO 4	10,000	2,730	1,020	352	83	
ISO 5	100,000	23,700	10,200	3,520	832	29
ISO 6	1,000,000	237,700	102,000	35,200	8,320	293
ISO 7				352,000	83,200	2,930
ISO 8				3,520,000	832,000	29,300
ISO 9				35,200,200	8,320,000	293,000

2.3.2. Photolithography

There are numerous lithography techniques for fabrication of microstructures. On the basis of energy beams involved, lithography techniques can be further subcategorised into photolithography, electron lithography, X-Ray lithography and ion lithography. However, photolithography is the most popular technique for microfluidic devices' fabrication [57]. Photolithography is limited to two-dimensional lateral structures and it employs a photosensitive emulsion layer called resist which is receptive of a desired design from a transparent mask. In most microfluidic applications that require complex structures, a mask derived from Autodesk AutoCAD software design is printed on a plastic transparency film by a high resolution (greater than 5000 dpi) commercial printer. There are three main processing steps describing photolithography illustrated in **Figure 2.2**:

i. *Alignment Process*: this involves the lateral positioning of the mask and the resist spin-coated substrate with adjustment of distance separating the mask and the substrate.

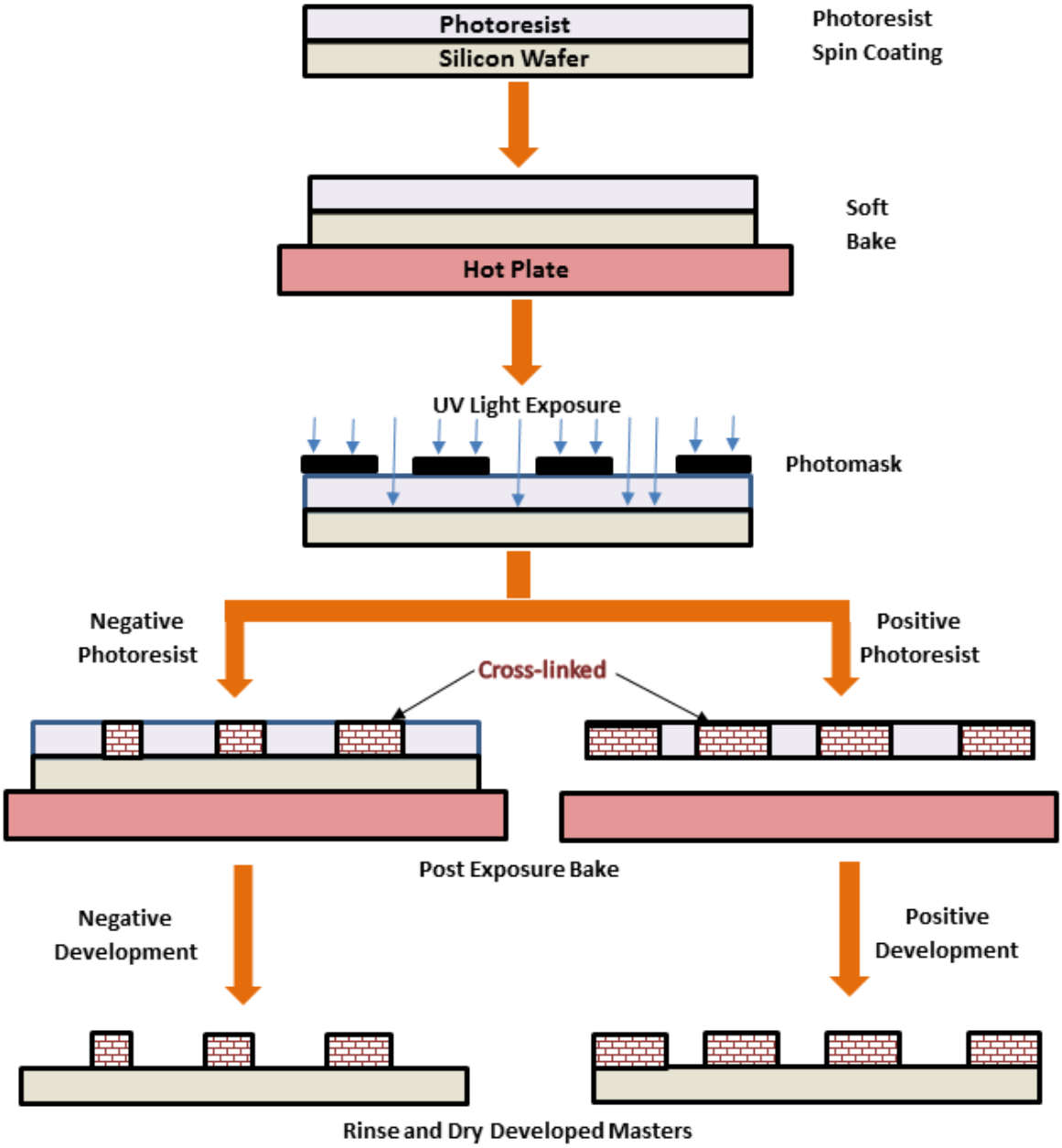

Figure 2.2|Schematic illustration of standard photolithographic protocol for master fabrication. Described in sequential order are the steps involved in photolithography. The first step involves coating the wafer with photo-reactive resist. A pre-exposure soft bake step follows to harden the photo-reactive resist. A photo-mask is placed in proximity or in contact with the photo-reactive resist coated wafer. The wafer is then exposed to UV-light using a photo-mask aligner. Depending on the nature of the photo-reactive resist employed (positive or negative), the cross-linking occurs accordingly. A post-exposure then carried out paving way for the development of the designed micro-features on the mold/master using the developing solutions. The masters are then finally rinsed and dried to complete their fabrication.[b]

[b] Concept redrawn after adaptation from http://www.photochembgsu.com/applications/photoresists

ii. *Exposure Process*: This process can be summarised as optical shining of the resist layer, thus transferring designs from the mask transparency to the photoresist by chemically altering the properties of the shone regions.

iii. *Development Process*: This is a process of dissolution (for negative resist) or etching (for positive resist) of the resist design in a developer solution to generate the desired features on the mold/master.

In general, photolithography is categorised into contact printing, proximity printing and projection printing. As the names suggest, the first two techniques involve bringing the mask close to the substrate; for contact printing, the transparent mask even touches the photoresist layer. For contact and proximity printing, the resolution b is computed using the following relation;

$$b = \frac{3}{2}\sqrt{\lambda s} \tag{10}$$

where λ is the wavelength and s is the distance between the photoresist layer and the mask. However as we consider projection printing, its resolution is given by;

$$b = \frac{\lambda s}{2NA} \tag{11}$$

where NA is the numerical aperture of the lens involved in the imaging [58].

2.3.3. Soft Lithography

Soft lithography is a microfabrication technique that typically use a two-component polymer (elastomer and curing agent) called polydimethylsiloxane (PDMS) for molding using the photoresist masters obtained from photolithography [59]. The features of the PDMS device are only limited by the master molds from which it is moulded from. This has greatly revolutionised the fabrication of microstructures with high degree of complexity using PDMS. This revolution has seen devices with complex multidimensional layers being fabricated for various applications. The popularity of soft lithography over glass/silicon micromachining emanates from it being less expensive and more suitable for biological applications [60]. **Table 2.2**[61] shows some of the physical and chemical properties of PDMS.

Table 2.2|PDMS Physical and Chemical Properties[c]

Property	Characteristics	Consequence
Optical	Transparent; UV cut-off, 240nm	Possible Optical detection between 240 and 1100nm
Electrical	Insulating; breakdown voltage, 2×10^{7} Vm^{-1}	Allows embedded circuits; intentional breakdown to open connections
Mechanical	Elastomeric; tunable Young's modulus, typical value of ~750kPa	Conforms to surfaces; allows actuation by reversible deformation; facilitates release from moulds
Thermal	Insulating; thermal conductivity, 0.2 $W(m\cdot k)^{-1}$; coefficient of thermal expansion, 310µm$(m\cdot°C)^{-1}$; stable up to ~300°C	Can be used to insulate heated solutions; does not allow dissipation of resistive heating from electrophoretic separation
Interfacial	Low surface free energy ~20 erg cm^{-2}	Replicas release easily from moulds; can be reversibly sealed to materials; not wetted by water unless oxidised to SiOH presenting surface
Permeability	Low permeability to liquid water; permeable to gases and nonpolar organic solvents	Contains aqueous solutions in channels; allows gas transport through the bulk material; incompatible with many organic solvents
Reactivity	Inert; can be oxidised by exposure to a plasma	Unreactive toward most reagents; surface can be etched; can be modified to be hydrophilic and also reactive toward silanes
Toxicity	Nontoxic	Can be implanted in vivo; supports mammalian cell growth

[c] Adapted from Basic microfluidic and soft lithographic techniques by Tang *et al.*

The **Figure 2.3** (below) shows the schematic illustration of steps involved in soft lithography that include PDMS dispensation, PDMS curing via oven baking, cutting the chip and punching inlet and outlet ports and bonding the chip to a holder substrate.

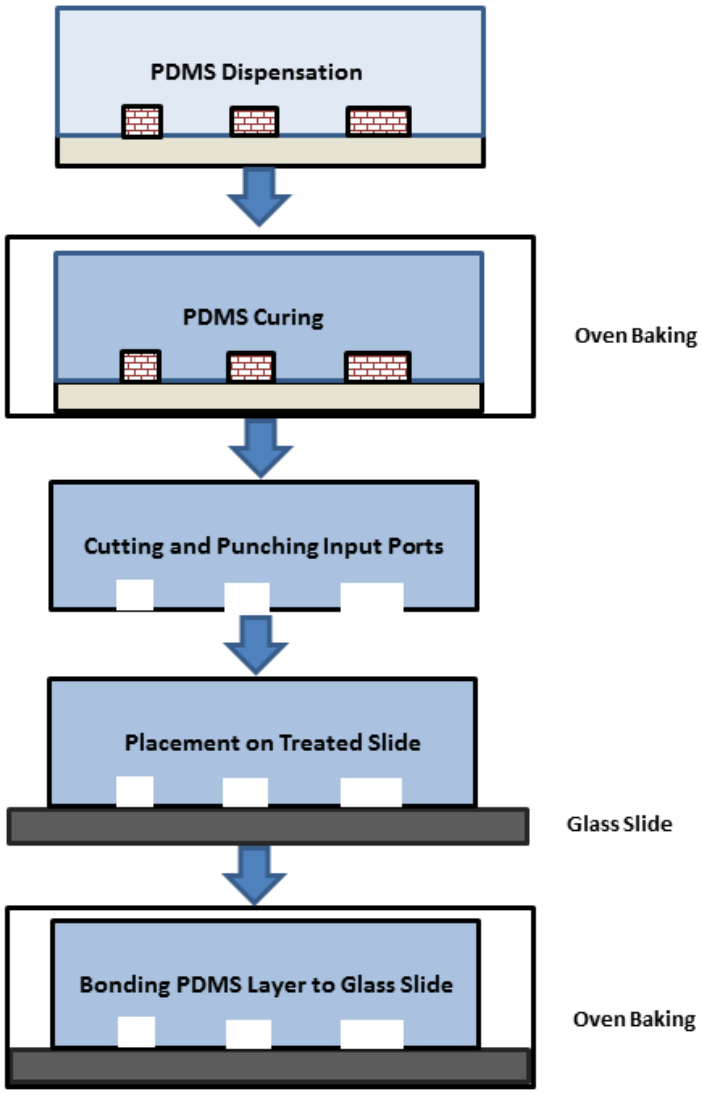

Figure 2.3| Schematic illustration of standard soft lithographic protocol for PDMS fabrication using the silicon wafer. Illustrated in sequential order are steps involved in soft lithography describing; PDMS dispensation; PDMS baking in an oven ensuring the PDMS to cure. Once cured the device is carefully cut along its periphery of the master; peeled off the master and input/outlet ports be punched with a punch press. The device is then placed on a pre-treated substrate such as a glass slide. The resulting hybrid device is then oven baked to ensure bondage of the glass substrate to the PDMS device.[d]

[d] Concept redrawn after adaptation from http://www.elveflow.com/microfluidic-tutorials/soft-lithography-reviews-and-tutorials/

2.4. Microfluidic Device Detection Methods

Detection mechanisms employed by biosensors that are integrated on microfluidic devices can be broadly classified into four different categories namely optical, electrochemical, thermal and mechanical [62]. Every biosensor design constantly aims to address and maximise strengths in sensitivity and selectivity. This makes detectors in microfluidic systems similar to those applied in conventional biosensors. However, with miniaturisation we approach the realm of lower volumes and concentrations. This realm therefore requires a low cost, highly selective and highly sensitive detector compatible with automation. The **Figure 2.4** (below) shows a schematic illustration of biosensor principle.

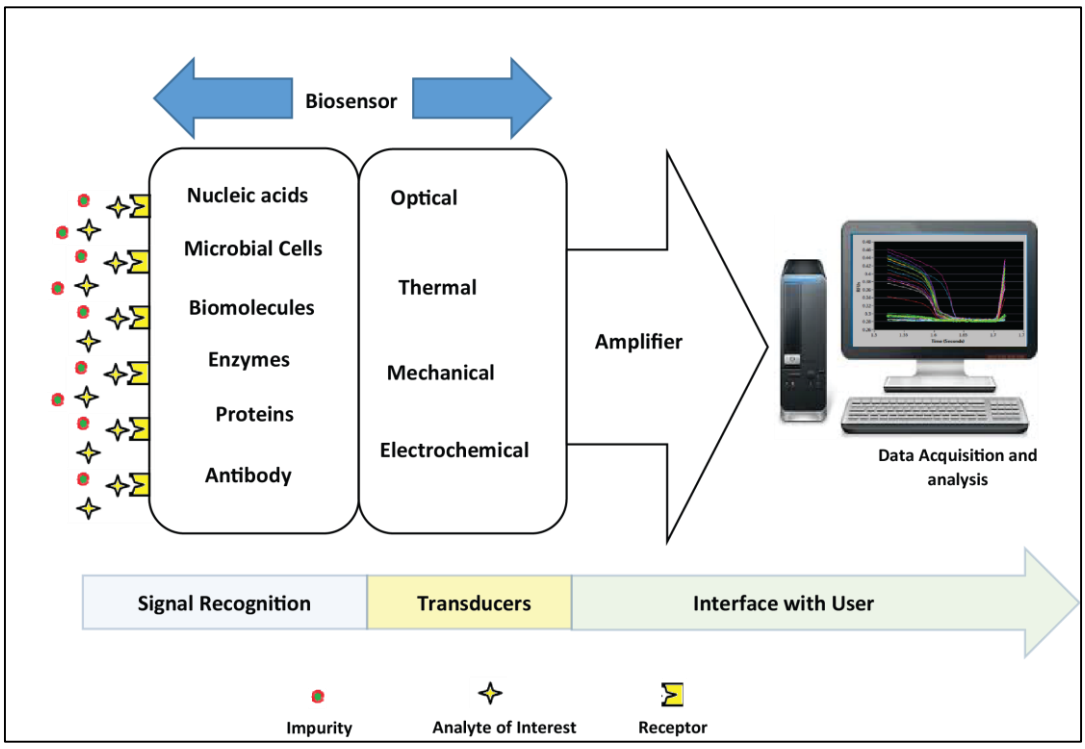

Figure 2.4| Schematic illustration of biosensor principle. The scheme shows the biomaterial detection mechanisms employed by biosensors that are integrated on microfluidic devices. There are several transducers that can be broadly classified into the shown four different categories namely optical, electrochemical, thermal and mechanical. After a specific signal recognition, the signal is transduced through the above stated mechanisms. This pave way for amplifiers such as the photomultiplier tubes (PMTs) to enhance the signal intensity so that it can be readable for analysis by a computer[63, 64].

2.4.1. Optical Detection Based Devices

In microfluidic biosensors, optical detection methods mostly rely on mechanisms that involve absorbance, fluorescence, chemiluminescence and surface plasmon resonance (SPR). In pursuit of high sensitivity and specificity, microscopes, lasers, spectrophotometers, charge coupled devices (CCDs) and photomultiplier tubes (PMTs) are still being coupled to microfluidic devices[65]. However, these fundamental components of optical detection are still very expensive and difficult to miniaturise. Given that for a true point-of-care system, microfluidic devices need to be cheap and user friendly, therefore this is a challenge that all future systems should aim to address [66].

2.4.1.1. Absorbance Based Devices

Absorption spectrometry is a traditional chemical analysis technique of determining the absorbance (A) of a specific wavelength of incident light by an analyte based on the Beer-Lambert law below;

$$A = -log_{10}\frac{P}{P_0} = \varepsilon cl \tag{12}$$

Where, P is the emergent beam radiant power (intensity); P_0 is the incident initial radiant power (intensity); ε is the absorptivity (extinction coefficient) of sample solution; c is the concentration of the absorbing analyte solution; and l is the path length of the cell [67]. In conventional laboratory settings UV absorption spectroscopy is mainly used to detect absorbance. Gustaffson and his team described their work on electrochromatographic separation on-chip utilising UV-transparent SiO_2 waveguides that they arranged in a silicon substrate and integrated within channels of a microfluidic system. Vykoukal *et al* described their absorbance based glucose colorimetric enzyme real-time assay that relies on CMOS image sensing [68]. A 5 hour long absorbance related assay for a cancer biomarker (HE4) was developed by Wang and team based on colorimetric sandwich ELISA. This assay works in conjunction with a CCD camera and has its resolution pegged at 19.5ng/mL [69]. Another on-chip absorbance detection platform was developed by Jokerst and team in 2012. Their colorimetric enzyme based assay detects *E. coli*, *Salmonella* and *Listeria* within 12 hours with a resolution of 10 CFU/cm^3 [70]. Despite these few attempts, microfluidic systems employing absorbance as a mechanism of detection are not very popular. The main drawback is that, a considerably long path length through which a specific wavelength beam of light has to travel within the sample at lower concentration is required for efficiency of this method. This renders the application of this detection method in microfluidic systems very challenging because the extremely narrow nature of microfluidic channels works against sensitivity to absorbance measurements. **Table 2.3** summarises some of the work done with the application of absorbance based microfluidic detectors.

Table 2.3| Summary of Devices Based on Absorbance Principle of Optical Detection

Analyte of interest	Type of Assay	Biosensor Technology	Analysis Duration	Detection Limit	Applicability at POC [a]	Ref.
Glucose	Colorimetric Enzymatic Assay	CMOS image Sensor	Real-Time	-	††	[68]
Cancer HE4 Biomarker	Colorimetric Sandwich ELISA	CCD Camera	5 h	19.5 ng/mL	†	[69]
E. Coli; Salmonella, Listeria	Colorimetric Enzymatic Assay	Visual (No sensor)	12 h	10 CFU/cm²	†	[70]

[a] Potential applicability for point-of-care: † Low; ††Moderate; ††† High

2.4.1.2. Fluorescence Based Devices

Fluorescence process involves a fluorophore or fluorescent dye undergoing three stages namely; excitation, excited state lifetime and emission[71]. The detection mechanism involves absorption of molecular light triggering emission of longer wavelength relative to the excitation wavelength[72]. In various applications fluorescent dyes derived from small molecules, proteins or quantum dots conjugated to proteins, nucleic acids or lipids have been developed[73-76]. This highly sensitive and highly selective fluorescent labelling has attracted diverse applications in microfluidic systems. Currently off-chip CCDs, microscope optics and PMTs coupled to these microfluidic systems still dominate fluorescence detection but work is underway to miniaturise and reduce their complexity[77]. As examples of fluorescence based microfluidic detection systems, Lee and his team used an optofluidics approach to develop a microscope technique that image a protozoan descent parasitic species *Giardia lamblia* cysts commonly found in environmental waters. Their technique is based on a CMOS image sensor with a time of analysis (~1 s) and the resolution is described with a focal plane of 0.8 µm [78]. Ramalingam and colleagues reported their work on real-time PCR based pathogen detection. They demonstrated parallel detection of genomic DNA belonging to multiple water borne pathogens namely; *Aeromonas hydrophilia, Klebsiella pneumonia, Staphylococcus aureus and Pseudomonas aeruginosa* with a resolution of about 50 CFU/mL using a CCD camera to detect fluorescence of EvaGreen dye which intercalates to DNA [79]. For environmental application, Yildirim and colleagues developed a competitive aptamer-based optical biosensor employing inorganic photodiodes that rapidly detects (in 10 min) 17-β-estradiol in water samples with a resolution of 0.6 ng/mL [80]. Another application was reported by Ishimatsu and colleagues when they developed a portable thin film organic photodiode that detects (within 5 min) alkylphenol polyethoxylates (resolution 2-4 ppb) using flow fluorescence based competitive immunoassay with magnetic micro-beads within a microfluidic channel [81]. The major drawback that affect fluorescence detection within microfluidic systems is that, the sensitivity is usually compromised by background signals emanating

from auto-fluorescence by the sample matrix. Currently the cost of fluorophores and fluorescent dyes is very high and often the fluorophores come with low shelf lives. Apart from factors such as temperature and pH influencing the shelf lives, the protocols for fluorescent labelling involve complex manipulation of fluid within micro-channels thus affecting the automation of assays[66]. **Table 2.4** (below) summarises some of the work done with the application of fluorescence based detectors in microfluidic devices.

Table 2.4 |Summary of Devices Based on Fluorescence Principle of Optical Detection

Analyte of interest	Type of Assay	Biosensor Technology	Analysis Duration	Detection Limit	Applicability at POC [a]	Ref.
Giardia Lamblia cysts	Microscopy	CMOS image sensor	~ 1 s	Focal plane of 0.8 µm	†	[78]
Bacterial DNA	PCR	CCD camera	Real-Time	~50 CFU/mL	†	[79]
17-β estradiol	Competitive aptamer	Inorganic Photodiodes	~10 min	0.6ng/mL	††	[80]
Alkylphenol polyethoxylates	Competitive immunoassay	Organic Photodiodes	~5 min	2-4ppb	††	[81]

[a] Potential applicability for point-of-care: † Low; ††Moderate; ††† High

2.4.1.3. Chemiluminescence Based Devices

Chemiluminescence is an optical detection method that involves the emission of light as a result of occurrence of a chemical reaction. When an analyte interacts with a receptor, a photochemical reaction occurs directly or with the aid of an enzyme label. This method has also been at the centre of attraction in many on-chip microfluidic technologies because it has no need for excitation light sources and emission filters. This results from the fact that, the photochemical reactions are very specific; therefore the likelihood of interference by matrix or background emission is largely minimized[82]. Xiang and colleagues have developed a 25 min long microfluidic based capillary chemiluminescence immunoassay for Hepatitis B antigen detection. Their biosensor technology employed a microplate reader and was able to register a limit of detection as low as 0.3ng/mL [83]. Hao and team developed an on-chip sandwich immunoassay for carcinoembryonic antigen detection using a PMT and were able to register a detection limit as low as 20 pg/mL [84]. Yang and colleagues also developed a 1 hour long sandwich immunoassay for Staphylococcal enterotoxin B detection using a CCD camera to obtain limit of detection as low as 0.1 ng/mL [85]. Harnessing the HRP luminol reactions coupled with inorganic photodiodes, Caputo and team were able to detect anti-HRP antibodies on-chip at a limit of detection of 0.2 amol within 1 h [86]. On-chip Streptavidin detection in real-time using HRP luminol reactions coupled with inorganic photodiodes was achieved by Lin and team at 4.76 nM limit of detection [87].

Wojciechowski and team successfully detected Staphylococcal enterotoxin B (within 60 – 70 s) by coupling an organic photodiode system to their sandwich immunoassay and obtained a limit of detection of 0.5 ng/mL [88].The major drawback of chemiluminescence is that, the photochemical signal is quite weak and usually requires sophisticated highly sensitive and computerised ultra-weak luminescence analysers to detect. **Table 2.5** (below) summarises some of the work done with chemiluminescence detection application in microfluidic devices.

Table 2.5| Summary of Devices Based on Chemiluminescence Principle of Optical Detection

Analyte of interest	Type of Assay	Biosensor Technology	Analysis Duration	Detection limit	Applicability at POC [a]	Ref.
Hepatitis B antigen	Capillary immunoassay	Microplate reader	25 min	0.3 ng/mL	†	[83]
Carcinoembryonic antigen	Sandwich immunoassay	PMT	-	20 pg/mL	†	[84]
Staphylococcal enterotoxin B	Sandwich immunoassay	CCD Camera	> 1 h	0.1 ng/mL	†	[85]
Anti-HRP antibody	HRP-luminol reactions	Inorganic Photodiodes	> 1 h	0.2 amol	††	[86]
Streptavidin	HRP-luminol reactions	Inorganic Photodiodes	Real-Time	4.76 nM	††	[87]
Staphylococcal enterotoxin B	Sandwich immunoassay	Organic Photodiodes	60 - 70 s	0.5 ng/mL	†††	[88]

[a] Potential applicability for point-of-care: † Low; ††Moderate; ††† High

2.4.1.4. Surface Plasmon Resonance (SPR) Based Devices

SPR optical detection methods are dependent on determining the change in the refractive index at a heavy metal (usually gold or silver) surface. This metal surface is typically functionalised with probe molecules usually antibodies, antigens or nucleic acid strands. As being illustrated in **Figure 2.5** [89], when an incident beam of light of specified wavelength passes through a prism at a specific angle towards a thin metal film, it excites a propagating surface plasmon at the surface of the metal film. As shown in **Figure 2.5**, the SPR angle is distinctively dependent on the mass of particles deposited on the opposite side of the metal thin film surface. The only scenario that changes the SPR angle is when the complementary analytes bind to the probe-functionalised metal surface registering a change in the mass of the surface film. In most detectors, this mass change at the metal surface film undergoes a transduction pathway through impacting a change in the resonant angle and this change can be recorded in real-time by plotting the resonance signal (a measure of mass change at the metal film surface) as a function of time[90, 91]. Krupin and colleagues have developed a real-time protein adsorption technique for Bovine Serum Albumin (BSA) detection using an infrared camera to obtain limit of detection as low as 12 pg/mm² [92]. Another SPR based real-time assay was developed by Ouellet and team, where they

detected human α-thrombin in a label free immunoassay using a CCD camera to reach a limit of detection of about 5 nM [91]. Foudeh and team using a CCD camera were also able to detect bacterial rRNA in an on-chip enzymatic colorimetric assay within 3 hours reaching a 0.45 fM detection limit [93]. Currently SPR technology has displayed tremendous sensitivity towards above -mentioned analytes; however, sophisticated equipment is still required to record SPR measurements.

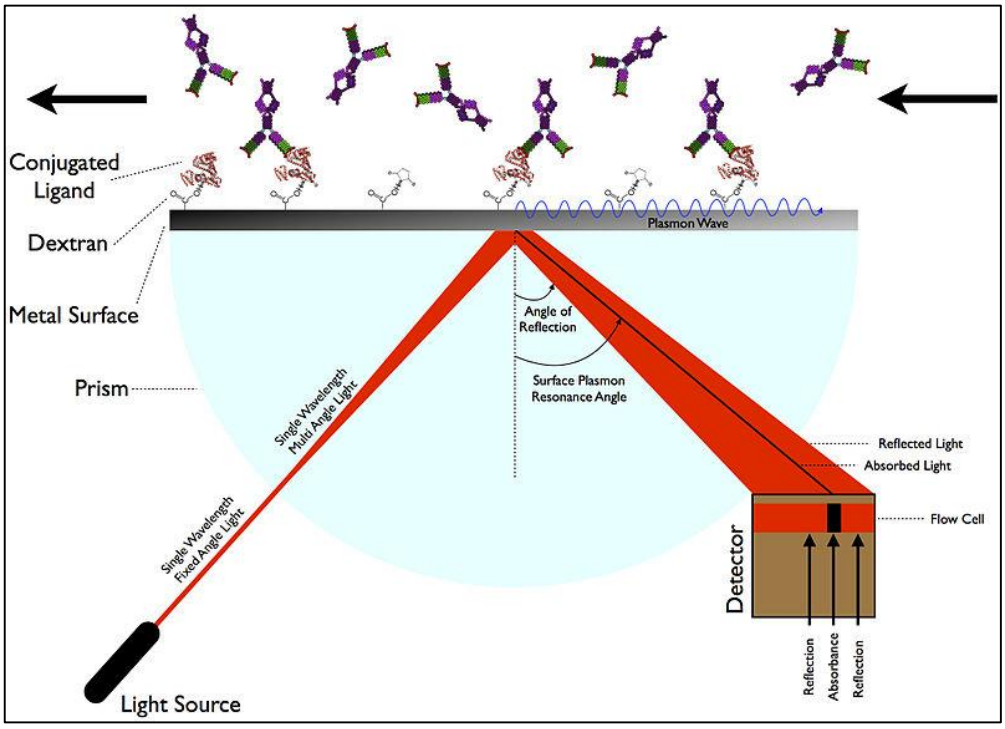

Figure 2.5| Illustration of the SPR principle. This figure illustrates that the surface is typically functionalised with probe molecules usually antibodies, antigens or nucleic acid strands. As being shown, when an incident beam of light of specified wavelength passes through a prism at a specific angle towards a thin metal film, it excites a propagating surface plasmon at the surface of the metal film. The SPR angle is distinctively dependent on the mass of particles deposited on the opposite side of the metal thin film surface. The only scenario that changes the SPR angle is when the complementary analytes bind to the probe-functionalised metal surface registering a change in the mass of the surface film.

Another factor that poses challenges is the microfluidic fabrication process due to the cost and complexity of embedding SPR sensors within the chip. SPR readings are also strongly affected by environmental conditions such as temperature and this ultimately has an impact on sensitivity of the method[94]. Another disadvantage is the gold and silver nanoparticles that have been largely applied; these precious metals are not sustainable for application in disposable point of care devices on grounds of cost and availability. **Table 2.6** summarises some of the work done through SPR detection in microfluidic devices.

Table 2.6|Summary of Devices Based on SPR Principle of Optical Detection.

Analyte of interest	Type of Assay	Biosensor Technology	Analysis Duration	Detection limit	Applicability at POC [a]	Ref.
Bovine Serum Albumin	Protein Adsorption	Infrared Camera	Real-Time	~12 pg/mm²	†	[92]
Human α-thrombin	Label-Free immunoassay	CCD Camera	Real-Time	~5 nM	††	[91]
Bacterial rRNA	Colorimetric Enzymatic Assay	CCD Camera	3 h	0.45 fM	†	[93]

[a] Potential applicability for point-of-care: † Low; ††Moderate; ††† High

2.4.2. Electrochemical Detection Based Devices

Detection using electrochemistry is a technology that relies on the interaction between chemical species with electric probes or electrodes[95]. This cross interaction culminates in generation of diverse signals that include potential, current, capacitance, inductance, conductance or impedance among others[96]. For the electrochemistry to occur and be measurable, charge or electron transfer (via reduction and oxidation reactions) has to occur through induction via the following major underlying principles[97]. (i) An electric current has to be passed through the analytical sample via an electrode system. (ii)The occurrence of a specific chemical reaction has to allow the electrode to register a response[66]. Electrochemical detection has numerous advantages that make it attractive for microfluidic applications. Electronics are very compatible with miniaturisation and this has inspired miniaturisation in various fields including fluidics. Electrochemical detectors usually have high sensitivity, low detection limits and are ideal detecting analytes usually embedded in complex matrices[97]. The commonly applied electroanalytical detection principles lie in categories of potentiometry, amperometry and conductometry or impedomerty[66].

2.4.2.1. Potentiometric Devices

Potentiometric biosensors measure the cell potential difference in an open circuit (at virtually zero current)[98]. The sensors produce a logarithmic concentration response allowing the measurement of extremely minute concentration changes with also a potential to do so in a continuous flow system. However, even with more refined ion selective field effect transistors (ISFETs) that can detect biological recognition events, potentiometry still has lower selectivity and higher detection limits in certain sample matrices[95]. Another set of drawbacks with this technology include facts that material immobilization techniques, packaging and fabrication are still very complex and expensive. Liao and colleagues have developed a potentiometry technique for detecting multiple biologically important ions using ion selective platinum microelectrodes. Their method was sensitive enough to obtain a limit of detection as

low as 10 µM[99]. Chou and team used a chemical species selective membrane sensor to potentiometrically detect glucose with a technique having a limit of detection of about 100 mg/dL[100]. **Table 2.7** (below) summarises some of the work on potentiometric detection in microfluidic devices.

Table 2.7 |Summary of Devices Based on Potentiometric Principle of Electrochemical Detection.

Analyte of interest	Type of Assay	Biosensor Technology	Analysis Duration	Detection limit	Applicability at POC [a]	Ref.
Multiple ions	Ion Selectivity	Platinum microelectrodes	–	10 uM	††	[99]
Glucose	Species Selectivity	Membrane Sensor	–	~100 mg/dL	†	[100]

[a] Potential applicability for point-of-care: † Low; ††Moderate; ††† High

2.4.2.2. Amperometric Devices

Amperometric biosensors measure the current linked to redox reaction(s) by an electrochemically active analyte at an interface of a working electrode relative to a reference electrode under conditions of constant potential difference[101]. In principle, there is a linear relationship between the analyte concentration and the registered current[102]. In instances where bio-molecular analytes do not a have a direct electron exchange relationship with the electrodes, redox intermediators that reversibly exchange electrons between the analyte and the electrode are employed[103]. The fact that most bio-molecular analytes do not have direct electron transfer relationships with electrodes poses limitations of this technology as very few redox reactions intermediators have been characterised. Gau and colleagues successfully harnessed a nucleic acid hybridisation assay coupled to an amperometric sensor to detect *E. coli* rRNA within 40min and with a limit of detection of about 1000 CFUs[104]. Using an immune-filtration assay and an amperometric sensor Abdel-Hamid and team were able to detect *E. coli* cells within 30 min at a limit of detection of about 100 cells/mL[105]. An ELISA based amperometric technique for Hepatitis B surface antigen detection at a detection limit of 0.005 µg/mL was also developed by Tang's team[106]. **Table 2.8** (below) summarises some of the work in which amperometric detection was applied in microfluidic devices.

Table 2.8 |Summary of Devices Based on Amperometric Principle of Electrochemical Detection.

Analyte of interest	Type of Assay	Biosensor Technology	Analysis Duration	Detection limit	Applicability at POC [a]	Ref.
E. coli rRNA	Hybridisation Assay	Amperometric sensor	40 min	~1000 CFUs	†	[104]
E. coli cells	Immunofiltration Assay	Amperometric sensor	30 min	~100 cells/mL	†	[105]
Hepatitis B (HBsAg)	ELISA	Amperometric sensor	–	0.005 µg/mL	†	[106]

[a] Potential applicability for point-of-care: † Low; ††Moderate; ††† High

2.4.2.3. Conductometric or Impedimetric Devices

Conductometric or impedimetric techniques measure the conductance or impedance of solutions that have ions (cations/anions) as charge carriers. Through AC electric field application between two electrodes, the conductometer/impedometer gathers the generated signals indicating changes in amplitude and/or phase angle. The amplitude signal is an indicator of serial resistance within the circuit under study. However, if DC electric field is applied, pure resistance signals are given and this property has been harnessed to make simpler instruments that are compatible with miniaturized microfluidic systems. The major demerit associated with conductometry in microfluidics is that if DC electric signal is applied through capillaries and microchannels, the potential difference is largely localised on the electric double layer on the electrode surface opposed to the analyte solution[107]. Bonanni and various teams have extensively applied gold nanoelectrodes for impedimetric genomic enterogation of various pathogens that include *Salmonella spp*, H1N1 swine flu virus and Cystic Fibrosis related DNA. **Table 2.9** (below) summarises some of the work that applied the principle of impedimetry in microfluidic devices [108-111].

Table 2.9 |Summary of Devices Based on Impedimetric Principle of Electrochemical Detection.

Analyte of interest	Type of Assay	Biosensor Technology	Analysis Duration	Detection limit	Applicability at POC [a]	Ref.
Salmonella spp	Double tagging PCR products	Impedimetric Sensor	–	–	†	[111]
DNA	DNA Hybridisation	Gold Nanoelectrodes	–	~3 µM	†	[109]
H1N1 virus DNA	DNA Probe Hybridisation	Nanoelectrode Sensor	–	577 pmol/L	†	[110]
Cystic Fibrosis Related DNA	DNA Hybridisation	Nanoelectrode Sensor	–	100 pM	†	[108]

[a] Potential applicability for point-of-care: † Low; ††Moderate; ††† High

2.4.3. Mechanical Detection Based Devices

Mechanical detectors comprise of mass sensitive sensors which rely on surface acoustic waves and effects first described in 1880 as piezoelectric[112]. The phenomenon of piezoelectricity is the ability of some crystalline and ceramic materials to generate an electric potential when subjected to stress. Physics laws dictate that rigid solid objects inherently resonate at certain frequencies and these frequencies can be shifted by incorporating an additional mass. Through some mathematical manipulation of this frequency one can determine the linked change in mass[113].

2.4.3.1. Quartz Crystal Microbalance (QCM) Based Devices

This instrument operates on a piezoelectric quartz crystal that can be manipulated to vibrate at elevated frequencies by an influence of an electric current thereby allowing for frequency based determination of biomolecular masses. The QCM can be easily converted into a biosensor by immobilizing a receptor on the quartz crystal surface. The subsequent binding/hybridization of the ligand molecule will register a change in the frequency of resonation[113]. An example of QCM application is where DNA hybridization processes have been studied with enough selectivity that discriminated complimentary and non-complimentary DNA strands using capture probe DNA immobilised on quartz crystal. This has been applied for end point detection and analysis of PCR products[114, 115]. Although a few researchers have reported success in the detection of multiplexed reactions, complexity of multiplexing still remains a major challenge with QCM popularity. However, the main drawback of the technique is that dry conditions are still a necessity with this technique; this implies that after receptor-ligand hybridisation, accurate measurements are still dependent on drying the QCM since liquid media cause a significant vibrational damping. Most bioanalytical approaches depend on liquid phase analysis therefore this renders the QCM applicable to limited cases[116]. Uludag and Tothill described their development of a point-of-care immuno-sensor that detects a cancer biomarker (total prostate-specific antigen, tPSA) using a quartz crystal microbalance (QCM) sensor platform in human serum samples. They performed a sandwich assay using antibody-modified gold nanoparticles [117]. García-Martinez and team used a 50 MHz quartz crystal microbalance (QCM) to detect DNA target concentrations higher than 50 ng/mL with resolution of 7.1 ng/cm^2 [118]. Xia and team developed a rapid piezoelectric quartz crystal microbalance (QCM) based nucleic acid biosensor using gold nanoparticles for detecting *S. epidermidis* in clinical specimens [119]. **Table 2.10** (below) summarises some of the microfluidic work in which quartz crystal microbalance (CQM) detection was applied.

Table 2.10 |Summary of Devices Based on Quartz Crystal Microbalance (CQM) Principle of Mechanical Detection.

Analyte of interest	Type of Assay	Biosensor Technology	Analysis Duration	Detection limit	Applicability at POC [a]	Ref.
Prostate Cancer Antigen	Sandwich Immunoassay	QCM Sensor	–	–	††	[117]
DNA	DNA Hybridisation	QCM Sensor	–	~50 ng/mL	†	[118]
Staphylococcus epidermidis	PCR Product Hybridisation	QCM Sensor	–	1.3×10^3 CFU/mL	†	[119]

[a] Potential applicability for point-of-care: † Low; ††Moderate; ††† High

2.4.3.2. Cantilever-Based Detection Based Devices

These systems have a miniaturised cantilever and are better alternatives to QCMs. These cantilevers that are usually made from ceramics or crystalline materials, rely on piezoelectric principles. The

measurements are derived from monitoring the deflection of a laser beam away from the tip of the cantilever. The readings are similar to QCM because they are translated from resonant frequency shifts as a result of ligand binding to the immobilized receptors. Literature suggests that this method has been used to sensitively detect single-base DNA mismatches and differentiating complementary and non-complementary DNA sequences[120]. The major drawback of the cantilever approach is its reliance on expensive laser systems for signal detection. Zhou and team reported the piezoresistive detection of p53 antibody, a biomarker for early-stage cancer diagnosis using a microcantilever biosensor with a 20 ng/ml limit of detection. In their work, they performed an on-surface immobilization of the probe to detect p53 antibody and measured the deflection of the microcantilever using integrated piezoresistors [121]. Hansen and team demonstrated the discrimination of DNA mismatches using a microcantilever-based optical deflection assay, without the need for external labelling. This work holds potential to characterize single-nucleotide polymorphisms (SNPs) which have become a major current focus in genomic research [122]. **Table 2.11** (below) summarises some of the work in which the microcantilever detection principle was applied in microfluidics.

Table 2.11 |Summary of Devices Based on Microcantilever Principle of Mechanical Detection.

Analyte of interest	Type of Assay	Biosensor Technology	Analysis Duration	Detection limit	Applicability at POC [a]	Ref.
p53 Cancer Antibody	Recognition Immunoassay	Microcantilever Bioensor	–	20 ng/ml	†	[121]
DNA SNPs	Probe-DNA Hybridisation	Microcantilever Biosensor	–	–	†	[122]

[a] Potential applicability for point-of-care: † Low; ††Moderate; ††† High

2.4.4. Thermal Detection Based Devices

From a thermodynamics standpoint, thermal methods detect characteristics of materials or chemical reactions by measuring the internal energy present in any state of the system's thermodynamic equilibrium by virtue of its temperature. The combination of thermal measurement techniques and microfluidic systems has allowed the feasibility of capturing different bioanalytical measurements with efficiency because of the associated low reagent consumption, high heating efficiency as well as minimized measurement time. Thermal measurement approaches can be categorised into thermal particle detection and calorimetry[123, 124].

2.4.4.1. Thermal Particle Detection (TPD) Based Devices

This technology uses heat transfer to detect and count particles in relation to their size. Thermal particle detection has attracted a considerable attention from researchers in microfluidics as they seek to find

detection applications for industrial, environmental and biological analysis [125]. TPD in contrast to most methods, complex optical, complex electrical set ups as well as complicated signal mathematical manipulation are minimised. The major limitation of this method is that it requires excessive insulation which might turn costly [124]. Vutha and colleagues recently demonstrated their employment of heat to quantify microscopic particles using a thermal particle detector (TPD). They were able to resolve particles with diameters of 90 and 200 µm as having relative temperature changes of 0.11 and-0.44 K, respectively, in their continuous flow sensor [126].

2.4.4.2. Micro-Calorimeter Inspired Thermal Characterisation Based Devices

This approach harnesses thermal conductivity and specific heat measurements to characterise materials using an on-chip calorimetric device. Some of the advantages of doing calorimetry at microscale in contrast to macroscale are that, reagent consumption is greatly reduced and automation results in increased precision and repeatability. Esfandyarpour and Davis developed an on-chip- integrated microfluidic calorimeter coupled to an on-chip sequential injector and multiplexing module. This device characterizes heat of reaction with 2-nW resolution strength in the nanoliter realm. These researchers were able to do real-time on-chip DNA "thermosequencing"[127]. **Table 2.12** (below) summarises some of the work on thermal detection based microfluidic devices.

Table 2.12 |Summary of Devices Based on Thermal Particle Detection (TPD) and Micro-Calorimeter Principles of Mechanical Detection.

Analyte of interest	Type of Assay	Biosensor Technology	Analysis Duration	Detection limit	Applicability at POC [a]	Ref.
Microscopic Particles	Resistive Change in Temperature	Thermal Paticle Detector	–	–	†	[126]
DNA SNPs	Thermosequensing	Micro-Calorimetry	–	2 nW RMS	†	[127]

[a] Potential applicability for point-of-care: † Low; ††Moderate; ††† High

2.5. Knowledge Gaps

Our literature findings in previous sections suggest that conventional TB diagnosis continues to rely on tests such as smear microscopy and culture methods despite them having known limitations. Efforts to develop tests for detection of drug resistance has yielded alternatives that are slow, costly, tedious and difficult to apply in field conditions. However, with recent advances in detection methods and emerging biosensor technologies, the diagnosis of active TB disease, and detection of drug resistance can be soon realised. We hereby propose new diagnostic tools that include newer versions of nucleic acid amplification tests for detection TB drug resistance conferring mutations. Although an ideal test for TB has not yet been created, considerable progress has been made over the past decade. This captured our interest in the development of a new tool for TB control with tangible benefits enabling it to reach the populations in developing countries that need cheaper diagnostic services the most.

Heterogeneity in TB lesions is also not well understood because of the limitations (stated in previous section) with current diagnostic tools. Lenaerts and her research team attributed the heterogeneity in TB to its lesions being complex and extremely dynamic microenvironments. Their research further suggests that the immunopathological diversity of cavities and granulomas creates a plethora of microenvironments that force *M. tuberculosis* bacilli to adapt. This ultimately affects processes such as metabolism, DNA replication and relatively the density of microbial subpopulation. All these factors subsequently lead to respective susceptibility or resistance to chemotherapeutic agents[128]. Therefore an ideal TB diagnostic tool must be able to detect heteroresistance from the onset.

CHAPTER 3

3. Microfabricated Devices for Detecting Mutants Using PCR & HRMA

3.1. Research Aims and Objectives

3.1.1. Research Aims

To harness to our advantage, the underlying principles of microfluidics through developing a cost effective, highly scalable platform—for fluorescence based genomic interrogation of *Mycobacterium tuberculosis* clinical isolates using real-time PCR and HRMA.

3.1.2. Research Objectives

1. To build a highly scalable, affordable, label-free-automated-microfluidic, fluorescence-based; real-time nucleic acid amplification and high resolution melt analysis (HRMA) system.
2. To demonstrate as a proof of principle, its potential to detect tuberculosis and rifampicin resistance based on DNA melting temperature (T_m) with high accuracy, specificity and sensitivity
3. To demonstrate as a proof of principle; the system's potential to do single copy nucleic acid amplification (Digital PCR); and subsequent HRMA for application in the detection of heteroresistance and heterogeneity in clinical samples based on DNA melting temperature (T_m) with high accuracy, specificity and sensitivity.
4. To design (in AutoCAD); fabricate (photolithography and soft lithography); and optimise PCR microfluidic devices.
5. To write a Matlab program with a code that automatically computes meaningful conclusions from the raw real-time PCR amplification and high resolution melt analysis data from the system.

3.2. Materials and Methods

3.2.1. Consumables

Table 3.1|Lithography Consumables

Consumables	Vendor/Reference Number
3 – 4" Silicon wafers (Type P), 500µm thick	WaferShipper
5x5" glass plate(s) for UV exposure	--
Acetone	Sigma-Aldrich, St Louis, MO 63103, U.S.A
Aluminium foil	SAPPHIRE
Compressed Air Gun	--
HMDS (hexamethyldisilzane)	Micro Chemicals, St Louis, MO 63103, U.S.A
ma-D 531 Developer	Microresist technologies, Berlin, Germany
MAP 1275 Photoresist	Microresist technologies, Berlin, Germany
PDMS GE 615 RTV (Part A)	Momentive, Waterford, New York 12188, U.S.A
PDMS GE 615 RTV (Part B)	Momentive, Waterford, New York 12188, U.S.A
Petri Dishes	Falcon
Photomasks	Outputcity (CAD/Art Services, Inc. 541-347-5315
Polyester Nanowoven Wipes	Amplitude Delta, Spartanburg, SC 29303, U.S.A
SU-8 Developer	Micro·Chem Corp, Newton, MA 02464, U.S.A
SU-8 Photoresists	Micro·Chem Corp, Newton, MA 02464, U.S.A
TCMS	Sigma-Aldrich, St Louis, MO 63103, U.S.A
Tygon® Tubing	AAD02103-CP
Wafer Tweezers	ETNEO

3.2.2. Equipment

Table 3.2|Equipment

Equipment	Vendor/Reference number
Contact Mask Aligner	SÚSS MicroTech MJB4
Flatbed Thermocycler	G-Storm GS-1, Somerset TA117JH, UK
Hard Baking Oven	Thermoscientific
Hot Plates	Torrey Pines Scientific Inc, Carlsbad, U.S.A.
Luca R EMCCD Camera	Andor
Microfluidic Chip/Mold Inspection Microscope	Olympus BX51, Tokyo, Japan
Mold Profilometer	KLA Tncor D-120, Milpitas, California 95035 U.S.A.
Olympus Alignment Light Source	KL 1600 LED, Tokyo, Japan
Olympus Alignment Light Source	KL 1500 LCD, Tokyo, Japan
PDMS Curing Oven	Binder, USA
PDMS Layer Alignment Microscope	Olympus SZX16, Tokyo, Japan
PDMS Mixer	THINKY Corporation Japan, Model ARE-250
PDMS punch Press	SCHMIDT Technology Corp, Cranberry, Germany.
Pull Vacuum Bell Jar	Bell-Art Products 1-800-4BEL-ART

Rocker	IKA ROCHER 3D digital
Spin Coater	Laurell Tech Corp (WS-650MZ-23NPP), North Wales
Spin rinse dryer	Laurell Tech Corp (WS-650MZ-23NPP), North Wales
Stereo Macroscope	Olympus MVX10, Tokyo, Japan
Temperature Sensing Probe NI USB-TC01	National Instruments, U.S.A.
Timers	Capital Lab Supplies, Durban, South Africa
UV Source	X-cite 120PC, New York, U.S.A
Weighing Balance	ADAM Equipment, AE75706064

3.2.3. Software

Table 3.3|Software

Software	**Providing Company**
AutoCAD 2013	Autodesk
GraphPad Prism Version 6.03	GraphPad
LabVIEW Student Version 2011(M7X44797)	National Instruments
MATLAB Student Version R2012a (7.14.079)	MathWorks

3.2.4. PCR and HRMA Reagents

Table 3.4 | Reagents for RealTime PCR and HRMA Assays

Reagent	**Supplier**
Buffer	Novagen®, Merk
dNTPs	Novagen®, Merk
LC Green Plus+	BioFire Diagnostics, Inc Salt Lake City, Utah U.S.A
F Primer	Inqaba Biotech, Pretoria, South Africa
R Primer	Inqaba Biotech, Pretoria, South Africa
KOD Polymerase Extreme Hot Start DNA Polymerase	Novagen®, MerK
1% Tween 20	Sigma-Aldrich, St Louis, MO 63103, U.S.A
PCR Grade Water	Novagen®, MerK

3.2.5. Characteristics of used clinical isolates

Table 3.5 |Characteristics of the Clinical Isolates Used for Comparison with H37RV[e]

	DR-Mutation(s) detected by Sanger Sequencing	*Mutation Class*	*Phenotype[f]*		
Isolates	***rpoB***		**RIF**	**INH**	**OFLX**
R 35	CTG → C**C**G (L533P)	1	Resistant	Resistant	Susceptible[g]
KZN 605	GAC → G**G**C (D516G)	1	Resistant	Resistant	Resistant[h]
	CTG → C**C**G (L533P)	1			
Tkk-01-062	GAC → G**T**C D516V	4	Resistant	Resistant	Susceptible[i]

[e] This sequencing data was jointly obtained with Ian Mbano from Inqaba Biotech
[f] The phenotypes were determined by Dr Adrie Steyn's and Dr Manormoney Pillay's research groups
[g] The phenotypes were determined by Dr Manormoney Pillay's research group
[h] The phenotypes were determined by Dr Manormoney Pillay's research group
[i] The phenotypes were determined by Dr Adrie Steyn's research group

3.3. Methods

3.3.1. AutoCAD photomask Design

Microfluidic-Bioengineering is a science at the intersection of biology and engineering, therefore its design procedures are heavily borrowed from techniques that are routinely used in engineering and architecture. The photomasks for microfluidic devices' fabrication were designed using the Autodesk AutoCAD software. This software is based on a hybridisation principle of command-line and 2D visual designing platforms. The designing process largely relied on the Stanford Microfluidic Foundry online guidelines (http://web.stanford.edu/group/foundry) that included:

- Initiation to AutoCAD
- Microfluidic chips basic designing rules
- Rules for photomask designing
- Basic Hitchhiker's guide to AutoCAD[129].

3.3.2. AutoCAD Design Fundamentals

Using the above-mentioned AutoCAD guidelines, the microfluidic device photomasks were designed with line based drawing tools that included lines, splines and polylines. However, for the purpose of conversion of the AutoCAD files (.dwg) into the format that is readable to a mask printer can read (.dxf), it was ensured that no open line segmentation existed in the drawings by employing the polyline tool. **Figure 3.1** shows some illustration of how Jerome Rogich designed the Spider PCR microfluidic chip using the AutoCAD software.

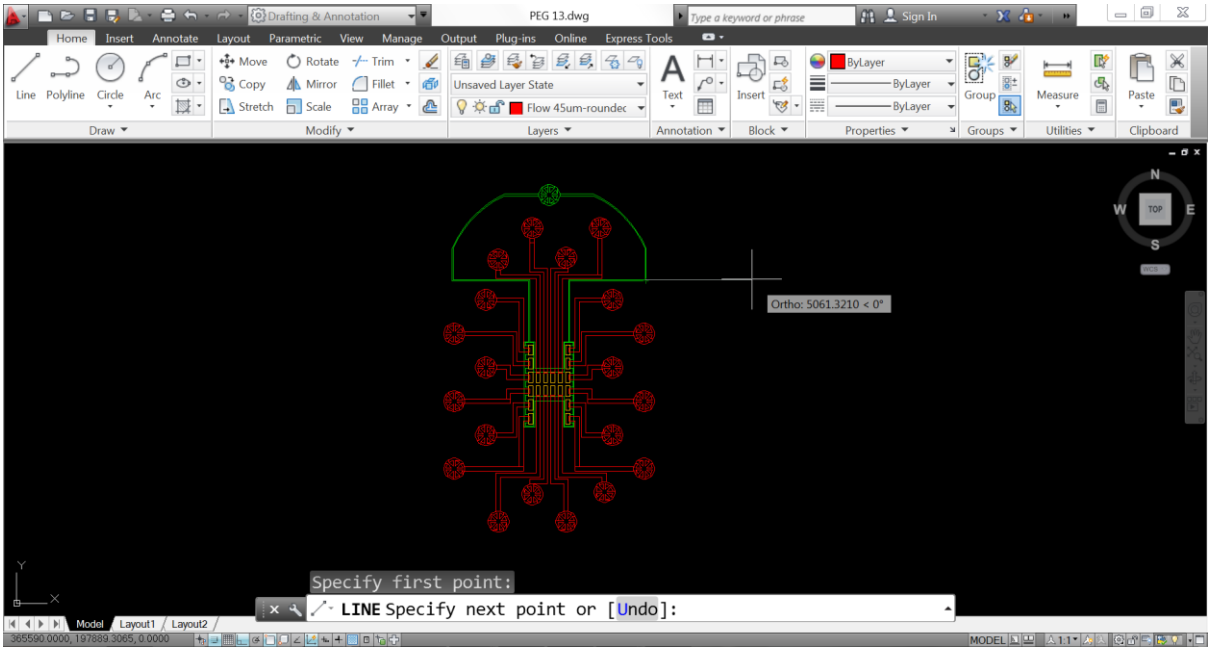

Figure 3.1 AutoCAD design illustration of the Jerome Rogich spider design microfluidic chip. AutoCAD allowed the design of microfluidic devices' photomasks. We employed line based drawing tools that included lines, splines and polylines shown on the window toolbar. However, for the purpose of conversion of the AutoCAD files (.dwg) into the format that is readable to a mask printer can read (.dxf), it was ensured that no open line segmentation existed in the drawings by employing the polyline tool on a complete design.

3.3.3. Patterning and Layering

Microfluidic designs consisted of some networked features that were repeat units, hence for maintaining precision and uniformity among similar features the "Array" tool was employed. These photomasks are characterised with regions of dark and light polarity. The "layering" tool was used to distinguish the regions of the mask that corresponded to the dark and light polarity on the AutoCAD design.

3.3.4. Considering Dimensions

3.3.4.1. Aspect Ratios and Feature Resolution Optimisation

In pursuit of firm and stable microfluidic features, the general principle that most stable features adhere to staying within the bounds of a minimum aspect ratio 1:10 (height:width) and a maximum aspect ratio of 5:1 was followed. This implied that on requiring the PCR chambers to have a height of 200 µm while retaining their stability/firmness without supporting features, the minimum and maximum width for the

flow photomask design was to be 20 µm and 1000 µm respectively. The **Figure 3.2** (below) illustrates how the aspect ratios were put into account for feature resolution in the designs.

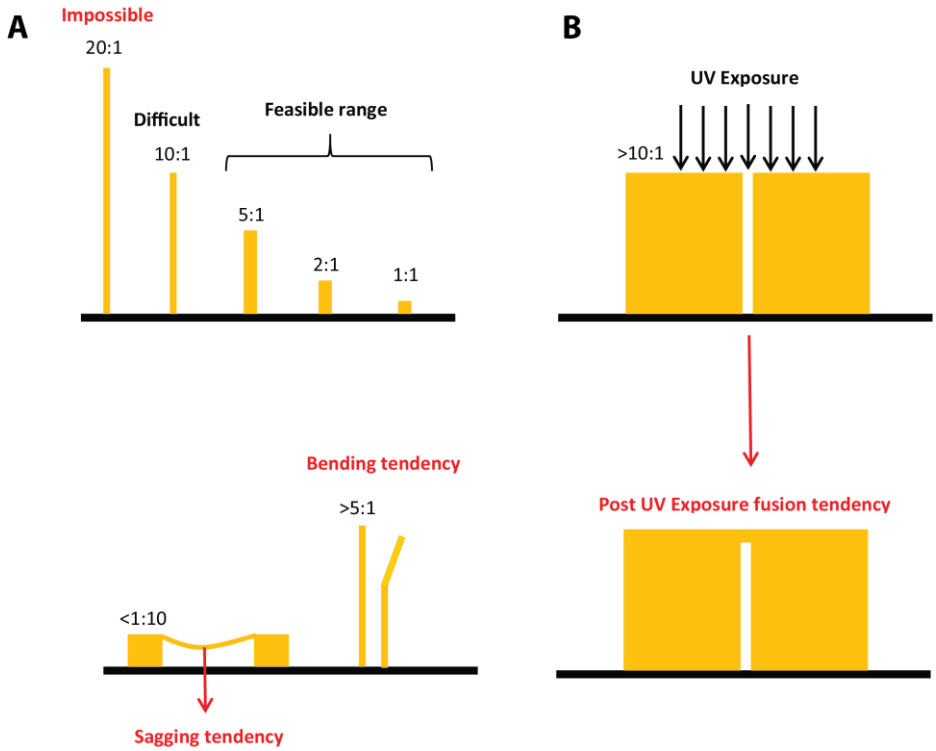

Figure 3.2| Illustration of the putting into account of aspect ratios. (**A**) Examples of levels of difficulty associated with fabricating features of various aspect ratios with photolithography and soft lithography. Ideal aspect ratios are $1{:}10 < x < 5{:}1$ (**B**) Illustration that aspect ratios are also crucial in gap features. Considerations were made in the photomask design such that the distance that resulted between SU-8 features was not too small, by this, avoidance of fusion at unintended locations due to UV diffraction during exposure and curing processes was ensured.

The design of inlet and output ports was done in a manner allowing fluids from a source into the device. Dimensional consideration of hollow stainless steel pins and Tygon® tubing to be employed were taken into account in relation to the size of the corresponding ports.

Completed photomask designs were shipped to Outputcity (CAD/Art Services, Inc. 541-347-5315 www.outputcity.com) for printing on flexible, inexpensive plastic films that generally guarantee feature resolution ranging between 5 and 10 µm. Before each photomask print a digital PDF format proof of each pattern was provided by Outputcity for re-inspection of design features ensuring all lines were polylines, no line gaps and no stray construction lines. The final photomask transparencies consisted of dark regions that corresponded to the "opaque" regions.

3.4. Microfabrication Process

At this stage the guidelines for microfluidic device master fabrication using photo lithography were used. The determination of each feature's desired height through optimising the parameters that included pre-baking time, post-baking time, exposure time, spin coating speed, choice of photoresist viscosity and developing time was done. Recommendations for some specifications on commonly used feature heights were sourced from MicroChem (website| http://www.microchem.com/) and in some instances when the desired height was not available among the recommendations, adjustments were made to the spin coating speed/acceleration, exposure time and photoresist choice.

3.4.1. Mold Fabrication:

3.4.1.1. Flow Mold

The 3' or 4' wafers had their surface first primed with HDMS (adhesion promoter) vapour for 1 min in a plastic container at standard room temperature and pressure (STP). The wafer was then placed and held by vacuum power on a Laurell technologies corporation (model WS-650MZ-23NPP) spin coater stage. After dispensing the photoresist of desired viscosity, the wafer was spun at a specified (rpm) speed and acceleration for a specified time that ensured desired photoresist film thicknesses. Soft contact baking on a hotplate at specified temperature and duration followed. Soon after soft bake, it was ensured that the photoresist was fully dry. The wafer were UV-exposed by a mask alignerfor a specified duration with a photomask in contact with it from the top to ensure photoresist curing in a manner defining the channel structures. The wafer was then developed in developing solution, rinsed with deionised H_2O and dried under house clean dry air. A hard baking step involving placing the mold in the oven and ramping the temperature from 120 °C to 180 °C, then held for 1 hr after which the oven was reversely ramped from 180 °C to 120 °C followed. This completed the first layer of the mold. However, in instances where the flow mold required was a hybrid, then a second layer of photoresist of desired viscosity was spun at a specified (rpm) speed and acceleration for a specified time in relation to the envisioned photoresist film thickness. Pre-exposure contact baking was performed using a hotplate at specified durations and temperatures (5 min x 65 °C / 20 min x 95 °C). The wafer was exposed to UV after the alignment of the mask of the subsequent top layer. This alignment was done in correspondence to the bottom layer with the aid of design alignment marks and a contact mask aligner (SÚSS MicroTech MJB4). The desired microwells were defined by the curing of UV-exposed regions of the mold. The exposed mold was subjected to post-exposure baking (1 min x 65 °C / 12 min x 95 °C / 1 min x 65 °C) and cooled to room temperature. For the fabrication of rounded channelled masters, the photoresist coated wafers were left at room temperature overnight and then baked by contact on a hotplate at 115

°C for 15 min. The final development was done in a developing solution for 5 min and rinsed with fresh developer solution and dried under house clean dry air. (See **Appendices A** for each mold design specifics)

3.4.1.2. Control Mold Fabrication

For all control molds, the wafer was placed and held by vacuum power on a spin coater (Laurell Tech Corp (WS-650MZ-23NPP), North Wales) stage. After SU8 2025 photoresist was dispensed, the wafer was spun at 3000 rpm for 1 min using an acceleration of 133 rpm^{-2} to attain film thicknesses of 25 microns on average. Pre-exposure contact baking followed using a hotplate (1 min at 65 °C / 5 min at 95 °C) and the wafer was then cooled to room temperature. The wafer was then exposed to UV-light through the control photomask for 15s to define control structures. Post-exposure bake (1 min at 65 °C / 5 min at 95 °C) followed. The wafers were then cooled to room temperature after which they were developed using developer solution for 5 minutes, rinsed with fresh developer solution and dried under house clean dry air. Final hard bake was carried out by contact hotplate (150 °C x 60 min). (See **Appendices A** for each mold design specifics).

3.4.2. Soft Lithography Process

All molds that resulted from above sections were subjected to trimethylchlorosilane (TMCS) vapor for 1 min in a plastic container at STP.

3.4.2.1. Flow Layer

For flow layer casting, the combination in 5:1 GE 615 RTV (A: B) of total amount in relation to the desired flow layer thickness was done. A hybrid mixer (THINKY Corporation Japan, Model ARE-250) was used for mixing with 5 min mixing time and 5 min degassing time. An amount of the mix in proportion to the desired thickness of the flow layer was poured onto the flow mold (petri dish lined with Aluminium foil). The flow layer was degassed via pull vacuum in bell jar (Bell-Art Products 1-800-4BEL-ART) --for approximately 30 minutes) and the residual bubbles were manually popped with an L-shaped spreader. The curing step of the flow layer was done by baking the wafer in a convection oven set at 80 °C for 40 min.

3.4.2.2. Control Layer:

The combined in 20:1 GE 615 RTV (40 g A: 2 g B) was mixed using a hybrid mixer set at 5 min mixing time and 5 min degassing time. A portion of 5 mL of the mixture was then dispensed on the control layer mold and spun it at 1800 rpm for 60 s at an acceleration of 500 rpm^{-2} to generate a film thickness of 25 microns. Curing of the control layer was done by baking in convection oven set at 80 °C for 40 min.

3.4.2.3. Dummy Layers:

The remaining 5 mL of 20:1 GE 615 RTV (40 g A: 2 g B) mix was spun (using a spin coater Laurell Tech Corp (WS-650MZ-23NPP), North Wales) on a blank wafer at 1800 rpm for 60 s at an acceleration of 500 rpm^{-2} generating a film thickness of 25 microns. Curing of the dummy layer was done by baking in convection oven set at 80 °C for 40 min.

3.4.2.4. Control/Flow Bonding

The flow layer was peeled off from the mold and the flow inlet and outlet ports were punched with a punch press. Thereafter, the punched flow layer was aligned (using Olumpus SZX16, Tokyo, Japan) to the control layer (still on the mold). The baking of the resulting hybrid was done in a convection oven at 80 °C for 40 min. After allowing the bonded hybrid device to cool to room temperature, cutting around the periphery of the thick layer and peeling of the hybrid device off the control layer mold as well as punching control inlet ports was done.

3.4.2.5. Flow/Control/Dummy Bonding

Finally, the control/flow hybrid structure was placed on the dummy layer bound to a blank wafer and it was ensured that there were no air bubbles and no collapsed valves/ control channels. The resulting device was baked in a convection oven (Binder, USA) at 80 °C for 8 hours. The final quality control of the device was done though inspection for air bubbles, linen, collapsed channels etc. This was done under a microscope (Olympus BX51, Tokyo, Japan) and became ready for use.

* Spin parameters needed to be optimized for each batch. (See **Appendix A**)

3.4.3. The LightForge System Set-Up

The Real-Time PCR and High Resolution Melt Analysis (HRMA) were done on a system that we developed in-house called The LightForge System which has the potential of bringing a new era to lab on a chip technologies. LightForge driver is built on a LabView (from National Instruments, USA) program that runs on a temperature feedback loop. **Figure 3.3** shows a schematic flow illustration of how the LightForge system operates. A microfluidic chip is installed with its base in contact with the flatbed of the thermocycler—(G-Storm GS-1, Somerset TA117JH, UK). A temperature sensing probe—National Instruments was also installed at the base of the microfluidic chip wired to a computer. PCR master mixes are pressure driven at 5 psi into the reactor chambers via Tygon® tubing. Each chamber is sealed via on-chip elastomeric control line valve closures as instructed by the LightForge computer program throughout the duration of PCR and HRMA. At each low temperature PCR cycle step, the computer program instructs the shutter mounted on the Olympus MVX10 stereo macroscope to open. This allows the chip to be excited by the UV light(x-cite) and simultaneously instructing the Luca R EMCCD Andor camera to take real-time images. The MATLAB script embedded into the LightForge (LabVIEW) program at the same time proportionally computes the pixels on each image in relation to the fluorescence signal. This is because as the PCR products accumulate, the relative fluorescence units also increase in a typical PCR sigmoidal fashion.

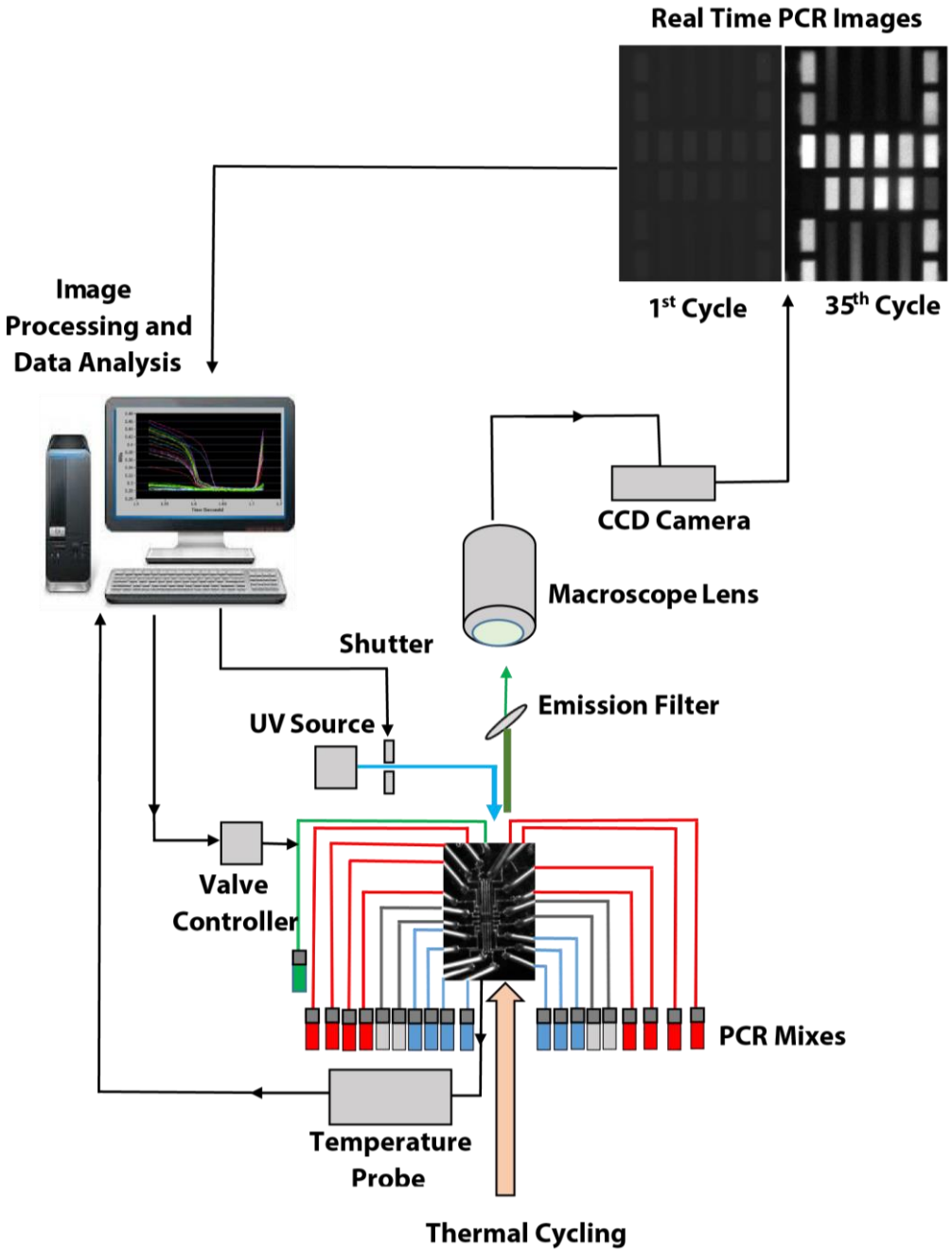

Figure 3.3| Schematic illustration of how The LightForge system works. The scheme shows the experimental setup used in this work. Individual reaction chambers of the chip are loaded with PCR specified PCR master mixes; microvials in red are replicates of the clinical isolate under study; microvials in blue are replicates of the reference H37RV standard; microvials in gray are the non-template control replicates; in green is the control line controlling opening and closure of valves on the chip with instructions from the LightForge computer program. The chip is connected to the temperature probe that send feedback to the LightForge computer program. This temperature feedback instructs the shutter to open at desired temperature allowing the CCD camera to capture a fluorescent image via a stereo macroscope. Images after every cycle are captured in real-time and the real-time PCR and HRMA data displayed on the computer screen after automated Matlab image processing.[i]

3.4.3.1. Matlab Image Processing

The LightForge System captures Real-Time PCR and High Resolution Melting images and processes them by generating arrays of pixel values that are proportional to the fluorescence brightness of the reactors. We then used a Student Version MATLAB®2012a software from MathWorks® (See **Appendix C** for the developed code) to translate this enormous pixel data into curves deducing the Real-Time PCR Amplification curves (Relative Fluorescence Units (RFUs) vs PCR Cycle Number), High Resolution Melt Analysis curves (Relative Fluorescence Units (RFUs) vs Temperature), 1st Derivative Melt Peaks ((–dRFUs/dt) vs Temperature).

3.4.3.2. Polymerase Chain Reaction (PCR) and High Resolution Melt Analysis (HRMA) Primer Design

As shown in **Table 3.6** (below)[130], we designed two pairs of primers for real-time PCR to amplify the *rpoB* and *gyrA* (positive control), specifically targeting sites at which mutations associated with drug resistance are found, namely, for *rpoB*, the 81-bp RIF resistance determining region (RRDR); and for *gyrA*, a region including several resistance-associated sites (OFLX resistance).

Table 3.6| PCR and HRMA Primer Design

Primer	Sequence 5'-3'	Amplicon Size (bp)	Anealing Temp (°C)	Nucleotide Locations	GenBank accession no.
rpoB-F rpoB-R	CGCGATCAAGGAGTTCTTC TGACAGACCGCCGGGCCC	118	65	2339-2357 2456-2439	L27989.1
gyrA-F gyrA-R	GGTGCTCTATGCAATGTTCG GCTTCGGTGTACCTCATCG	234	63	2467- 24861 2700-2682	L27512.1

3.4.3.3. DNA Extraction

Genomic DNA from *M. tuberculosis*- H37RV (reference susceptible lab strain) and clinical isolates of KZN 605, R35 and R271was extracted and provided by research groups of Drs Adrie Steyn and Manormoney Pillay from KwaZulu Natal Research institute for TB and HIV(K|RITH) and University of KwaZulu Natal(UKZN) respectively.

3.4.3.4. Polymerase Chain Reaction (PCR) and High Resolution Melt Analysis (HRMA)

The (On-Chip) bulk PCR mixture was prepared and optimised in relation to the (Off- Chip) commercial Roche LightCycler® 96 system requirements as shown in the **Table 3.7**.

Table 3.7| Used Optimised on-Chip PCR Master Mix Derived from off-Chip Master Mix

Component	On- Chip Master Mix		Off-Chip Master Mix	
	Volume	Activity	Volume	Activity
Buffer	37.5	0.5	25	0.5
dNTPs	15	0.2	10	0.2
LC Green	7.5	0.1	5	0.1
F Primer	2.25	0.03	1.5	0.03
R Primer	2.25	0.03	1.5	0.03
KOD Polymerase	1.5	0.02	1	0.02
1% Tween 20	6	0.06	_	_
PCR Grade Water	_	_	1	0.02
Total Volume	75	1	50	1

*~ 50 ng of DNA template

PCR amplification was performed using the G-Storm GS1 flatbed thermal cycler (Somerset TA117JH, UK), with optimised initial denaturation at 97°C for 8 min, followed by 35 cycles of 98°C for 60 s, 60°C for 115 s, and 74.5°C for 130 s and a final elongation at 72°C for 10 min. A non-template control containing sterile distilled water was included in the experiment.

For HRMA, we melted the PCR products from 75 to 95 °C with fluorescence data acquisition being carried out at regular increments—at 0.25 °C/step at a rate of 0.5 °C/sec—with specified holds at each step. The HRMA curves were analyzed using Student Version MATLAB®2012a software from MathWorks®. The melting temperatures of replicated clinical isolates' plots were generated and compared to the wild-type (rifampicin susceptible H37RV) melting profile after normalizing the melting profiles of both the examined clinical isolates and the wild-type.

CHAPTER 4

4. Results

4.0. Temperature Conduction Optimisation

Since PDMS is a poor conductor of heat, inorder for PCR to work on a chip, it is important for the PDMS microdevice to be placed on a base that has the ability to rapidly gain and rapidly lose heat. This facilitates the heating and cooling essential for PCR thermal cycling efficiency.

4.0.1. Glass Substrate Base

We conducted an experimental iteration to investigate the effect of attaching a glass base to the PDMS microfluidic device on a flatbed thermal cycler. This setup revealed that although glass is a cheaper material to work with in disposable POC devices, its thermal properties did not allow efficient heat transfer. The poor conducting nature of glass resulted in the 3 stage PCR reactions requiring longer time frames at each stage to allow the chip to attain the required temperature.

4.0.2. Thinner Glass Substrate Base

We hypothesised that the inefficient heating—from the iteration above—was probably as a result of the glass slide base being too thick, therefore we reduced the thickness of the glass and employed a thinner glass cover slip base. Despite improvement in the heating efficiency, the PCR duration was still very long and the cover slip proved to be delicate and largely affecting our yield of chips.

4.0.3. Thermal Grease

We then reached the hypothesis that the inefficient heating was probably as a result of lack of close contact between the glass bases and the flatbed of the thermal cycler. To test this hypothesis, we smeared a thin film of silicone heat transfer compound (Unick Chemical Corp) between the flatbed of the thermal cycler and the chip glass base. The heating efficiency improved slightly. However, the grease being a lubricant, it resulted in the lateral movement of the chip such that the regions of interest on the chip were out of their initial positions within a couple of PCR cycles. Therefore we concluded the use of thermal grease to be unfavourable.

4.0.4. Polysilicon Substrate Base

We then performed the final iteration of employing a silicon substrate as a base of the PDMS microfluidic device. As shown in **Figure 4.1**, the experimental results reveal that the LightForge temperature log profile from a polysilicon substrate base provided the most improved heating efficiency.

Figure 4.1A shows how the LightForge system can complete the entire real-time PCR coupled to HRMA within 3 ½ hrs. We can also see the high degree of reproducibility of temperature profile from one cycle to the other. Silicon being a semiconductor demonstrated a strong ability to gain and lose heat in a manner sufficient for reasonably long PCR experiments. Hence the use of a polysilicon substrate base fulfilled our need of achieving the desired heating and cooling conditions for PCR cycles.

4.0.5. General Description of the LightForge System's Temperature Kinetics.

We optimised our temperature measurement by a contact temperature sensor method to get an initial understanding of PCR kinetics in our microfluidic system. As can be seen on **Figure 4.1**, there is a hot start activation step that is about 10 mins long—this duration was seen to be long enough to dissociate the anti-*thermococcus kodakaraenis*—KOD-- DNA polymerase antibodies and/or accessory proteins that keep the polymerase inactive at lower pre-PCR temperatures. Depicted also by **Figure 4.1** also, are the defined periodical repetitions of three different temperature zones—melting, annealing and extension zones.

a. *DNA melting temperature zone*: this was the highest temperature attained in each periodic PCR cycle. This can be seen in **Figure 4.1**(**B**) to be just below 95 °C on average on this LightForge platform—congruous to the acceptable temperature range for DNA denaturation that is between 90 and 95 °C.
b. *Primers' annealing temperature zone*: from **Figure 4.1**(**B**), this zone follows the melting temperature zone. Since this temperature is optimised for each primer pair because of its dependence on the nucleic acid sequence, we can see in **Figure 4.1**(**B**) that we optimised the annealing temperature to be around 60 °C.
c. *Primer extension temperature zone*: as can be seen on **Figure 4.1**(**B**), this was the medium temperature zone that was averaging at 73 °C.

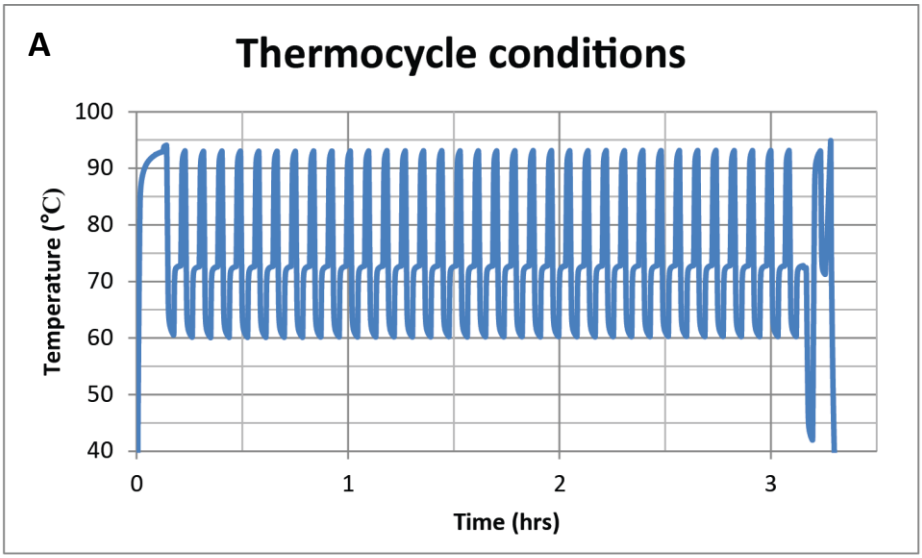

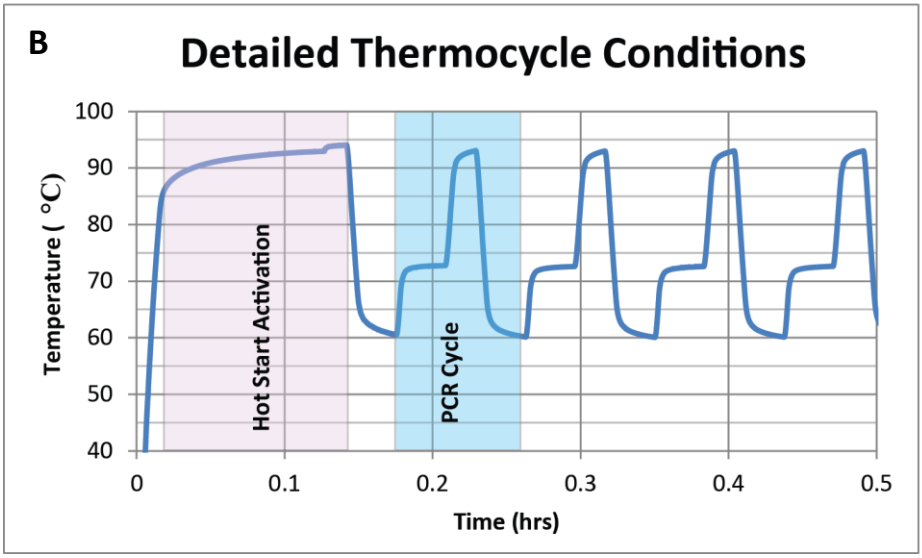

Figure 4.1|LightForge System PCR polysilicon base thermal profiling. **A**) Illustration of 35 PCR cycles and HRMA. **B**) Detailed thermal cycling conditions of the first 4 PCR cycles On **Figure 4.1B;** shown in detail are the steps performed by LightForge. Initially there is a denaturation step for the enzyme activaton. Each PCR cycle has a 60 °C step for anealing, 72 °C extension step and a 93 °C denaturation step.

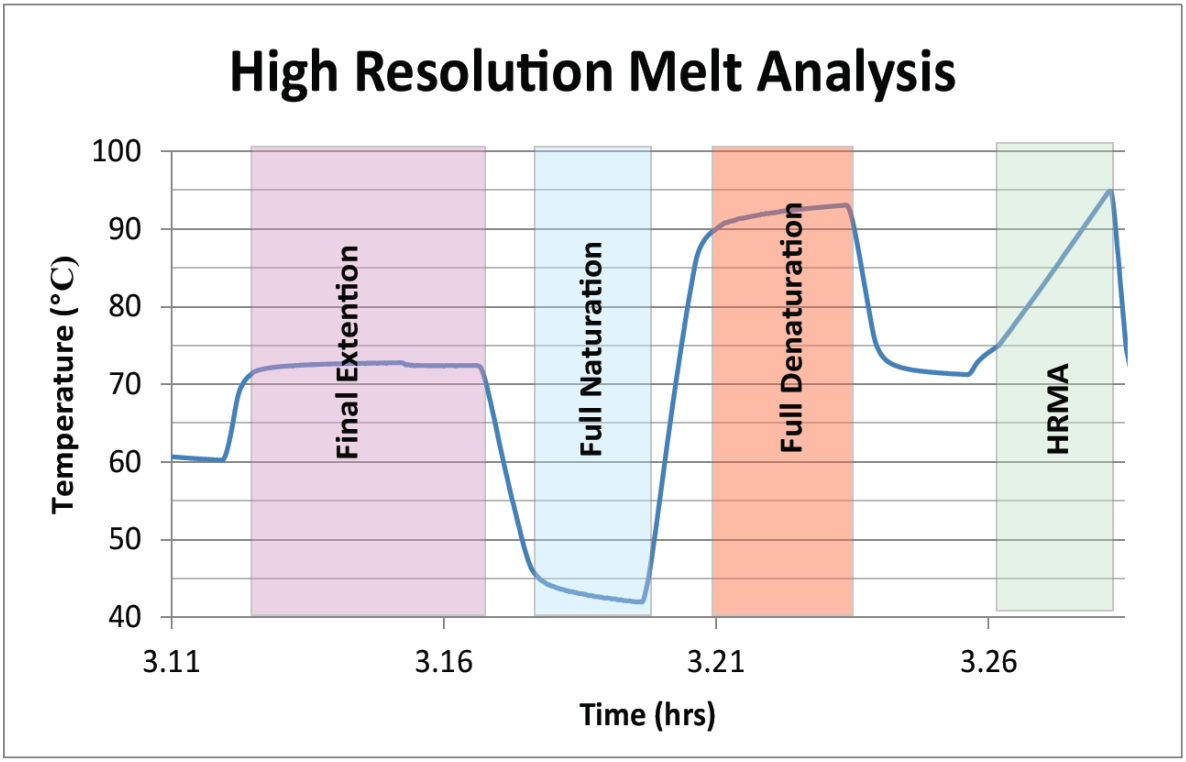

Figure 4.2| Illustration of LightForge HRMA perfomance. shown above are the steps after the 35th PCR cycle; the temperature feedback loop program allows LightForge to enter a final extension step which is then followed by full a naturation step to ensure naturation of all PCR products. A full denaturation step follows later to eliminate primer dimers. The system is then lowered to a temperature sufficient for only PCR products excluding primer dimers to hybridize. It is only at this stage that the HRMA is initiated through ramping the temperature from 75 °C to 95 °C at 0.25°C/step at a ramp rate of 0.5 °C/sec.

In **Figure 4.2** (above), it can be seen that after the periodic repetitions of PCR cycles, there is a final extension step with a mean temperature around 73 °C for 8 mins. The system is then cooled down to 42 °C for full DNA hybridisation. This low temperature of 42 °C signals the end of PCR periodic cycles and triggers the LightForge computer program to enter into a high resolution melt analysis (HRMA) phase. The initial step in this HRMA phase is the full denaturation of the PCR products at 92 °C for 2 mins. The products are then cooled to a medium temperature of 75 °C where the temperature is ramped to 95 °C at 0.25 °C/step at a rate of 0.5 °C/sec.

At this stage we had a prototype system that could perform PCR in real-time as well as HRMA with periodic fluorescent image acquisition. We then hypothesised that:

1. Can we do PCR in a microfluidic device that has19 nL reaction chamber volumes—2 632 times reaction volume reduction in comparison to current conventional PCR volumes which can be 50 µL?

To test this hypothesis we fabricated the microfluidic chip designed by Jerome Rogich shown in **Figure 4.3**. Each of the reaction chambers in this chip have a 19 nL volume. The channels in red are 10 µm high. They are rounded channels and have a diameter of 200 µm. This makes each of the chambers shown in yellow in **Figure 4.3(B)** to have a volume of 19 nL as the height of each yellow chamber is 190 µM. The chambers are sealed by pressurised elastomeric valves in the green layer of the microfluidic chip. The height of this green layer is 23 µm.

4.1. Jerome Rogich Spider Design Chip

This chip was designed to test the possibility of conducting PCR on a Microfluidic chip. **Figure 4.3** (below) shows the AutoCAD complete design of the chip with 20 PCR reaction chambers(in yellow) independent of one another. Each chamber has its own input therefore 20 independent PCR experiments can be conducted on this chip. The total volume of each reactor is 19 nL.

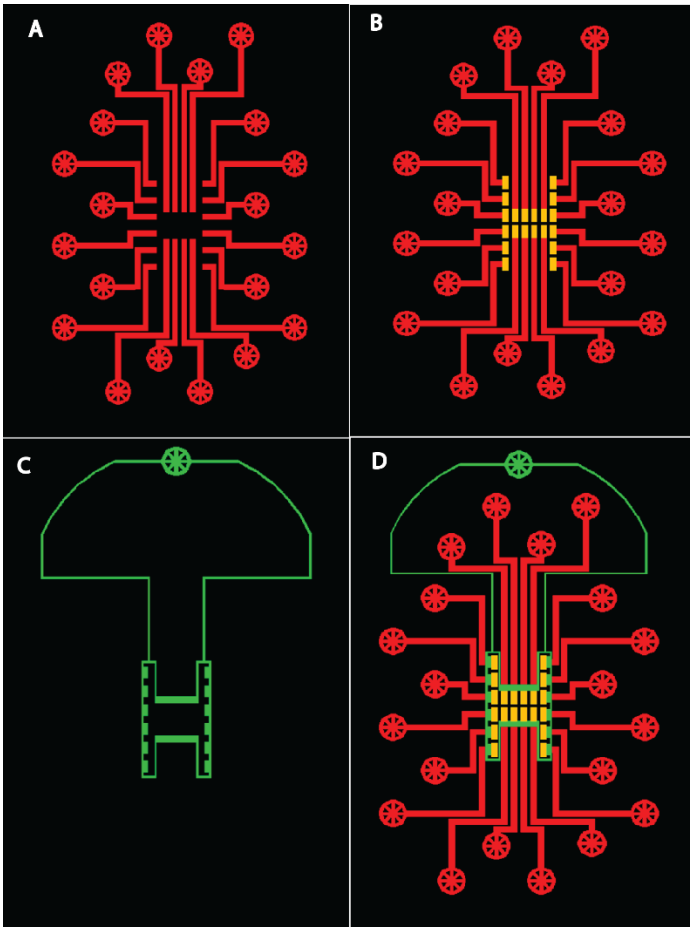

Figure 4.3| Representation of Jerome Chip Fabrication. (**A**) The rounded first flow layer that has a height of 11 microns, consists of channels providing pathway to the reactors, the circular features are the inlet ports of the chip. (**B**) The hybrid structure that resulted from layering the 190 microns high PCR reaction chambers (the yellow layer) on top of A thereby yielding a complete Flow Layer mold; (**C**) shows the 23 microns high Control mold monolayer that seals each of the PCR chambers in an elastomeric valve fashion; (**D**) is the complete Spider Design Chip showing how the aligned three layers function in conjunction with one another.[j]

[j] Designed by Jerome Rogich and fabricated by Tawanda Mandizvo

The chips produced from soft-lithography and photolithography processes were plugged into the LightForge system and loaded with PCR reaction mixtures. The automated sensing of temperature and real-time imaging allowed for twenty PCR experiments to be executed without the need for user intervention. As shown in **Figure 4.4** experimental layout below, in each of the 20 PCR reaction chambers a unique real-time PCR progression signal was produced. Using LightForge, a custom software developed in-house in LabView (National Instruments) we controlled image acquisition and data processing.

4.1.1. Experimental Layout

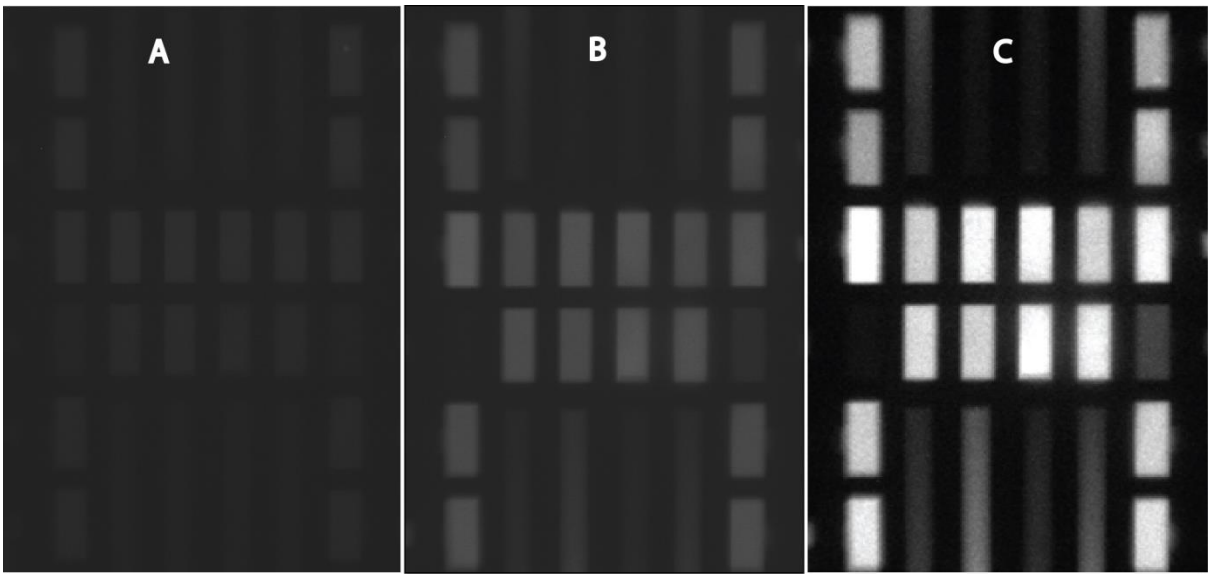

Figure 4.4| Spider design chip Real-Time monitoring of PCR progression using the LightForge System. (**A**) Raw image taken by LightForge after the 1st PCR cycle at 60 °C. (**B**) Raw image taken by LightForge after the 35th PCR cycle 60 °C. (**C**) Matlab processed image taken by LightForge after the 35th PCR cycle 60 °C. **A** and **B** show raw images that the lightForge system captured, with relatively low fluorescence intensity was observed at the beginning of the experiment (**A --**1st PCR cycle). As the PCR experiment progressed towards the 35th cycle (**B)** the fluorescence intensity signal got relatively stronger; (**C**) shows that by lowering the background signal, the reactors' fluorescence intensity became even more pronounced. The reactors (4th row 1st and last columns) that harboured the non-template control maintained relatively weaker fluorescence signal even up to the 35th PCR cycle.[k]

We successfully conducted PCR and HRMA using this microfluidic chip. **Figure 4.4** (above) shows how we organised our PCR/HRMA experiments. A fluorescent double stranded DNA saturating dye LC Green was used to monitor the experimental progression. A fluorescent image was being acquired in real-time after every PCR cycle. However, in **Figure 4.4**, we only show the images of the 1st and the

[k] This data was jointly obtained with Ian Mbano, with whom I worked with on some aspects of the project

35th PCR cycles. The summary of overall observation from **Figure 4.4** is that the fluorescence intensity of the 20 PCR reactions gradually get stronger as the cycle number increases—which is in consistent with the theoretical accumulation of PCR products. The HRMA was also conducted successfully after every 35th PCR cycle to determine the thermal properties of our PCR products.

Since we could conduct PCR and HRMA on a microfluidic chip, we were prompted again to ask the following questions:

a. Is the LightForge system able to interrogate Mtb clinical isolates for the presence of drug resistance conferring mutations (SNPs)?
b. Can we tally a high resolution melting temperature (T_m) or a melting curve profile to a specific clinical Mtb isolate—so that we can predict drug resistance?

We attempted to answer these questions with the LightForge system using:

1. The genomic material from R35 multidrug resistant (MDR) clinical isolate. This clinical strain is known to have rifampicin resistance associated with a class 1 SNP mutation within its rpoB region—a rifampicin resistance determining region (RRDR).
2. The genomic material from KZN 605 extensively drug resistant (XDR) clinical isolate. This strain was first isolated in Tugella Ferry in KwaZulu Natal province of South Africa. KZN 605 is known to have rifampicin resistance associated with two class 1 SNP mutations within its rpoB region—a rifampicin resistance determining region (RRDR).
3. The genomic material from Tkk 062 multidrug resistant (MDR) clinical isolate. This clinical strain is known to have rifampicin resistance associated with a class 4 SNP mutation within its rpoB region—a rifampicin resistance determining region (RRDR).

The data for the R35 clinical isolate is shown in **Figure 4.5**. As can be seen (**A**) shows the real-time PCR amplification curves that are similar to those observed in conventional PCR commercial systems. Detectable levels of PCR products were registered after the 15th cycle. Shown in **red** are replicates for the R35 strain. In **blue** are the replicates for the standard H37RV reference strain. In black are the non-template control replicates. The normalised HRMA data shown in (**B**) reveal the differences in the thermal properties of the PCR products of each loaded sample. Computing the –dRFU/dt in (**C**) it can be seen that all the three sample types gave distinct peak signatures. As theoretically expected, the R35 isolate with a cytosine residue SNP substitute (C**C**G) had a higher melting peak temperature (T_m ~86.3 °C); in comparison to the (C**T**G) for the reference strain H37RV (T_m ~83.9 °C). The non-template control in black had a broad peak signature with its –dRFU/dt maximum value at ~81 °C. The figure (**D**) shows the independence of the melt peak temperature to the fluorescence intensity—the melt peak temperature is related to the clinical isolate identity and not the intensity of the fluorescence in each PCR reaction chamber.

Shown in **Figure 4.6** is the data for the KZN 605 clinical isolate. As can be seen (**A**) shows the real-time PCR amplification curves that are similar to those observed in conventional PCR commercial systems. Detectable levels of PCR products were registered after the 15th cycle. Shown in **red** are replicates for the KZN 605 strain. In **blue** are the replicates for the standard H37RV reference strain. In black are the non-template control replicates that amplified around the 25th PCR cycle. The normalised HRMA data shown in (**B**) reveal the differences in the thermal properties of the PCR products of each loaded sample. Computing the –dRFU/dt in (**C**) it can be seen that all the three sample types gave distinct peak signatures. As theoretically expected, the KZN 605 isolate with cytosine residue and guanine residue SNP substitutes—(C**C**G) and (G**G**C)—had a higher melting peak temperature (T_m ~83.0 °C); in comparison to the—(C**T**G) and (G**A**C)—respectively for the reference strain H37RV (T_m ~82.0 °C). Despite KZN 605 having two class 1 SNPs, it was surprising to it having a smaller relative temperature difference in comparison to R35 which has one class 1 SNP. The non-template control in black had no amplicon domain peak signature, with its –dRFU/dt remaining flat in the studied high resolution melting region. The figure (**D**) shows the independence of the melt peak temperature to the fluorescence intensity—the melt peak temperature is related to the clinical isolate identity and not the intensity of the fluorescence in each PCR reaction chamber.

The data for the Tkk 062 clinical isolate is shown in Figure 4.7. As can be seen (**A**) shows the real-time PCR amplification curves that are similar to those observed in conventional PCR commercial systems. Shown in **red** are replicates for the Tkk 062 strain. In **blue** are the replicates for the standard H37RV reference strain. Also introduced in **green** are the H37RV gyrA positive control replicates. In black are the non-template control replicates. The normalised HRMA data shown in (**B**) reveal the differences in the thermal properties of the PCR products of each loaded sample. Computing the –dRFU/dt in (**C**) it can be seen that all the three sample types gave distinct peak signatures. As theoretically expected for a class 4 mutation, the Tkk 062 isolate with an adenine SNP substitute (G**T**C) had a closely similar melting peak temperature (T_m ~82.5 °C); in comparison to the (G**A**C) for the reference strain H37RV (T_m ~82.3 °C). The non-template control in black had no amplicon domain peak signature, with its –dRFU/dt remaining flat in the studied high resolution melting region. As also expected the gyrA positive control had its own unique peak signature (T_m ~85.4 °C). The figure (**D**) shows the independence of the melt peak temperature to the fluorescence intensity—the melt peak temperature is related to the clinical isolate identity and not the intensity of the fluorescence in each PCR reaction chamber.

4.1.2. Interrogation of R35 Clinical Isolate

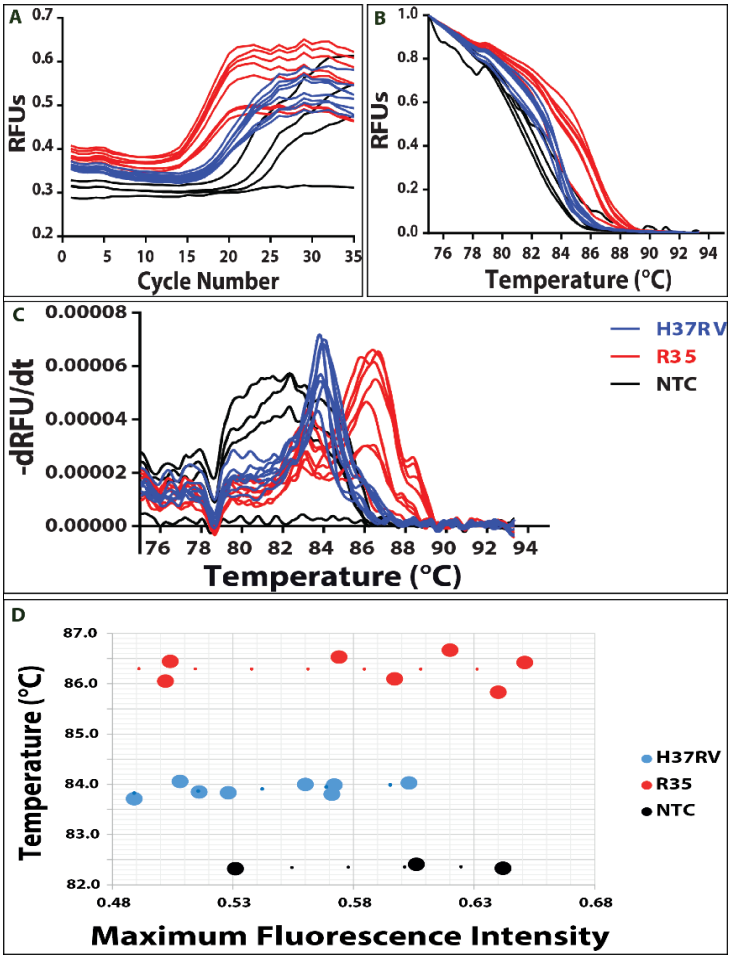

Figure 4.5| Real-Time PCR and High Resolution Melt Analysis data for a rifampicin resistant MTB clinical isolate R35.[ii] (R35 = 7 in **Red** replicates) relative to a rifampicin susceptible (H37RV = 8 in **Blue** replicates). The (3 **black** replicates) are the non-template controls **NTC**. (**A**) The realtime amplification curves for 35 PCR cycles (**B)** Normalised High Resolution Melt Analysis curves ranging from 75 – 95 °C. (**C**) The 1st derivative melt plots of the Normalised High Resolution Melt Analysis curves ranging from 75 – 95 °C. (**D**) Melting temperature peak in relation to maximum fluorescence intensity data display. From (**A**) it can be seen how the detectable concentrations of PCR products were achieved after 15 cycles and it can be confirmed that the PCR experiment proceeded to saturation. The **NTCs** amplified after the 20th cycle. In (**B**) there is a distinction between the HRMA signatures of H37RV and R35. (**C**) show the profound differences from the 1st Derivative melt plot (-dRFU/dt vs temperature); (**D**) shows that H37RV had an average melting temperature (max –dRFU/dt) of 83.90813314 °C while R35 had an average melting temperature max (–dRFU/dt) of around 86.2908122°C. Although the NTCs amplified, their melt temperature signature was localised and distinct in relation to the sample signatures. [b]

[b] This data was jointly obtained with Ian Mbano, with whom I worked with on some aspects of the project

4.1.3. Interrogation of KZN 605 Clinical Isolate

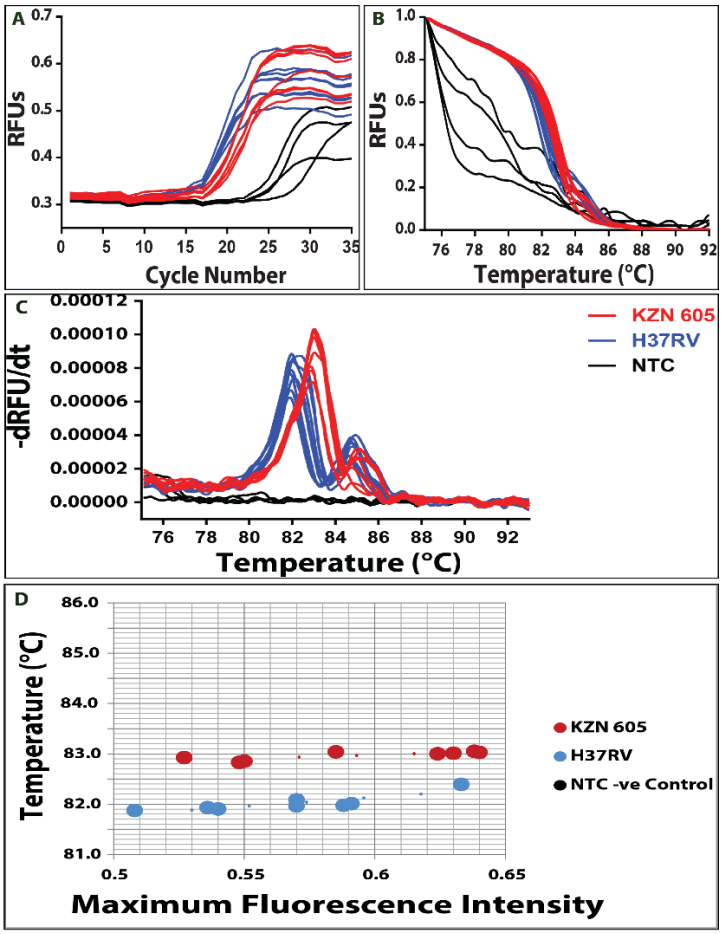

Figure 4.6| Real-Time PCR and High Resolution Melt Analysis data for a rifampicin resistant MTB clinical isolate KZN 605(KZN 605 = 8 replicates in **Red**) relative to a rifampicin susceptible (H37RV = 8 replicates in **Blue**). In (**black**) is the non-template control **NTC**. (**A**) The real-time amplification curves for 35 PCR cycles (**B)** Normalised High Resolution Melt Analysis curves ranging from 75 – 95 °C. (**C**) The 1st derivative melt plots of the Normalised High Resolution Melt Analysis curves ranging from 75 – 95 °C. (**D**) Melting temperature peak in relation to maximum fluorescence intensity data display. From (**A**) it can be seen how the detectable concentrations of PCR products were achieved after 16 cycles and it can be confirmed the PCR experiment proceeded to saturation. The **NTCs** amplified after the 24th cycle. In (**B**) there is a slight distinction between the HRMA signatures of H37RV and KZN 605; (**C**) shows the exacerbated differences from the 1st Derivative melt plot (-dRFU/dt vs temperature); (**D**) shows that H37RV had an average melting temperature max (–dRFU/dt) of 82.01705253 °C while KZN 605 had an average melting temperature max (–dRFU/dt) of around 82.96774752 °C. Though the NTCs amplified, their melt peak signature was not registered according to (**C**).[iii]

[c] This data was jointly obtained with Ian Mbano, with whom I worked with on some aspects of the project

4.1.4. Interrogation of TKK-062 Clinical Isolate

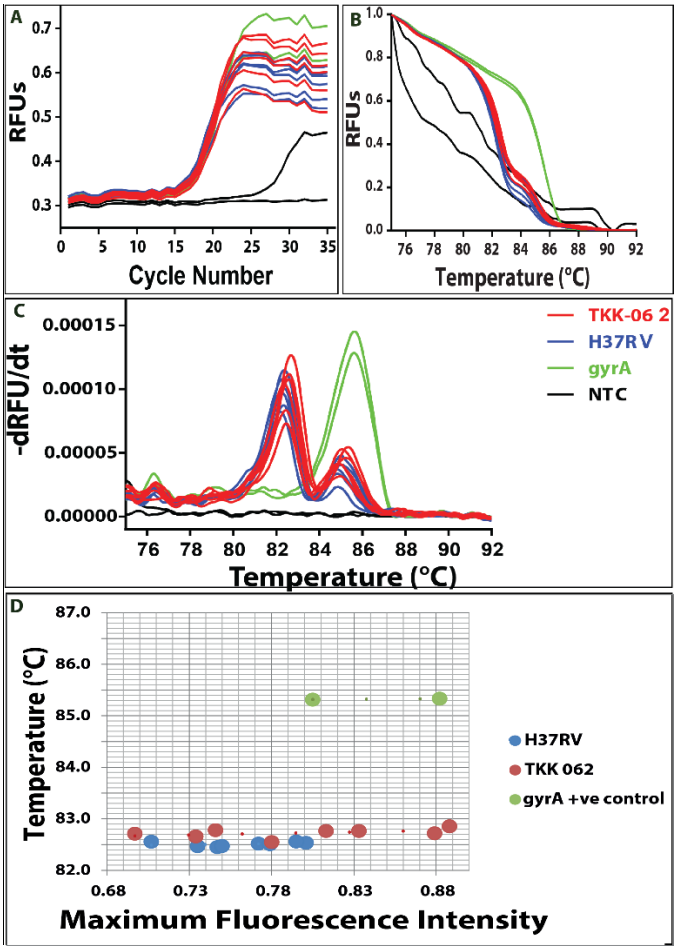

Figure 4.7| Real-Time PCR and High Resolution Melt Analysis data for a rifampicin resistant MTB clinical isolate TKK 062(TKK 062 = 8 replicates in **Red**) relative to a rifampicin susceptible (H37RV = 8 replicates in **Blue**). In (**black**) is the non-template control (**NTC**). The two replicates in **green** are the gyrA positive controls from the H37RV genome. (**A**) The realtime amplification curves for 35 PCR cycles (**B)** Normalised High Resolution Melt Analysis curves ranging from 75 – 95 °C. (**C**) The 1st derivative melt plots of the Normalised High Resolution Melt Analysis curves ranging from 75 – 95 °C. (**D**) Melting temperature peak in relation to maximum fluorescence intensity data display. From (**A**) (above) it can be seen how the detectable concentrations of PCR products were achieved after 15 cycles and it can be confirmed that the PCR experiment proceeded to saturation. In **(B**) there is a slight distinction between the HRMA signatures of H37RV and Tkk -01-062; (**C**) shows the exacerbated differences from the 1st Derivative melt plot (-dRFU/dt vs temperature); (**D**) shows that H37RV had an average melting temperature max (–dRFU/dt) of 82.30025716 °C while Tkk -01-062 had an average melting temperature max (–dRFU/dt) of around 82.53506398 °C. Though one of the NTCs amplified after the 26th cycle, there was no melt peak signature according to (**C**)**.** In this assay we also incorporated the positive control where we amplified (gyrA, **green**) a different region of the MTB genome. As expected the peak for gyrA was distinctly positioned at about 85.4 °C.[iv]

4.1.5. Summary of the Clinical Isolates Data

Table 4.1| Summary of Strain HRMA Assays Data in Relation to H37RV

	DR-Mutation(s) detected by Sanger Sequencing	*Mutation Class*	*HRMA data*		
Isolates	***rpoB***		**Mean H37RV T_m (°C)**	**Mean Isolate T_m (°C)**	**Relative Difference to H37RV T_m (°C)**
R 35	CTG → C**C**G (L533P)	1	83.90813314	86.2908122	2.382679057
KZN 605	GAC → G**G**C (D516G)	1	82.01705253	82.96774752	0.950694994
	CTG → C**C**G (L533P)	1			
Tkk-01-062	GAC → GTC D516V	4	82.30025716	82.53506398	0.234806817

Table 4.1 above summarises the data from figures **4.5, 4.6** and **4.7.** For the *R35* clinical isolate that was described as resistant to rifampicin (RIF), isoniazid (INH) but susceptible to ofloxacin (OFLX) (See **Table 3.5** in Materials and Methods Section Chapter 3); we focused on the *rpoB* region which had a class 1 mutation CTG → C**C**G (L533P). The mean melting temperature for *R35* was 86.2908122 °C while that of the reference susceptible strain *H37RV* was 83.90813314 °C; owing to a 2.382679057 °C relative difference between the two strains.

The *KZN 605* clinical isolate that was described as resistant to RIF, INH and OFLX (See **Table 3.5** in Materials and Methods Chapter 3); we also focused on the *rpoB* region which had two class 1 mutations CTG → C**C**G (L533P) and GAC → G**G**C (D516G). The mean melting temperature for *KZN 605* was 82.96774752°C while that of the reference susceptible strain *H37RV* was 82.01705253 °C; owing to a 0.950694994 °C relative difference between the two strains.

The *Tkk 062* clinical isolate that was described as resistant to RIF, INH but susceptible to OFLX (See **Table 3.5** in Materials and Methods Chapter 3); we also focused on the *rpoB* region which had a class 4 mutation GAC - GTC. The mean melting temperature for *Tkk 062* was 82.53506398 °C while that of the reference susceptible strain *H37RV* was 82.30025716 °C; owing to a 0.234806817 °C relative difference between the two strains.

The results at this point showed that; PCR can be conducted on a LightForge platform for only 20 reaction chambers on Jerome Rogich design chip. The findings further reveal that 19 nL reaction volume is sufficient for PCR on the lightForge platform. These outcomes prompted us to ask the following questions in a bid to save reagents and time:

1. Can the LightForge platform perform PCR simultaneously in 720 reactions chambers?
2. Can the LightForge platform conduct PCR in 1.8 nL reaction volumes—10.6 times reduction in comparison to the Jerome Rogich chip?
3. Can the LightForge platform achieve individual Mtb genome interrogation per chamber—digital PCR (dPCR)?

We designed and fabricated the following microfluidic chips in an attempt to answer the above questions:

a. *The serpentine design dPCR chip*: This is shown in **Figure 4.8**. We derived its name from the serpent fashion of its flow layer shown in red in **Figure 4.8**(**B**). The volume of each of the reaction chambers is1.8 nL. The chip has four quadrants with each quadrant having 180 reaction chambers.
b. *The web randomising design dPCR chip*: This chip is shown in **Figure 4.11**. Its name is derived from the web/net interconnection fashion of PCR reaction chambers to allow random filling of the chambers. This design is shown in detailed in **Figure 4.12**(**E**). The volume of each of the reaction chambers is1.8 nL. The chip has four quadrants with each quadrant having 180 reaction chambers to make a total of 720 chambers.
c. *Dead ended design dPCR chip*: This chip is shown in **Figure 4.15**. Its name is derived from the fact that each row of chambers have a dead end. The volume of each of the reaction chambers is1.8 nL. The chip has four quadrants with each quadrant having 180 reaction chambers to make a total of 720 chambers.

Through these iterations we used the reactor brightness patterns (in figures **4.10**, **4.13** and **4.16**) to identify the dead ended design dPCR chip as the best candidate for the for future dPCR experiments on a LightForge platform. The post PCR image showing fluid dynamics for the serpentine design dPCR chip in **Figure 4.10** (**C**) reveal an undesirable effect that the DNA sample distribution favoured some rows at the expense of others. Another unfavourable outcome can be seen in the web randomising design dPCR chip's post PCR images. This again can be seen in **Figure 4.13**(**C**) and **4.14** where it is revealed that there is confinement of the brighter reactors at the periphery of the studied quadrant. The bias can be seen in that, the reactors in the middle of the quadrant were of uniformly weaker intensity in comparison to the peripheral reactors. However, **Figure 4.16**(**C**) which shows the post PCR image for the dead ended design dPCR chip shows a random reaction chamber fluorescence that we would expect for a digital PCR experiment. This signifies the expected random positive and negative reaction occurrence.

4.2. Serpentine Design dPCR Chip

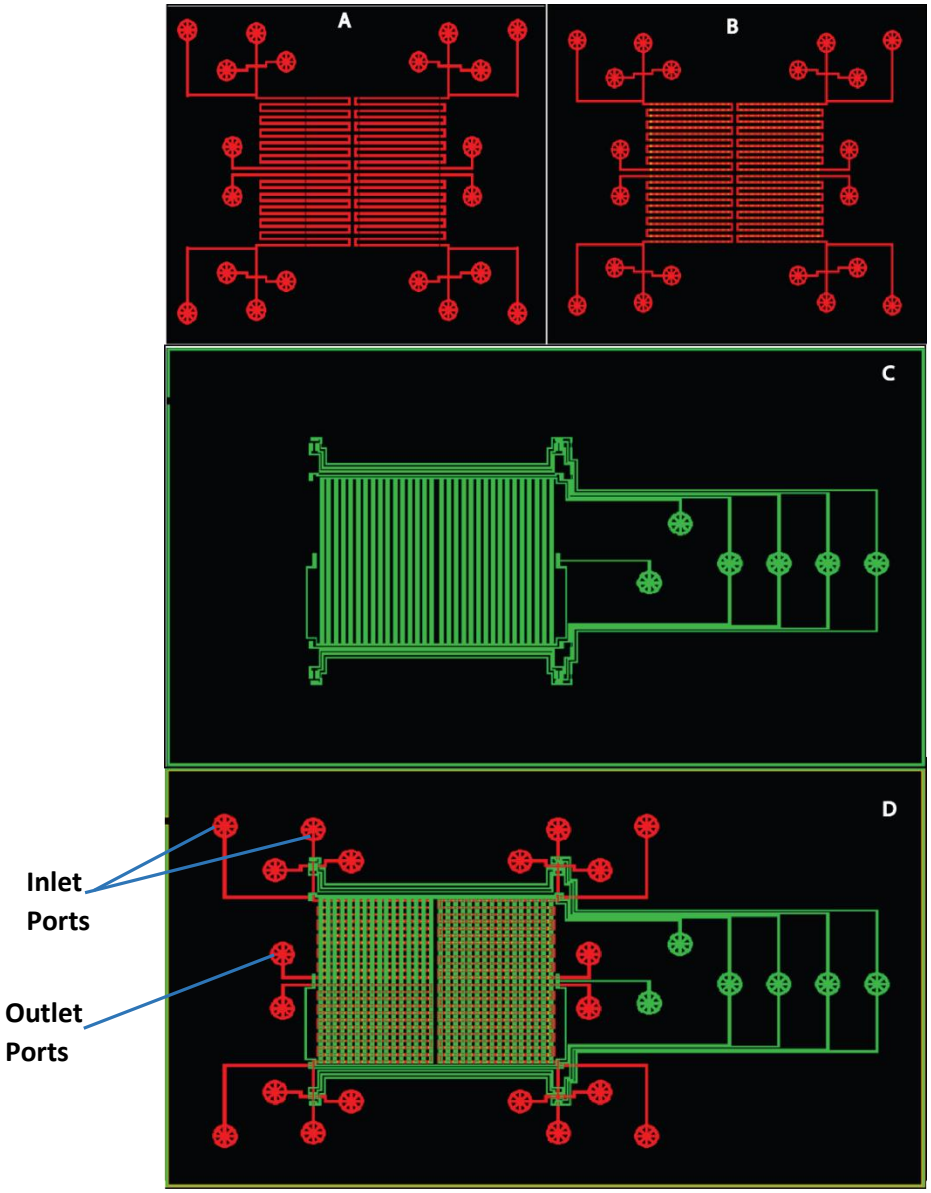

Figure 4.8| Serpentine Design dPCR chip. (**A**) The rounded "serpentine "first flow layer that has a height of 13 microns, consists of channels linking PCR reaction chambers all the way to the outlets, the circular features are the inlet/outlet ports of the chip. (**B**) The hybrid structure that resulted from layering the 180 microns high PCR reaction chambers (the yellow layer) on top of (**A**) thereby yielding a complete Flow Layer mold; (**C**) is the 23 microns high control mold monolayer consisting of valves that control the sequential flow of reagents; (**D**) is the complete Serpentine Design dPCR chip showing how the aligned three layers function in conjunction with one another. The Serpentine Design dPCR chip shown above has four identical quadrants. Each quadrant has four inlet ports and one outlet port. One of the inlet ports is for inputting PCR master mix while the extra three were meant for inputting surface pre-treatment reagents but however, these later become redundant.

4.2.1. Zooming into Serpentine Design dPCR Chip

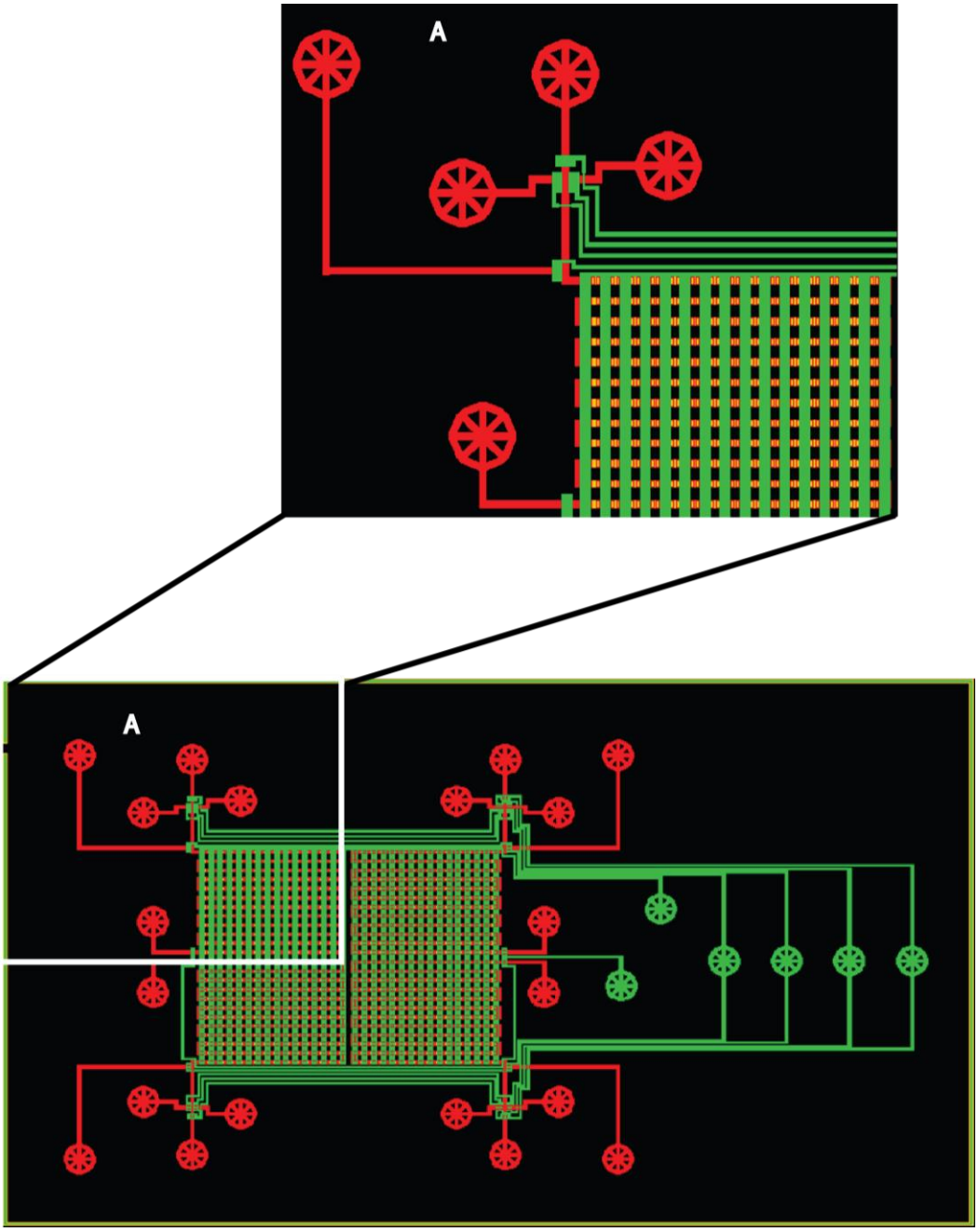

Figure 4.9| Zooming into one of the four quadrants of the Serpentine Design dPCR chip. (A) The PCR reaction chambers become visible. The figure above shows a more detailed figural display of one quadrant of the Serpentine Design dPCR chip. Each of the four quadrants can be seen to have 180 PCR reaction chambers in yellow (12 rows x 15 columns). The serpentine design derived from the literal word serpent describes the series arrangement of the PCR reaction chambers. The cross interaction between the contents of adjacent reaction chambers is prevented by the giant vertical valves (in green) intercepting flow within each row. Each Reaction chamber (in yellow) is 1.8 nL. The total number of reaction on this chip are (4 quadrants× 12 rows × 15 columns) = 720 reaction chambers

4.2.2. Digital PCR Attempt Using Serpentine Design dPCR Chip

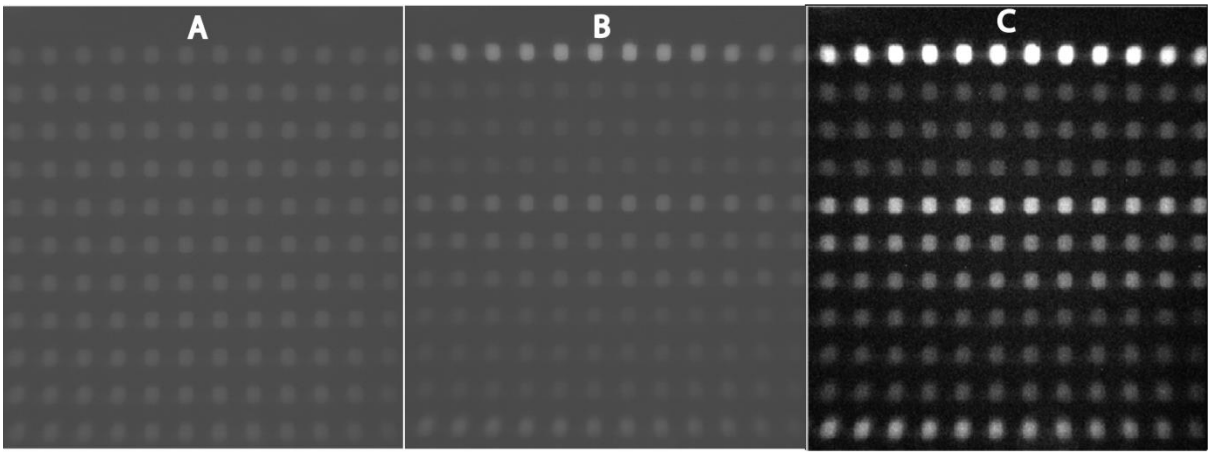

Figure 4.10| Serpentine Design dPCR chip Real-Time monitoring of PCR progression using the LightForge System. (A) Raw image taken by LightForge after the 1st PCR cycle. (B) Raw image taken by LightForge after the 35th PCR cycle. (C) Matlab processed image taken by LightForge after the 35th PCR cycle; (**A**) and (**B**) show raw images that the lightForge system captured, showing relatively low fluorescence intensity at the beginning of the experiment (1st PCR cycle). As the PCR experiment progressed towards the 35th cycle the fluorescence intensity signal relatively got stronger; (**C**) shows that by lowering the background signal, the reactor fluorescence intensity became even more pronounced. The reactors (4th row 1st and last columns) that harboured the non-template control maintained relatively weaker fluorescence signal even up to the 35th PCR cycle. The 35th cycle image shows that the 1st, 5th, 6th, 7th and 11th rows confined brightness more than other rows. This confirmed some systematic bias of the serpentine chip design because there was no randomness in the pattern of fluorescence signal strength.

4.3. Web Randomising Design dPCR Chip

The **Figure 4.11** (below) shows the Web Randomising Design dPCR chip we designed with the idea of randomising the flow of the sample. In contrast to the serpentine design described previously, the adjacent reactors of the web randomising chip are interconnected allowing fluid to flow in multiple directions.

4.3.1. The Web Randomising Design dPCR Chip

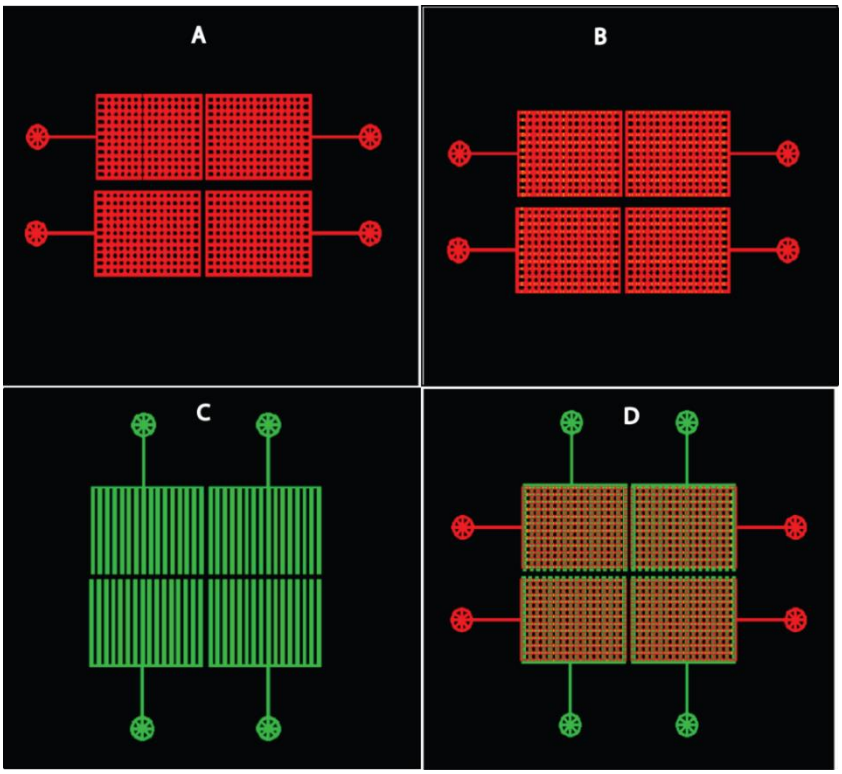

Figure 4.11| Web Randomising Design dPCR Chip. (**A**) The rounded interconnected first flow layer that has a height of 12 microns, consists of channels linking PCR reaction chambers without outlets, the circular features are the inlet/outlet ports of the chip; (**B**) The hybrid structure that resulted from layering the 180 microns high PCR reaction chambers (the yellow layer) on top of A thereby yielding a complete Flow Layer mold; (**C**) is the 23 microns high Control mold monolayer consisting of valves that control the sequential flow of reagents; (**D**) is the complete Web Randomising Design dPCR Chip showing how the aligned three layers function in conjunction with one another. As can be seen above, the chip is a lot simpler because the redundant inlet ports were eliminated. There is only one remaining inlet port and the outlet ports were also eliminated to make the chip dead ended. Each Reaction chamber (in yellow) is 1.8 nL. The total number of reaction on this chip are (4 quadrants× 12 rows × 15 columns) = 720 reaction chambers

4.3.2. Zooming The Web Randomising Design dPCR Chip

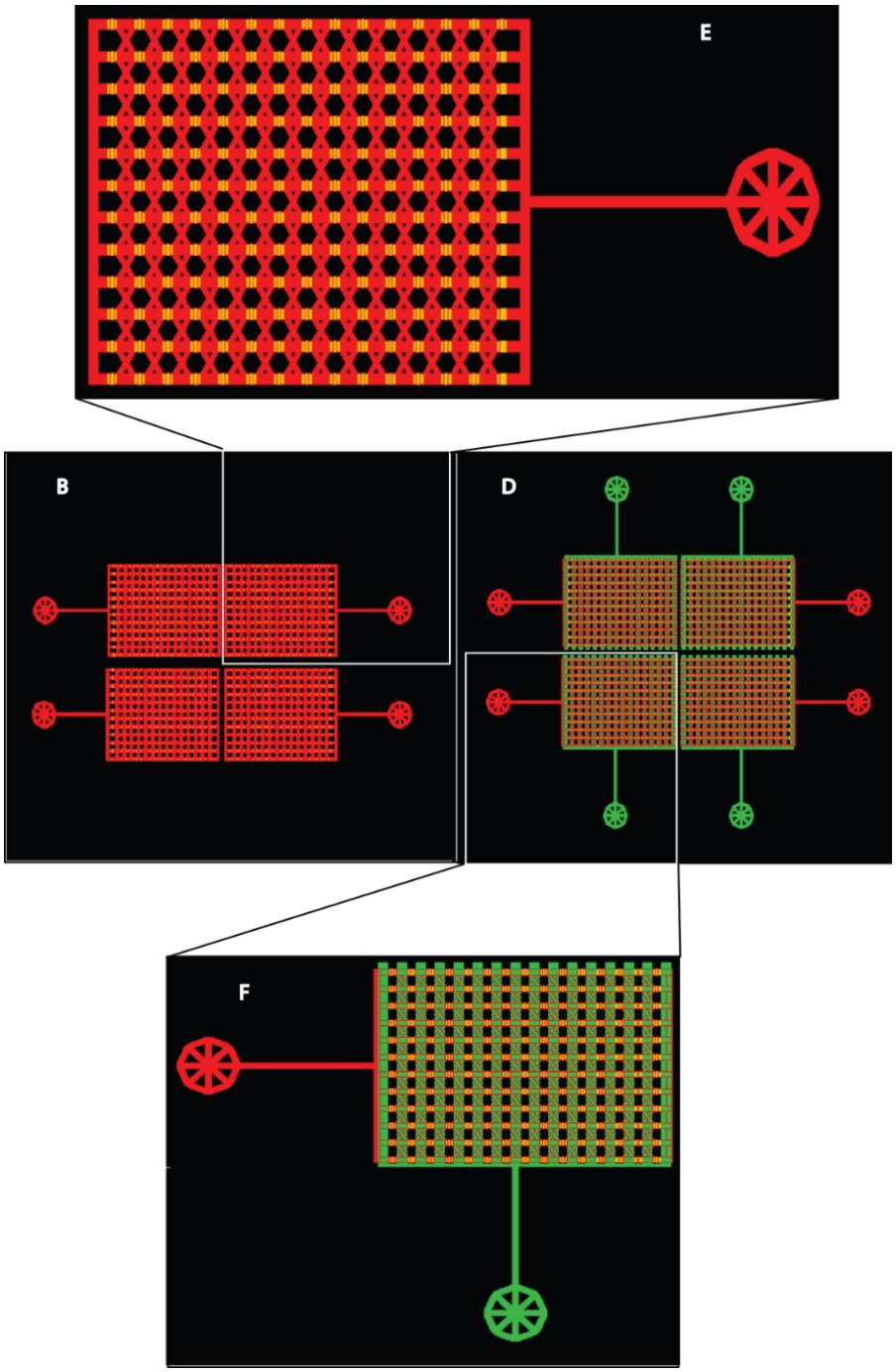

Figure 4.12| Zooming into one of the four quadrants of the Web Randomising Design dPCR Chip. (**E**) Shows the detailed features of how the flow layer mold, the PCR reaction chambers (in yellow) become clearly visible. (**F**) Shows the detailed features of the complete Web Randomising Design dPCR Chip, in red are the flow lines, in green are the control lines and in yellow are the PCR reaction chambers.

4.3.3. Digital PCR Attempt Using the Web Randomising dPCR Chip

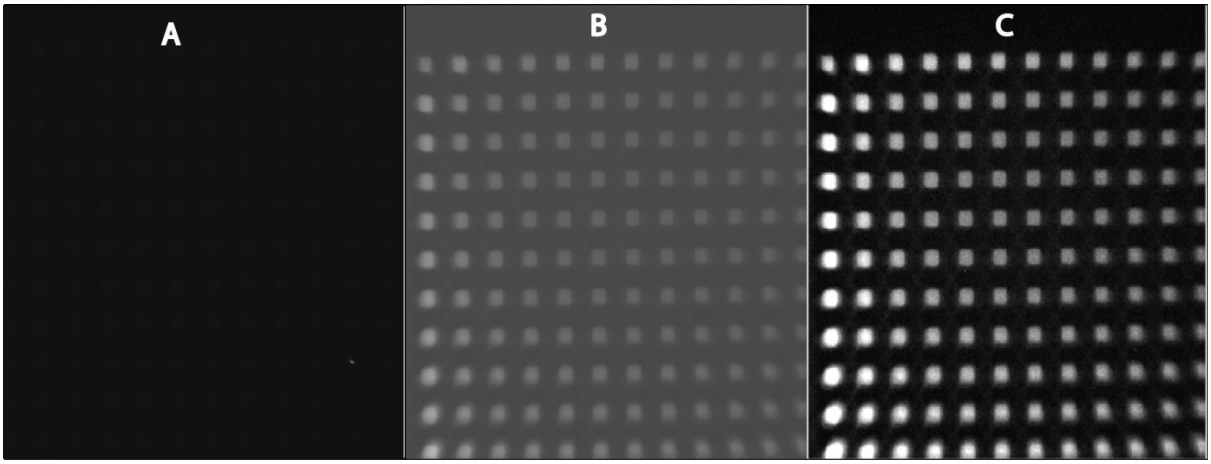

Figure 4.13| Web Randomising Design dPCR Chip Real-Time monitoring of PCR progression using the LightForge System. (**A**) Raw image taken by LightForge after the 1st PCR cycle. (**B**) Raw image taken by LightForge after the 35th PCR cycle. (**C**) Matlab processed image taken by LightForge after the 35th PCR cycle; (**C**) also shows that the reactors of strong intensity are confined to the quadrant peripheries.

4.3.4. Deduced Fluid Dynamics when Using the Web Randomising dPCR Chip

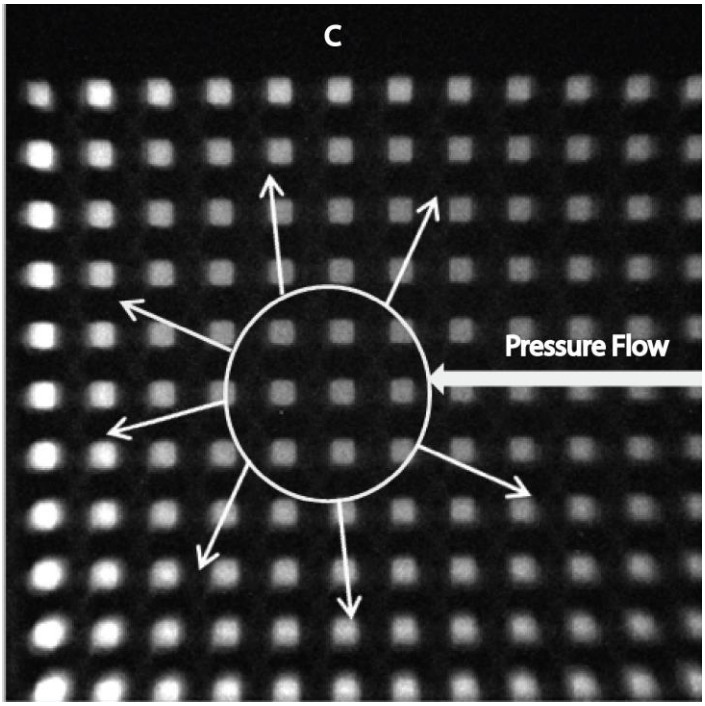

Figure 4.14| Web Randomising Design dPCR Chip showing evidence of pressure radiating from the centre of the quadrant and confining the brightness towards the edges of the chip. It can be seen that the reactors at the centre of the quadrant have relatively low fluorescence intensity compared to peripheral reactors.

4.4. Dead Ended Design dPCR Chip

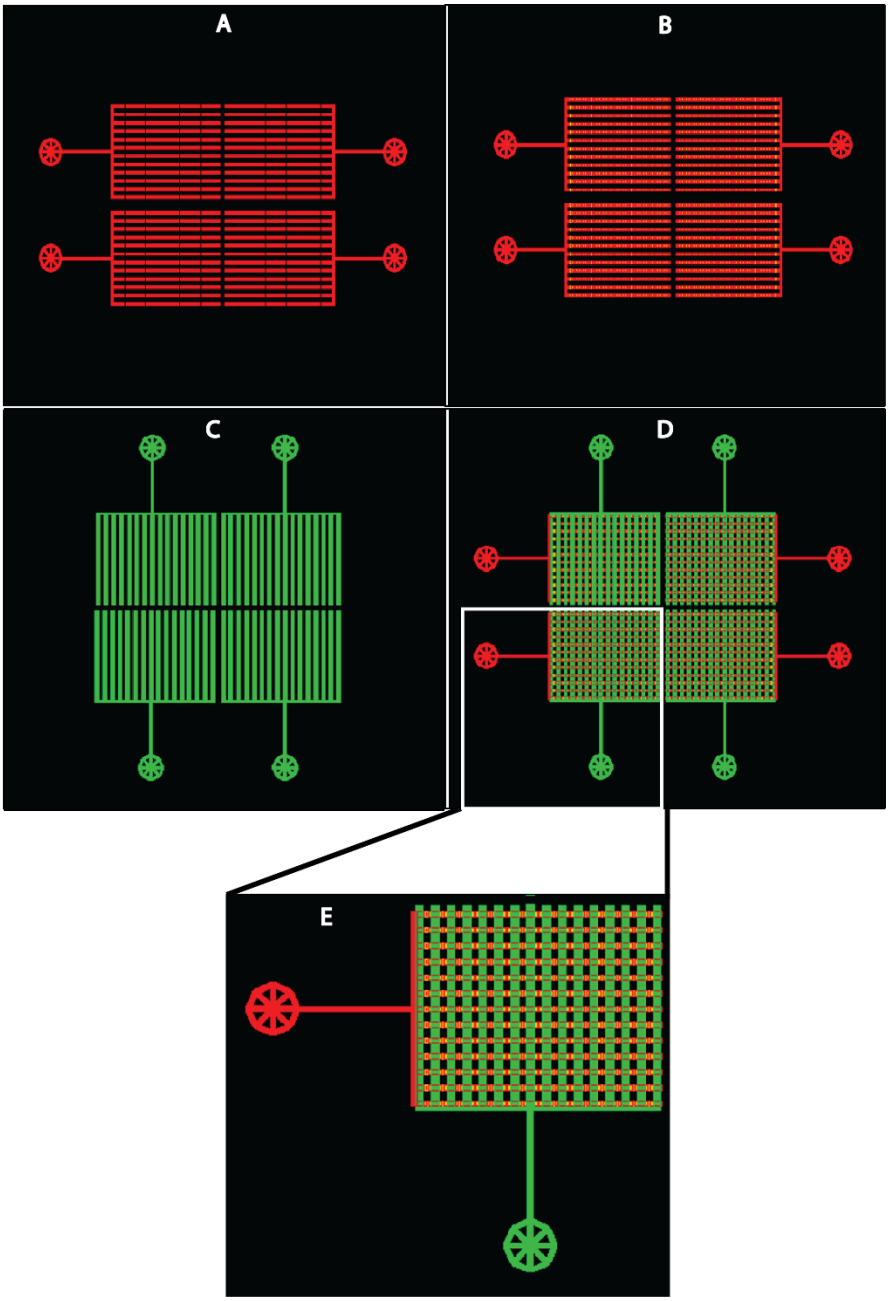

Figure 4.15| Dead Ended Design dPCR Chip. (**A**) The rounded rows of first flow layer that have a height of 12 microns, consists of channels linking PCR reaction chambers without outlets; the circular features are the inlet ports of the chip. (**B**) The hybrid structure that resulted from layering the 180 microns high PCR reaction chambers (the yellow layer) on top of A thereby yielding a complete flow layer mold; (**C**) is the 23 microns high Control mold monolayer consisting of valves that control the sequential flow of reagents; (**D**) is the complete Dead Ended Design dPCR chip showing how the aligned three layers function in conjunction with one another. Each Reaction chamber (in yellow) is 1.8 nL. The total number of reaction on this chip are (4 quadrants× 12 rows × 15 columns) = 720 reaction chambers

4.4.1. Digital PCR Attempt Using the Dead Ended Design dPCR Chip

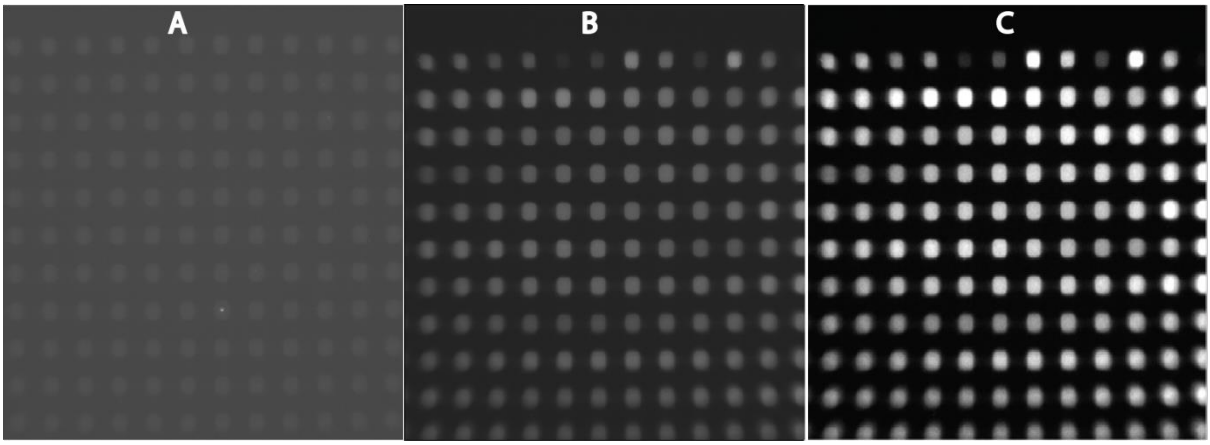

Figure 4.16| Dead Ended Design dPCR Chip Real-Time monitoring of PCR progression using the LightForge System. (**A**) Raw image taken by LightForge after the 1st PCR cycle. (**B**) Raw image taken by LightForge after the 35th PCR cycle. (**C**) Matlab processed image taken by LightForge after the 35th PCR cycle, (**C**) also show some randomness in the brightness pattern in which the PCR chambers lit up. This is a random series of positive and negative PCR reactions fashion that we would expect for digital PCR.

In **Figure 4.17** we show the demonstrated ability of the LightForge system to simultaneously process data from individual PCR reaction chambers. The chambers are numbered sequentially in columns from top to bottom as depicted by **Figure 4.17**(**B**). In **Figure 4.17**(**C**) we only show the data for the first 12 reactors in the first column. It can be seen that the reactors of weaker fluorescence intensity in **Figure 4.17**(**B**) also had a corresponding weaker real-time amplification signal in **Figure 4.17**(**C**). As expected again, it can be seen that the reactors of stronger fluorescence intensity in **Figure 4.17**(**B**) also had a corresponding stronger real-time amplification signal in **Figure 4.17**(**C**). The data for the rest of the reactors is shown in **Appendix B**. This reveals the potential of the LightForge system to be a highly scalable platform for real-time PCR and HRMA; because we can monitor in real-time, the progression of the assays in each chamber shown in **Figure 4.17**(**C**) simultaneously.

4.4.2. LightForge Scalability

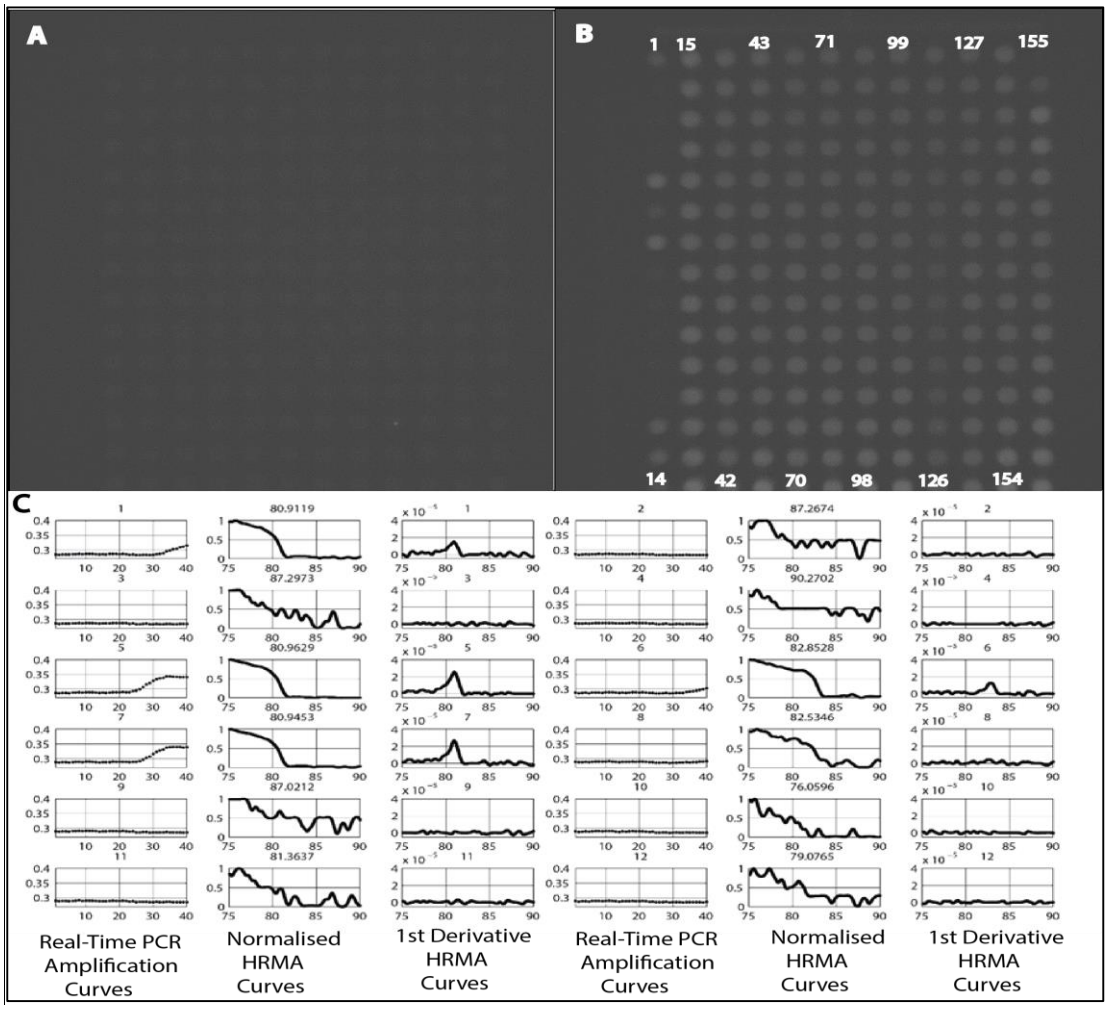

Figure 4.17| Dead Ended Design dPCR Chip Real-Time monitoring. With 50% H37RV rpoB region PCR amplicons using the LightForge System. (**A**) Raw image taken by LightForge after the 1st PCR cycle. (**B**) Raw image taken by LightForge after the 35th PCR cycle. (**C**) Multi-graph plot showing the real-time amplification, Normalised HRMA curve and the negative 1st derivative plot of some of the PCR reaction chambers in the 1st column (See Appendices for profiles corresponding to each of the reactors shown in image (**C**) In (**B**) we see that the PCR chamber 1 amplified as its relative fluorescence intensity increased in comparison to (**A**). This observation is in consistency with what (**C**) shows the reactor numbering system done by the LightForge system (sequentially from top to bottom); for reactor 1 there is a significant real-time amplification signal, a normalised HRMA curve with a corresponding melting temperature of 80.9119 °C. This temperature was determined by taking the temperature that corresponded to the maximum value of y on the 1st derivative melt plot for this PCR reaction chamber. It was also observed that reaction chambers 5, 6 and 7 had melting temperatures of 80.9629 °C, 82.8528 °C and 80.9453 °C respectively. PCR reaction chambers 2, 3, 4, 8, 9, 10, 11 and 12 did not yield a legitimate peak implying the initial absence of a DNA copy in them at the beginning of the experiment. The LightForge microfluidic system we developed demonstrated the capability of processing large amounts of real time fluorescence data from different reaction chambers in parallel.[v]

CHAPTER 5

5. Discussion

5.1. LightForge Real-Time PCR and HRMA

Amidst nucleic acid amplification tests (NAATs), qPCR has been widely employed for molecular diagnosis and technological applications that detect and quantify pathogens [131]. PCR microfluidic systems of various designs have been developed for effective and fast DNA amplification by many research groups. These comprise of chamber stationary PCR[132, 133] and flow-through PCR[134], as well as thermal convection-driven PCR[135]. Alternatively, we have now built an automated rapid prototype instrument shown in **Figure 3.3** (Materials and Methods Section Chapter 3) that rapidly performs PCR and HRMA using microfluidic chips of different designs. Real-time PCR, High Resolution Melt Analysis (HRMA) and SNP genotyping with fluorescent DNA saturating dyes can be performed within a disposable LightForge microfluidic chip at over two thousand-fold reduction in analysis volume from current conventional PCR commercial systems. The LightForge PCR and HRMA system takes over 3 hours to complete the assay. However, future embedding the PCR reaction chambers with thin film resistive heaters and temperature sensors will enable thousands of real-time PCR experiments to rapidly occur in parallel followed by detection at endpoint using HRMA.

5.2. Single Nucleotide Polymorphism (SNP) Resolution

In comparison with conventional PCR instruments, the LightForge system dramatically allows for highly scalable assays because of automated sample operation. To demonstrate data quality of HRMA melting curves for this study, we have developed PCR/HRMA assays to detect particular mutations associated with drug resistance within *rpoB*, the 81-bp rifampicin resistance determining region (RRDR). We performed this for rifampicin resistant conferring SNPs present in Mtb clinical isolates, namely, *R35*, *KZN 605* and *TKK-01-062*. The reference for this detection was an *rpoB* region of a rifampicin susceptible strain *H37RV*. The *gyrA* (wild type), a 234-bp region that includes several resistance-associated sites (OFLX resistance in other strains) was used as a positive control.

The development of non-specific ds-DNA binding dyes that include SYTO 9 and LC Green has increased the stability and sensitivity of HRMA assays by making it possible to distinguish minute melting temperature differences[136]. In summary according to the Bioline website, the following commercial systems; (ABI 7300, 7500 FAST, Qiagen Rotor-Gene™ 6000, Eppendorf Mastercycler® ep realplex, Illumina® Eco™, Roche LightCycler®; 96 and 480, Bio-Rad Opticon®, CFX96™, CFX384™, Idaho LightScanner® 32 (LS32™), Takara Thermal Cycler Dice (TP800)) as shown in **Table 5.1**

(below) for instance, (> 0.5 °C for SNP class 1 and 2 mutations); (> 0.2 °C and < 0.5 °C for SNP class 3 mutations); and (< 0.2 °C for SNP class 4 mutations) T_m differences are registered if the SensiFAST™ HRM-kit is used[137]. In this project as we investigated class 1 and 4 SNP T_m differences on the LightForge platform we found them to be largely exacerbated in comparison to the systems noted above. However, this exacerbation occurred in a trend that is in harmony with what is observed for most commercial bulk PCR systems. **Table 5.1** (below) shows that the LightForge system is at least two-fold better at detecting Class 1 SNPs. When we considered Class 4 SNPs which are a lot more difficult to detect in most commercial systems, LightForge showed potential to distinguish these by greater than 0.2 °C (as opposed to less than 0.2 °C offered by current commercial systems).

Table 5.1|Comparison between LightForge and the Bioline SensiFAST™ HRM-kit commercial system melting temperatures (T_m).

SNP Class	Base Change	T_m Curve Shift	
		SensiFAST™ Commercial System	LightForge
1	C↔T and G↔A	Large > 0.5 °C	> 1 °C
2	C↔A and G↔T	Large > 0.5 °C	
3	C↔G	Small 0.2 - 0.5 °C	
4	A↔T	Small < 0.2 °C	> 0.2 °C

5.3. LightForge Perfomance

In this section we discuss our LightForge system in relation towards its satisfying the following criteria fundamentally important for a clinically useful molecular diagnostic tool:

1. *Scalability*: In comparison to single stationary chamber PCR microfluidics that has been developed and widely investigated by other groups [138-141], the LightForge platform provides a highly scalable multi-chamber stationary PCR microfluidics. This has improved factors such as PCR throughput, analysis time and minimised errors through automation. Nonetheless investigation into the thermal design to ascertain temperature uniformity between the chambers is still to be conducted. The temperature uniformity is very critical since it bears influence on reliability, repeatability, sensitivity, efficiency and specificity of PCR amplification across different chambers[142].

2. *Assay time*: The LightForge system demonstrated that it requires over 3 ½ hours to complete real-time PCR and HRMA. In comparison to the flow-through PCR, this duration is relatively long. In flow-through PCR microfluidics the stationary chambers are replaced by flowing the PCR master mix solution continuously and repeatedly through three different temperature zones required for PCR amplification [143]. However, this advantage of having shorter PCR time is achieved at costs that are partly addressed by the LightForge system. The costs include a fixed number of cycles that are dictated by the chip design, automation of realtime data acquisition and multiplexing of assays which are very challenging when using the flow-through PCR microfluidics approach. It can also be argued that 3 ½ for thousands of PCR experiments on a LightForge platform can certainly be better than conducting a few hundreds of PCR experiments for 1 hour in conventional systems such as the Roche LightCycler® 480[144].

3. *Surface treatment*: The LightForge platform demonstrated its capability to do real-time PCR and HRMA on a chip. This was only achieved as a proof of principle by employing the dynamic surface passivation approach. In this approach the passivation occurred during the practical operation of the microfluidic PCR when we added the non-ionic surfactant Tween 20 to the PCR master mix solution as a passivation agent. Although we only optimised Tween 20 in our assays, there are several passivation agents that can be investigated in pursuit of an improved signal in future. These agents include protein adjuvant-Bovine Serum Albumin (BSA) and polymer based solutions such as polyethylene glycol (PEG)[142]. LightForge microfluidic chips can also be subjected to static passivation where we pre-coat the inner surfaces of the channels using substances compatible with PCR during fabrication. This may involve silicon oxide or chemicals that act as salinizing agents[145, 146].

4. *Data acquisition*: Many researchers have explored end point detection of PCR products by measuring fluorescence after PCR completion to establish the success or failure of amplification[132, 147]. However, this approach of inferring initial target DNA concentration based on the ultimate amplified PCR products is very unreliable[142]. The LightForge system we have developed has the potential to resolve some of these challenges as it can kinetically quantify fluorescence signals that result from the binding of LC Green fluorescence dye as a function of the increasing double stranded DNA copies. We have also demonstrated that LightForge has the ability to detect the yields of a PCR as soon as the products increase appreciably to the detection threshold in contrast to waiting until completion of all pre-programed PCR cycles.

5. *Sensitivity*: Analytical sensitivity is a very critical parameter of any diagnostic qPCR test especially with *Mycobacteria tuberculosis* where research has shown paucibacillary nature in

paediatrics and immunocompromised individuals [148, 149]. The aspects affecting sensitivity of PCR microfluidics have not been widely studied despite research showing that detection of rare targets or trace genomic material from environmental and/or clinical samples is a great challenge for microfluidic devices [150]. In addition, inconsistencies in the reaction chemistry (e.g., in salt concentration) is known to significantly alter the HR-Melting temperature[151]. In this study, the LightForge platform in conjunction with the dead ended digital PCR chip (**Figure 4.15** Results Chapter 4) with reactor chamber volumes of 1.8 nL demonstrated its potential to detect DNA concentrations within the digital realm (individual Mtb genomes per chamber). The 81-bp RIF resistance determining region (RRDR) *rpoB,* was adequately amplified with a total of 35 cycles in about 3 ½ hrs. The sensitivity of LightForge PCR microfluidics was demonstrated with its ability to amplify the *rpoB* gene at concentrations of DNA that theoretically allow only 50% of 180 PCR chambers of the dead ended digital PCR chip to brighten up. This shows potential for future heterogeneity studies on this LightForge platform.

6. *Specificity*: By definition this is the fraction of samples without the target analyte that generates a positive result and technically an ideal assay should have this fraction as zero[149]. The signal that was detectable using the LightForge real-time PCR assay step had contribution from both specific and non-specific products; hence this bears implication on the qualitative or quantitative result of the analysis. To circumvent this problem, the post PCR HRMA using LC Green DNA saturating fluorescent dye confirmed the specificity of the assay since distinct melt profiles were recorded for specific samples. For instance; i) replicated overlapping 1st derivative melt peaks corresponding to the 81-bp RIF resistance determining region (RRDR) *rpoB* amplicon, ii) replicated overlapping positive control peaks for 234-bp *gyrA* region amplicons that includes several OFLX resistance-associated sites (See **Figure 4.7** Results Chapter 4) and iii) distinctly profiled non template control signal were differentiated. However, as previously discussed the temperature uniformity of the heating block was unreliable and imprecise from one experiment to the next. This is a very critical drawback of the system that bore influence on efficiency and specificity of PCR amplification across different chambers thereby restricting us to confidently tally a specific melting temperature to an Mtb clinical strain mutation. However, our incorporation of a susceptible H37RV standard as a reference strain allowed us to distinguish specific classes of SNP genotyping within drug resistant Mtb strains. This distinction was done in a manner that is in agreement with what most commercial systems do.

7. *Simplicity*: We chose PCR as a diagnostic assay since it has been well renowned for many years and its advantages and disadvantages are widely understood[149]. Furthermore, with the recent invention of HRMA as a simple and effective method for characterising PCR products[136], we saw this as an opportunity to develop a SNP genotyping platform. The LightForge system we

have built does not only integrate PCR and HRMA but also has the ability to automatically handle and manipulate fluids at a nanoscale. This strength gives it potential to contribute towards accuracy and repeatability of assays by minimum need for human involvement. The LightForge system has a controlling computer algorithm that runs on a temperature feedback loop. This implies that the sequence of events carried by the system is dictated by the thermal instructions allowing the 3 step PCR to occur and HRMA directly following. The Cepheid GeneXpert® has shown promise as an automated desktop machine with capability of conducting real-time PCR and simultaneously detecting Mycobacrteria tuberculosis as well as rifampicin resistance directly from sputum[27]. This is the typical simplicity we project for the highly scalable LightForge platform by future incorporation of a sputum processing module that is able to extract microbes and lyse them leading to the release of genomic material prior to real-time PCR and HRMA.

8. *Cost*: The trend towards smaller reaction volumes by PCR microfluidics is being largely influenced by the fact that PCR reagents are very expensive. Furthermore, the communities that are largely in need of diagnostic services cannot afford currently available assays. The current PCR-based gold standard, the Cepheid GeneXpert®, presents with an important limitation because of its cost which is highly prohibitive for a disease that principally affects poor community settings. The pricing of the GeneXpert has been tiered and heavily subsidised for developing countries. A single Cepheid GeneXpert® machine costs between US$17,000-$62,000. Furthermore the single use disposable test-cartridges cost between US$17-$120[27]. Our miniaturized LightForge PCR microfluidic devices bring many improvements towards decreased cost of fabrication and usage. The system we have built shows potential towards reduced consumption of biological sample and reagents necessary for PCR; label free detection; long shelf life; and economical disposal of the used PCR chips. In addition, the LightForge system's ability to cost effectively perform large numbers of parallel PCR amplifications and HRMA analyses on a single PCR microfluidic chip can lead to the generation of more accurate information. This will ultimately translate to a greater understanding of particular bioassays, which are currently costly, challenging, impractical, or even hopeless to perform on macro-scale PCR devices. Since TB mainly affects people in low income settings who cannot afford to pay the current costs for diagnostics and treatment, the potential principal solution to this challenge is the LightForge system. Therefore, we believe that the LightForge system has the potential to present a more sustainable business model capable of significantly reducing the cost per patient.

5.4. Possible Future LightForge System Applications

5.4.1. Digital PCR

The current PCR based gold standard systems for diagnosis, are analog in nature, with a population averaged diagnostic indicator being measured from the total sample volume[152]. With the high scalability nature of the LightForge system, it has potential to bring a solution to this problem by utilising digital PCR (dPCR). Digital PCR is a refinement of conventional PCR that is performed by partitioning a minimally diluted sample and conventional PCR mixture into very large number of separate reaction volumes, such that there is either one target molecule or zero per individual reaction[23]. The LightForge system demonstrated the fundamental concept of making digital measurements as can be seen in **Figure 4.16**(**C**) (Results Chapter 4) which shows the image after thermal cycling performed to endpoint. All target containing reaction chambers became brightly fluorescent while compartments without targets only displayed background fluorescence. This approach can be statistically validated by Poisson distribution statistics where the chances of target molecules to be co-located in the same chamber can be calculated and put into account[153]. Having true single target molecules to be interrogated in isolation allows for multiplex or heterogeneity investigating assays to be conducted[23].

Lenaerts and her team recently reported that Tuberculosis lesions are complex and consist of extremely dynamic microenvironments. They further suggest that immunopathological diversity of cavities and granulomas creates a plethora of microenvironments that force *M. tuberculosis* bacilli to adapt. This ultimately affects processes such as metabolism, DNA replication and relatively the density of microbial subpopulation. All these factors subsequently lead to respective susceptibility or resistance to chemotherapeutic agents[128]. This mechanism is believed to be another major driving force towards heterogeneity as well as MDR and XDR-TB development among patients. Therefore the future applications of LightForge are directed towards detecting this heterogeneity from the onset to guide proper dispensation of medicines. Digital PCR (dPCR) is a very versatile technique with many research groups having demonstrated its versatility. For instance, it has been used for the detection of rare alleles in cancer cells or genetic disorders as well as RNA viral load detection[154, 155]. It has also been used to study gene expression and copy number variations in heterogeneous cell populations as well as to run a quality control tests on DNA samples before sequencing [156-158]. This technology can also be applied to assays with limited sample material. These are some of the future possibilities that the LightForge system may be able to fulfil in future.

5.4.2. Other Applications

The versatility of LightForge PCR microfluidics through compatibility with a variety of architectures, displays wide future biomedical and bioanalytical applications conveniently at a cheaper cost. Some of these applications may involve bacterial contamination and/or infection detection- including *E.coli*[159]; *Salmonella typhimurium*[160]; *M. tuberculosis*[161]. Viral infection detection including Human Immunodeficiency Virus (HIV)[162]; human papillomavirus (HPV)[133]; hepatitis virus[163]; and Protozoan parasitic infection detection including malaria[164]. Another possible area of application would be in pharmacogenetics, where we could use the system to rapidly detect inherited differences in drug targets, and drug disposition in the form of drug receptors as well as drug transporters[165]. However it should be noted that the applications of LightForge PCR microfluidics are not potentially confined to the fields we mentioned here. Principally, in future the LightForge system technology can be applied to many cases where minute nucleic acid materials DNA/RNA have to be amplified and analysed subsequently. These are just some of the possibilities that the LightForge system can achieve and with time this can be escalated to broader research spheres.

CHAPTER 6

6. Conclusions

Principally we have demonstrated that the fully automated LightForge system we have developed at K-RITH offers a highly scalable microfluidic platform for interrogation of tuberculosis strains using Real-Time PCR and High Resolution Melt Analysis (HRMA) on a chip. We have used this system to identify clinical TB strains resistant to rifampicin—a frontline drug used to treat tuberculosis; relative to a susceptible strain H37RV, based on mutations in the *rpo*B gene. This system has the potential to contribute towards a low-cost solution for diagnosis of multidrug resistant tuberculosis—a critical global healthcare challenge. LightForge system has detected mutations linked to rifampicin resistance, including single nucleotide polymorphisms (SNPs), in a manner harmonious with commercial systems. In preparation for diagnosis of clinical isolates, this LightForge approach is now being expanded to incorporate detection of genetic markers linked with resistance to other TB drugs that include *gyr*A for fluoroquinolones; and *kat*G/Mab-*inh*A for isoniazid[166]. Future PCR assays that are attuned to any resistance conferring molecular signature can be developed using appropriate probes to improve LightForge specificity. Our top priority at the moment is to make further efforts to improve the LightForge system's sensitivity; specificity; speed; heteroresistance detection capacity—through dPCR; and simplicity towards low cost solution to *Mycobacterium tuberculosis* resistance detection. The real-time PCR and HRMA demonstrated by the LightForge system are potentially applicable not only to *Mycobacterium tuberculosis* but also to other pathogens. This includes the capability to accurately diagnose mixed infections, detect drug-resistant strains, and render other genetic markers available as diagnostic tools for laboratory and field environments. We also plan to integrate PCR with sample preparation on a single chip as currently sample pre-preparation is still required. This is useful when using environmental or otherwise very complex samples such as whole blood that may contain PCR inhibiting contaminants. Although the current version of the LightForge system relies on a microscope and a camera, future improvement considerations include employing other methods amenable with miniaturization such as surface plasmon resonance (SPR).

In conclusion, it is conceivable that the LightForge system could address not only *Mycobacterium tuberculosis* but also a variety of other tropical diseases in both developed and underserved regions. This research highlights the immense diversity of creating such a system that can be escalated to achieve universal welfare.

THE END

British Prime Minister Robert Peel on Michael Faraday's discoveries on electricity and magnetism

Prime Minister: *"What good is it?"*

Faraday: *"What good is a new-born baby?"*

THESIS APPENDICES

Appendix A: Microfabrication Protocols of PCR Microfluidic Chips.

Jerome Rogich Spider Design Chip Mold Fabrication.

Flow Mold

Layer 1 (Positive Photoresist)

Priming:	HDMS vapor 2 min in plastic container (STP)
Spin MAP 1275:	1200 rpm x 60 s, Acceleration=133rpm/sec
	Film thickness = 11 microns
Soft Bake:	contact bake on hotplate
	95 °C x 90 s
Expose Wafer:	15 sec on mask aligner
Develop:	ma-D 531 Developer, rinse with deionised water (H_2O)
	and dry under house dry air with and air gun
Incubate:	Overnight at room temperature, light shielded
Rounding:	Contact bake on hotplate
	65 °C x 3 min and115 °C x 15 min
Profile:	Profilometer (KLA Tencor D-120) to establish height and geometry
Hard Bake:	Thermoscientific oven: a) Set oven to 120 °C and place mold
	b) Ramp up 120 °C to 180° C
	c) Hold oven for 1 hr at 180 °C
	d) Ramp down180 °C to 120 °C
Cooling:	To room temperature

Layer 2 (Negative Photoresist)

Spin SU8 100:	1200 rpm x 60 s, Acceleration = 100 rpm/sec
	Film thickness = 190 microns
Pre-Exposure Bake:	contact bake on hotplate
	5 min x 65 °C / 30 min x 95 °C / 1 min x 65 °C
Expose Wafer:	150 sec
Post-Exposure Bake:	2 min x 65 C / 12 min x 95 C / 1 min x 65 C

Develop: 100 % SU-8 Developer, rinse with fresh developer
dry under house dry air with an air gun

Control Mold (Negative Photoresist)

Spin SU8 2015: 1500 rpm x 60 s, Acceleration= 270 rpm/sec
Film thickness = 23 microns
Pre-Exposure Bake: contact bake on hotplate
3 min x 65 °C / 5 min x 95 °C
Expose Wafer: 5 sec
Post-Exposure Bake: 5 min x 65 °C / 15 min x 95 °C
Develop: 100 % SU-8 Developer, rinse with fresh developer
dry under house dry air with an air gun

MSL Fabrication

Priming: all molds except for dummy layer,
TMCS vapor 3 min in plastic container (STP)

Flow layer

Cast Flow Layer: combine 5:1 GE 615 RTV (75 g A: 15 g B)
mix hybrid mixer: 5 min mix / 5 min degas
Molding: 60 g onto flow mold (150mm petri dish lined with Al foil)
Degas Flow Layer: pull vacuum in bell jar (approx 30 minutes)

Control Layer

Spin Control Layer: combine 20:1 GE 615 RTV (40 g A: 2 g B)
Mix hybrid mixer: 5 min mix / 5 min degas
Molding: dispense 5 mL on control layer
1800 rpm x 60 s / Acceleration =500 rpm/sec
Film thickness = 28 microns

Dummy layer

Spin Blank Layer:	combine 20:1 GE 615 RTV (40 g A: 2 g B)
mix hybrid mixer:	5 min mix / 5 min degas
Molding:	dispense 5 mL on blank 3’ wafer 2000 rpm x 60 s / 15 s ramp
	Film thickness = 30 microns

Curing

Cure Flow Layer:	Binder® oven 80 C x 40 min
Cure Control Layer:	Binder® oven 80 C x 40 min
Cure Blank Layer:	C x 40 min

Bonding

Flow Peeling:	Peel flow layer from mold, punch all flow inlet and outlet ports
Cutting:	Cut around periphery of desired flow layer area.
Control/ Flow Bonding:	Align to control layer using the Olympus SZX16 microscope
	Bake in convection oven 80 C x 40 min
Cutting:	Cut around periphery of thick layer avoiding damage to the mold
Peel Hybrid:	Peel bonded hybrid device from control mold
	Punch all control ports
Blank/Hybrid Bonding:	Place control/flow hybrid structure on blank,
	ensuring no air bubbles, no collapsed valves
	Binder® oven 80 °C x 8 hours
Final Inspection:	Quality control is done through inspection using the
	Olympus SZX16 microscope

* spin parameters need to be optimized for each batch.

Serpentine Design dPCR Chip Mold Fabrication.

Flow Mold

Layer 1 (Positive Photoresist)

Priming: HDMS vapor 2 min in plastic container (STP)

Spin MAP 1275: 1200 rpm x 60 s, Acceleration=133rpm/sec
Film thickness = 11 microns

Soft Bake: contact bake on hotplate
95 °C x 90 s

Expose Wafer: 15 sec

Develop: ma-D 531 Developer, rinse with deionised water (H_2O)
and dry under house dry air with air gun

Incubate: Overnight at room temperature, light shielded

Rounding: Contact bake on hotplate
65 °C x 3 min and115 °C x 15 min

Profile: Profilometer (KLA Tencor D-120) to establish height and geometry

Hard Bake: Thermoscientific oven: a) Set oven to 120 °C and place mold
b) Ramp up 120 °C to 180° C
c) Hold oven for 1 hr at 180 °C
d) Ramp down180 °C to 120 °C

Cooling: To room temperature

Layer 2 (Negative Photoresist)

Spin SU8 100: 1200 rpm x 60 s, Acceleration = 100 rpm/sec
Film thickness = 180 microns

Pre-Exposure Bake: contact bake on hotplate
5 min x 65 °C / 30 min x 95 °C / 1 min x 65 °C

Expose Wafer: 150 sec

Post-Exposure Bake: 2 min x 65 C / 12 min x 95 C / 1 min x 65 C

Develop: 100 % SU-8 Developer, rinse with fresh developer
dry under house dry air with an air gun

Control Mold (Negative Photoresist)

Spin SU8 2015: 1500 rpm x 60 s, Acceleration= 270 rpm/sec

Film thickness = 23 microns

Pre-Exposure Bake: contact bake on hotplate

3 min x 65 °C / 5 min x 95 °C

Expose Wafer: 5 sec

Post-Exposure Bake: 5 min x 65 °C / 15 min x 95 °C

Develop: 100 % SU-8 Developer, rinse with fresh developer

dry under house dry air with an air gun

MSL Fabrication

Priming: all molds except for dummy layer,
TMCS vapor 3 min in plastic container (STP)

Flow layer

Cast Flow Layer: combine 5:1 GE 615 RTV (75 g A: 15 g B)

mix hybrid mixer: 5 min mix / 5 min degas

Molding: 60 g onto flow mold (150mm petri dish lined with Al foil)

Degas Flow Layer: pull vacuum in bell jar (approx 30 minutes)

Control Layer

Spin Control Layer: combine 20:1 GE 615 RTV (40 g A: 2 g B)

Mix hybrid mixer: 5 min mix / 5 min degas

Molding: dispense 5 mL on control layer

1800 rpm x 60 s / Acceleration =500 rpm/sec

Film thickness = 28 microns

Dummy layer

Spin Blank Layer: combine 20:1 GE 615 RTV (40 g A: 2 g B)

mix hybrid mixer: 5 min mix / 5 min degas

Molding: dispense 5 mL on blank 3’ wafer 2000 rpm x 60 s / 15 s ramp

Film thickness = 30 microns

Curing

Cure Flow Layer: Binder® oven 80 C x 40 min

Cure Control Layer: Binder® oven 80 C x 40 min

Cure Blank Layer: C x 40 min

Bonding

Flow Peeling: Peel flow layer from mold, punch all flow inlet and outlet ports

Cutting: Cut around periphery of desired flow layer area.

Control/ Flow Bonding:	Align to control layer using the Olympus SZX16 microscope
	Bake in convection oven 80 C x 40 min
Cutting:	Cut around periphery of thick layer avoiding damage to the mold
Peel Hybrid:	Peel bonded hybrid device from control mold
	Punch all control ports
Blank/Hybrid Bonding:	Place control/flow hybrid structure on blank,
	ensuring no air bubbles, no collapsed valves
	Binder® oven 80 °C x 8 hours
Final Inspection:	Quality control is done through inspection using the
	Olympus SZX16 microscope

* spin parameters need to be optimized for each batch.

Web Randomising Design dPCR Chip Mold Fabrication.

Flow Mold

Layer 1 (Positive Photoresist)

Priming: HDMS vapor 2 min in plastic container (STP)

Spin MAP 1275: 1200 rpm x 60 s, Acceleration=133rpm/sec
Film thickness = 11 microns

Soft Bake: contact bake hotplate
95 °C x 90 s

Expose Wafer: 15 sec

Develop: ma-D 531 Developer, rinse with deionised water (H_2O)
and dry under house dry air with an air gun

Incubate: Overnight at room temperature, light shielded

Rounding: Contact bake on hotplate
65 °C x 3 min and115 °C x 15 min

Profile: Profilometer (KLA Tencor D-120) to establish height and geometry

Hard Bake: Thermoscientific oven: a) Set oven to 120 °C and place mold
b) Ramp up 120 °C to 180° C
c) Hold oven for 1 hr at 180 °C
d) Ramp down180 °C to 120 °C

Cooling: To room temperature

Layer 2 (Negative Photoresist)

Spin SU8 100: 1200 rpm x 60 s, Acceleration = 100 rpm/sec
Film thickness = 168 microns

Pre-Exposure Bake: contact bake on hotplate
5 min x 65 °C / 30 min x 95 °C / 1 min x 65 °C

Expose Wafer: 150 sec

Post-Exposure Bake: 2 min x 65 C / 12 min x 95 C / 1 min x 65 C

Develop: 100 % SU-8 Developer, rinse with fresh developer
dry under house dry air with an air gun

Control Mold (Negative Photoresist)

Spin SU8 2015: 1500 rpm x 60 s, Acceleration= 270 rpm/sec
Film thickness = 23 microns

Pre-Exposure Bake: contact bake on hotplate
3 min x 65 °C / 5 min x 95 °C

Expose Wafer: 5 sec

Post-Exposure Bake: 5 min x 65 °C / 15 min x 95 °C

Develop: 100 % SU-8 Developer, rinse with fresh developer
dry under house dry air with an air gun

MSL Fabrication

Priming: all molds except for dummy layer,
TMCS vapor 3 min in plastic container (STP)

Flow layer

Cast Flow Layer: combine 5:1 GE 615 RTV (75 g A: 15 g B)

mix hybrid mixer: 5 min mix / 5 min degas

Molding: 60 g onto flow mold (150mm petri dish lined with Al foil)

Degas Flow Layer: pull vacuum in bell jar (approx 30 minutes)

Control Layer

Spin Control Layer: combine 20:1 GE 615 RTV (40 g A: 2 g B)

Mix hybrid mixer: 5 min mix / 5 min degas

Molding: dispense 5 mL on control layer
1800 rpm x 60 s / Acceleration =500 rpm/ sec
Film thickness = 28 microns

Dummy layer

Spin Blank Layer: combine 20:1 GE 615 RTV (40 g A: 2 g B)

mix hybrid mixer: 5 min mix / 5 min degas

Molding: dispense 5 mL on blank 3’ wafer 2000 rpm x 60 s / 15 s ramp
Film thickness = 30 microns

Curing

Cure Flow Layer: Binder® oven 80 C x 40 min

Cure Control Layer: Binder® oven 80 C x 40 min

Cure Blank Layer: C x 40 min

Bonding

Flow Peeling:	Peel flow layer from mold, punch all flow inlet and outlet ports
Cutting:	Cut around periphery of desired flow layer area.
Control/ Flow Bonding:	Align to control layer using the Olympus SZX16 microscope
	Bake in convection oven 80 C x 40 min
Cutting:	Cut around periphery of thick layer avoiding damage to the mold
Peel Hybrid:	Peel bonded hybrid device from control mold
	Punch all control ports
Blank/Hybrid Bonding:	Place control/flow hybrid structure on blank,
	ensuring no air bubbles, no collapsed valves
	Binder® oven 80 °C x 8 hours
Final Inspection:	Quality control is done through inspection using the
	Olympus SZX16 microscope

* spin parameters need to be optimized for each batch.

Dead Ended Rows Design dPCR Chip Mold Fabrication.

Flow Mold

Layer 1 (Positive Photoresist)

Priming: HDMS vapor 2 min in plastic container (STP)

Spin MAP 1275: 1200 rpm x 60 s, Acceleration=133rpm/sec
Film thickness = 11 microns

Soft Bake: contact bake hotplate
95 °C x 90 s

Expose Wafer: 15 sec

Develop: ma-D 531 Developer, rinse with deionised water (H_2O) and dry under house dry air with an air gun

Incubate: Overnight at room temperature, light shielded

Rounding: Contact bake on hotplate
65 °C x 3 min and115 °C x 15 min

Profile: Profilometer (KLA Tencor D-120) to establish height and geometry

Hard Bake: Thermoscientific oven: a) Set oven to 120 °C and place mold
b) Ramp up 120 °C to 180° C
c) Hold oven for 1 hr at 180 °C
d) Ramp down180 °C to 120 °C

Cooling: To room temperature

Layer 2 (Negative Photoresist)

Spin SU8 100: 1200 rpm x 60 s, Acceleration = 100 rpm/sec
Film thickness = 158 microns

Pre-Exposure Bake: contact bake hotplate
5 min x 65 °C / 30 min x 95 °C / 1 min x 65 °C

Expose Wafer: 150 sec

Post-Exposure Bake: 2 min x 65 C / 12 min x 95 C / 1 min x 65 C

Develop: 100 % SU-8 Developer, rinse with fresh developer
dry under house dry air with air gun

Control Mold (Negative Photoresist)

Spin SU8 2015: 1500 rpm x 60 s, Acceleration= 270 rpm/sec
Film thickness = 23 microns

Pre-Exposure Bake: contact bake on hotplate

3 min x 65 °C / 5 min x 95 °C

Expose Wafer: 5 sec

Post-Exposure Bake: 5 min x 65 °C / 15 min x 95 °C

Develop: 100 % SU-8 Developer, rinse with fresh developer

dry under house dry air with an air gun

MSL Fabrication

Priming: all molds except for dummy layer,
TMCS vapor 3 min in plastic container (STP)

Flow layer

Cast Flow Layer: combine 5:1 GE 615 RTV (75 g A: 15 g B)

mix hybrid mixer: 5 min mix / 5 min degas

Molding: 60 g onto flow mold (150mm petri dish lined with Al foil)

Degas Flow Layer: pull vacuum in bell jar (approx 30 minutes)

Control Layer

Spin Control Layer: combine 20:1 GE 615 RTV (40 g A: 2 g B)

Mix hybrid mixer: 5 min mix / 5 min degas

Molding: dispense 5 mL on control layer

1800 rpm x 60 s / Acceleration =500 rpm/ sec

Film thickness = 28 microns

Dummy layer

Spin Blank Layer: combine 20:1 GE 615 RTV (40 g A: 2 g B)

mix hybrid mixer: 5 min mix / 5 min degas

Molding: dispense 5 mL on blank 3’ wafer 2000 rpm x 60 s / 15 s ramp

Film thickness = 30 microns

Curing

Cure Flow Layer: Binder® oven 80 C x 40 min

Cure Control Layer: Binder® oven 80 C x 40 min

Cure Blank Layer: C x 40 min

Bonding

Flow Peeling: Peel flow layer from mold, punch all flow inlet and outlet ports

Cutting: Cut around periphery of desired flow layer area.

Control/ Flow Bonding: Align to control layer using the Olympus SZX16 microscope

Bake in convection oven 80 C x 40 min

Cutting:	Cut around periphery of thick layer avoiding damage to the mold
Peel Hybrid:	Peel bonded hybrid device from control mold
	Punch all control ports
Blank/Hybrid Bonding:	Place control/flow hybrid structure on blank,
	ensuring no air bubbles, no collapsed valves
	Binder® oven 80 °C x 8 hours
Final Inspection:	Quality control is done through inspection using the
	Olympus SZX16 microscope

* spin parameters need to be optimized for each batch.

Appendix B: LightForge Data for a Single Experiment

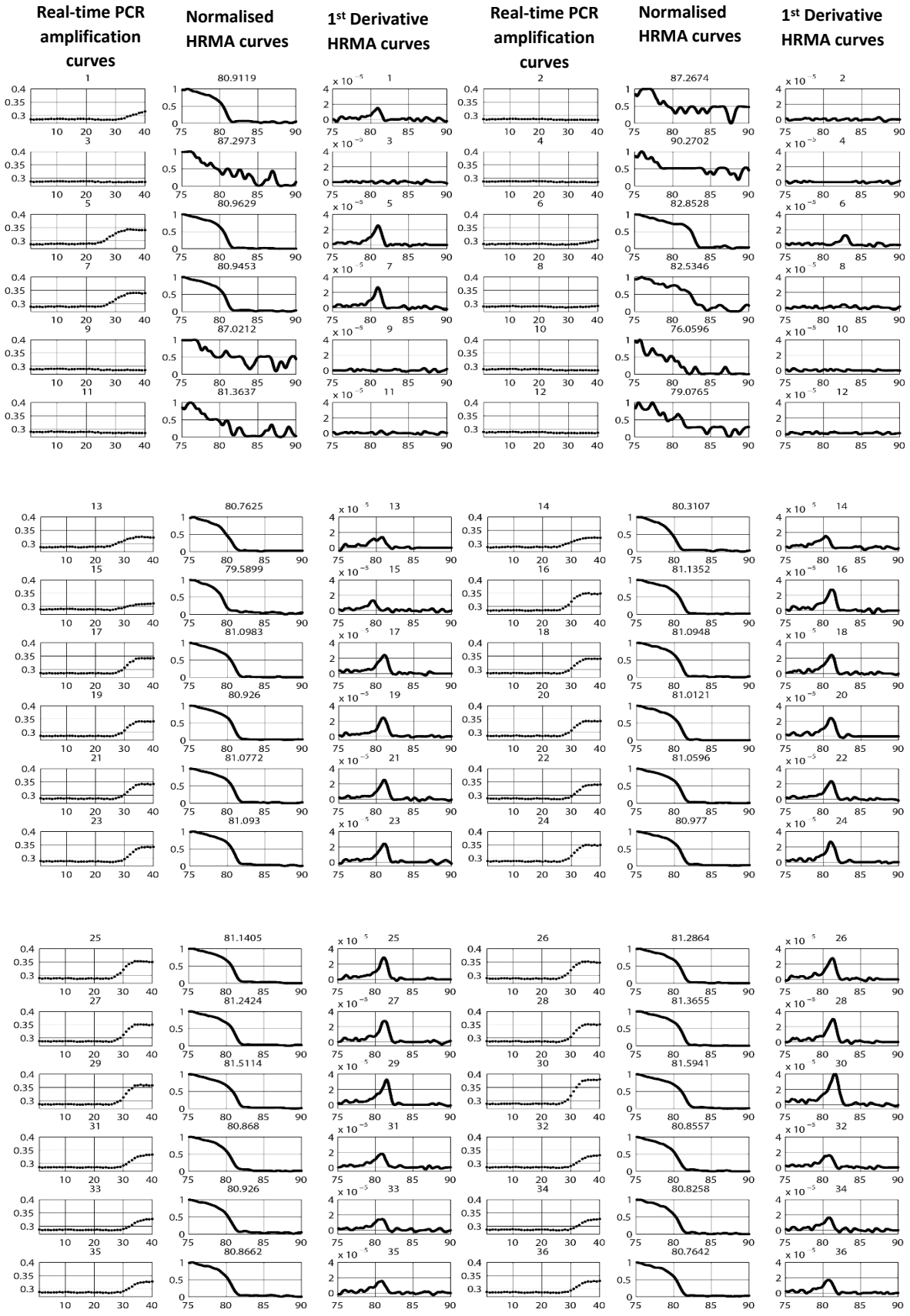

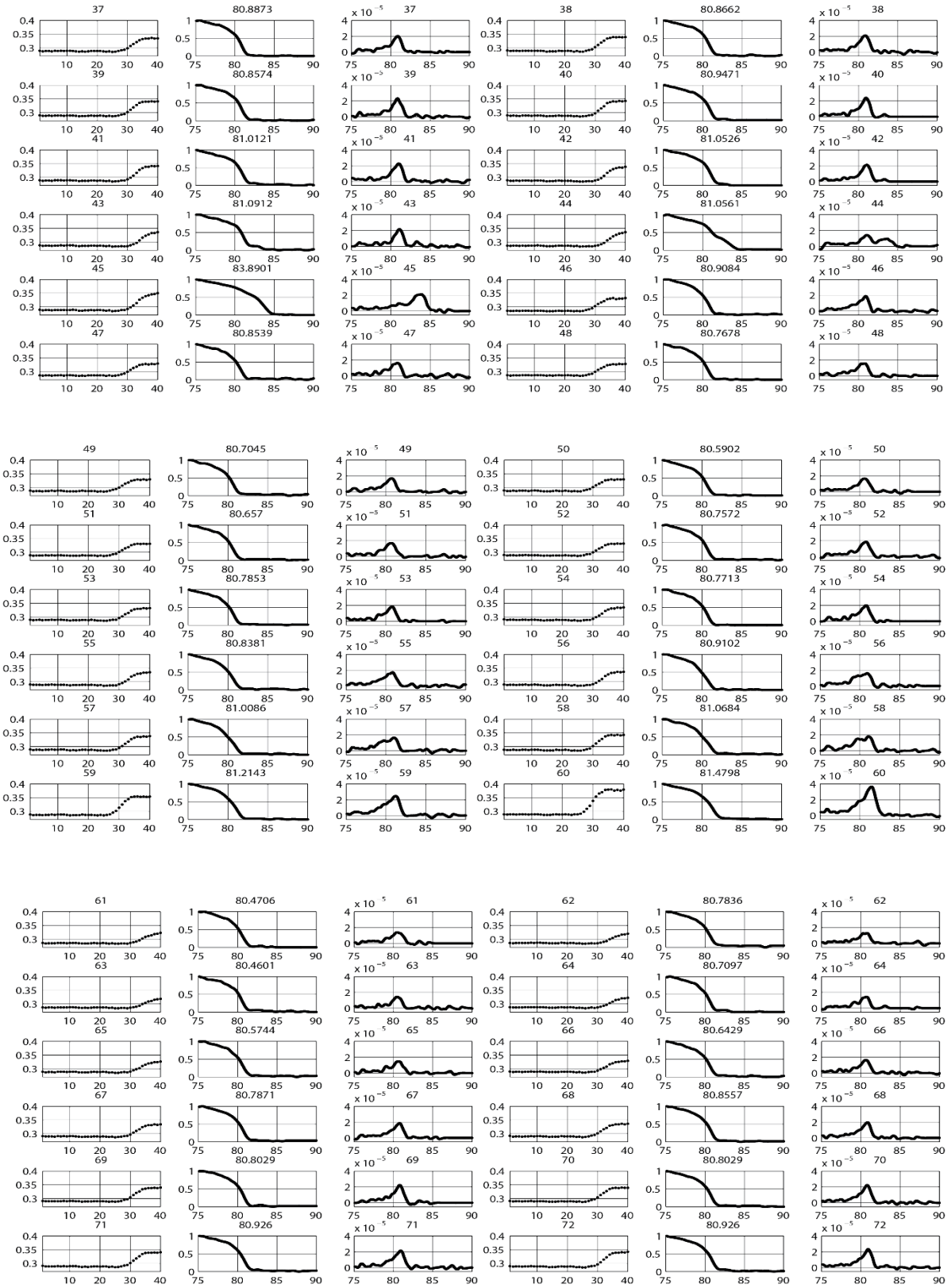
37 80.8873 37 38 80.8662 38
39 80.8574 39 40 80.9471 40
41 81.0121 41 42 81.0526 42
43 81.0912 43 44 81.0561 44
45 83.8901 45 46 80.9084 46
47 80.8539 47 48 80.7678 48
49 80.7045 49 50 80.5902 50
51 80.657 51 52 80.7572 52
53 80.7853 53 54 80.7713 54
55 80.8381 55 56 80.9102 56
57 81.0086 57 58 81.0684 58
59 81.2143 59 60 81.4798 60
61 80.4706 61 62 80.7836 62
63 80.4601 63 64 80.7097 64
65 80.5744 65 66 80.6429 66
67 80.7871 67 68 80.8557 68
69 80.8029 69 70 80.8029 70
71 80.926 71 72 80.926 72

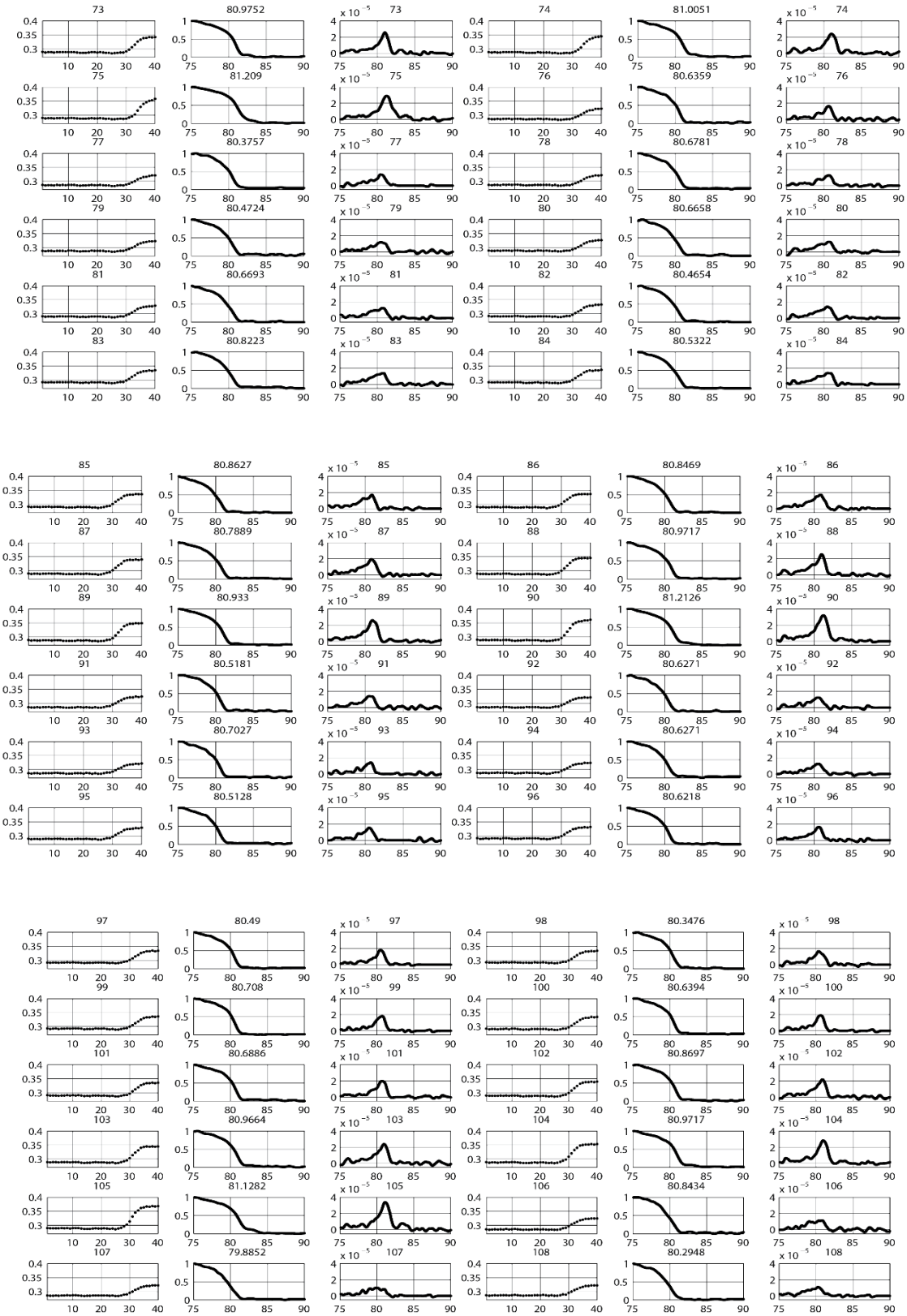
73
80.9752
73
74
81.0051
74
75
81.209
75
76
80.6359
76
77
80.3757
77
78
80.6781
78
79
80.4724
79
80
80.6658
80
81
80.6693
81
82
80.4654
82
83
80.8223
83
84
80.5322
84
85
80.8627
85
86
80.8469
86
87
80.7889
87
88
80.9717
88
89
80.933
89
90
81.2126
90
91
80.5181
91
92
80.6271
92
93
80.7027
93
94
80.6271
94
95
80.5128
95
96
80.6218
96
97
80.49
97
98
80.3476
98
99
80.708
100
80.6394
100
101
80.6886
102
80.8697
102
103
80.9664
104
80.9717
104
105
81.1282
106
80.8434
106
107
79.8852
108
80.2948
108

Appendix C: MATLAB Data Processing Code

```
%Author: Tawanda_Mandizvo

%K-RITH Bioengineering%
%%%%%%%%%%%%%%%%%%%%%%%%%%%%%%%%%%%%%%%%
fclose all; clear all; close all;
tic;
%Set up directories
%%%%%%%%%%%%%%%%%%%%%%%%%%%%%%%%%%%%%%%%%%%%%%%%%%%
file_name = 'High_Resolution_MeltRecords.xls';
file_name2 = 'Real_time_PCR_Records.xls';

data_directory = 'C:\Usersxxxxxxx'
my_file_name = strcat(data_directory,'\',file_name);
my_file_name2 = strcat(data_directory,'\',file_name2);

Temp_inc = 0.00001;
num_pts = 10000;

Amplif_data_array(1,1) = 0;
Amplif_Array = dlmread(my_file_name2);
my_ampliffile_name = strcat(file_name2,'Amplif.xls');

Melt_data_array(1,1) = 0;
Melt_Array = dlmread(my_file_name);
my_meltfile_name = strcat(my_file_name,'melt.xls');

Smoothed_data_array(1,1) = 0;
Smoothed_array = dlmread(my_file_name)
my_smoothedfile_name = strcat(my_file_name,'smooth.xls');

Norm_smoothed_data_array(1,1) = 0;
Norm_smoothed_array = dlmread(my_file_name);
my_norm_smoothedfile_name = strcat(my_file_name,'norm_smooth.xls');

Raw_data_array(1,1) = 0;
Raw_array = dlmread(my_file_name);
my_rawfile_name = strcat(my_file_name,'raw.xls');

%Melt_Array = dlmread('C:\Users\tawanda.mandizvo\Documents\Masters Research\Matlab\mbano man
rpob03Jun2014_03_45PM0\Records_MeltC.txt');

X0 = Melt_Array(:,3);
max_index = find(X0 == max(X0(:)));  %max_index = find(Array == max(Array))
X = X0(1:max_index);

MeltDD(1,1)=0;
Fullw(1,1)=0;

reactor_count = 0;

%%%%%%%%%%%%%%%%%%%%%%%%%%%%Amplification
Curves%%%%%%%%%%%%%%%%%%%%%%%%%%%%%%%%%%%%%%%%%%%%%%%%%%%%%%%%
%%%
```

```
for react = 5:41  %5:25

   reactor_count = reactor_count+1;
   Y0 = Melt_Array(:,react);
   Y = Y0(1:max_index);

   %Y = (Y1 - min(Y1)) / ( max(Y1) - min(Y1) );

%%%%%%%%%%%%%%%%%%%%%%%%%%%%%%%%%%%%%%%%%%%%%%%%%%%%%%%%%
%%%%%%%%%%%%%%%%%%%%%%%%%%%%%
   f_ = clf;
   figure(f_);
   set(f_,'Units','Pixels','Position',[658 269 688 485]);
   % Line handles and text for the legend.
   legh_ = [];
   legt_ = [3];
   % Limits of the x-axis.
   xlim_ = [Inf -Inf];
   % Axes for the plot.
   ax_ = axes;
   set(ax_,'Units','normalized','OuterPosition',[0 0 1 1]);
   set(ax_,'Box','on');
   axes(ax_);
   hold on;

   % --- Plot data that was originally in data set "Y vs. X"
   X = X(:);
   Y = Y(:);
   h_ = line(X,Y,'Parent',ax_,'Color',[0.333333 0 0.666667],...
      'LineStyle','none', 'LineWidth',1,...
      'Marker','.', 'MarkerSize',12);
   xlim_(1) = min(xlim_(1),min(X));
   xlim_(2) = max(xlim_(2),max(X));
   legh_(end+1) = h_;
   legt_{end+1}z = 'Y vs. X';

   % Nudge axis limits beyond data limits
   if all(isfinite(xlim_))
      xlim_ = xlim_ + [-1 1] * 0.01 * diff(xlim_);
      set(ax_,'XLim',xlim_)
   else
      set(ax_, 'XLim',[74.819999999999993, 93.180000000000007],'FontSize', 30);
   end

   % --- Create fit "fit 1"
   fo_ = fitoptions('method','SmoothingSpline','SmoothingParam',0.991);
   ok_ = isfinite(X) & isfinite(Y);
   if ~all( ok_ )
      warning( 'GenerateMFile:IgnoringNansAndInfs',...
         'Ignoring NaNs and Infs in data.' );
   end
   ft_ = fittype('smoothingspline');

   % Fit this model using new data
   cf_ = fit(X(ok_),Y(ok_),ft_,fo_);
```

```
%%%%%%%%%%%%%%%%%%%%%%%%%%%%%%%%%%%%%%%%%%%%%%%%%%%%%%%%%%%%%%%%%
%%%%%%%%%%%%%%%%%%%%%%%%%%%%%%

   newX = linspace(min(X), max(X), num_pts);

   my_y = (cf_(newX));
   my_t = newX;
   my_y2 = (my_y - min(my_y)) / ( max(my_y) - min(my_y) );
   % %    ---------------------------------------------------------------------------
   %% Plot -dRFU/dT from Fitted Melt Data
   %%---------------------------------------------------
   dy2 = -diff((cf_(newX)));
   dt2 = my_t(2:length(my_t));


%%%%%%%%%%%%%%%%%%%%%%%%%%%%%%%%%%%%%%%%%%%%%%%%%%%%%%%%%%%%%%%%%
%%

   Melt_peak_index = find(dy2 == max(dy2(:)));
   Melt_temp = dt2(Melt_peak_index);

   %%%%%%%%
   %1. Raw data:                X, Y
   %1. smoothed data:           my_t, my_y
   %1. normalized smoothed data:   my_t, my_y2
   %1. MELT profile:            dt2,dy2


%%%%%%%%%%%%%%%%%%%%%%%%%%%%%%%%%%%%%%%%%%%%%%%%%%%%%%%%%%%%%%%%%
%%%%%%%%%%%%%%%%%%%%%%%%%%


   %Record Melt Data in file
   fid = fopen(my_meltfile_name, 'a'); %a === append to existing file, w === overwrite existing fil (create new
file)

   n = size(dt2);;
   n2 = n(2);


   for k3 = 1:n2
      if reactor_count==1
         Melt_data_array(k3,1) = k3;
         Melt_data_array(k3,2) = dt2(k3);
         Melt_data_array(k3,reactor_count+2) = dy2(k3);
      else
         Melt_data_array(k3,reactor_count+2) = dy2(k3);
      end

   end


%%%%%%%%%%%%%%%%%%%%%%%%%%%%%%%%%%%%%%%%%%%%%%%%%%%%%%%%%%%%%%%%%
%%%%%%%%%%%%%%%%%%%%%%%%%%%%
   %      Record Raw Data in file
   fid = fopen(my_rawfile_name, 'a'); %a === append to existing file, w === overwrite existing fil (create new
file)
```

```
    n = size(X);;
    n2 = n(2);


    for k3 = 1:n2
        if reactor_count==1
            Raw_data_array(k3,1) = k3;
            Raw_data_array(k3,2) = X(k3);
            Raw_data_array(k3,reactor_count+2) = Y(k3);
        else
            Raw_data_array(k3,reactor_count+2) = Y(k3);
        end

    end

%%%%%%%%%%%%%%%%%%%%%%%%%%%%%%%%%%%%%%%%%%%%%%%%%%%%%%%%%%%%%%%%%%%%%%%%%%%%%%%%%%%%%%%%%
    %Record norm smoothed Data in file
    fid = fopen(my_smoothedfile_name, 'a'); %a === append to existing file, w === overwrite existing fil (create
new file)

    n = size(my_t);;
    n2 = n(2);


    for k3 = 1:n2
        if reactor_count==1
            Smoothed_data_array(k3,1) = k3;
            Smoothed_data_array(k3,2) = my_t(k3);
            Smoothed_data_array(k3,reactor_count+2) = my_y(k3);
        else
            Smoothed_data_array(k3,reactor_count+2) = my_y(k3);
        end

    end
    % %

%%%%%%%%%%%%%%%%%%%%%%%%%%%%%%%%%%%%%%%%%%%%%%%%%%%%%%%%%%%%%%%%%%%%%%%%%%%%%%%%%%%%%%%%%%%%
    %Record norm smoothed Data in file
    fid = fopen(my_norm_smoothedfile_name, 'a'); %a === append to existing file, w === overwrite existing fil
(create new file)

    n = size(my_t);;
    n2 = n(2);


    for k3 = 1:n2
        if reactor_count==1
            Norm_smoothed_data_array(k3,1) = k3;
            Norm_smoothed_data_array(k3,2) = my_t(k3);
            Norm_smoothed_data_array(k3,reactor_count+2) = my_y2(k3);
        else
            Norm_smoothed_data_array(k3,reactor_count+2) = my_y2(k3);
        end

    end
```

```
    n = size(reactor_count);;
    n2 = n(2);


    for k3 = 1:n2
        if reactor_count==1
            Max_data_array(k3,1) = k3;
            Max_data_array(k3,2) = reactor_count(k3);
            Max_data_array(k3,reactor_count+2) = max(dy2), k3;
        else
            Max_data_array(k3,reactor_count+2) =  max(dy2), k3;
        end

    end

end
%%%%%%%Random Number Generation
r1 = rand(1000,1);

Rand_num_array(1,1) = 0;

for sk = 1:reactor_count

    Rand_num_array(:,sk) = r1(sk,1);
end

for nk = 1:reactor_count

    Max_temp_index = find(Melt_data_array(:,2+nk) == max(Melt_data_array(:,2+nk)));
    Max_temp = Melt_data_array(Max_temp_index,2);

    MeltDD(nk,1)= nk;
    MeltDD(nk,2)= Max_temp

end

%%%%%%%%%%%%%%%%%%%%%%%%%%%%%%%%%%%%%%%%%%%%%%%%%%%%%%%%%%%%%%%%%%%%%%%%%%%%%%%%%%%%%%%%%%%%%%%%%%%%%%%%%%
for pCount = 1:reactor_count
    if ((pCount >= 1) && (pCount <= 49)) %if ((p == 1) || (p == 2) || (p == 4) || (p == 5)) % if((p == 1) && (p ==
2) && (p == 4) && (p == 5))
        if ((pCount == 2))% || (pCount ==9))
            hold on;
plot(Norm_smoothed_data_array(:,2),Norm_smoothed_data_array(:,pCount+2),'Color',[Rand_num_array(:,pCo
unt-1) Rand_num_array(:,pCount) Rand_num_array(:,pCount-1)],...
                'LineStyle','-', 'LineWidth',2,...
                'Marker','.', 'MarkerSize', 1);
        else
            if (pCount == 1)
                figure( 'Name', 'Normalized Smoothed Data' );
                plot(Norm_smoothed_data_array(:,2),Norm_smoothed_data_array(:,pCount+2), 'Color',[0 0 0],...
                    'LineStyle','-', 'LineWidth',2,...
                    'Marker','.', 'MarkerSize', 1);


                xlabel( 'Temperature', 'FontSize', 25 );
```

```
            ylabel( 'Ultra Fitted -dRFU/dT', 'FontSize', 25 );
            grid off;
        else
            hold on;
plot(Norm_smoothed_data_array(:,2),Norm_smoothed_data_array(:,pCount+2),'Color',[Rand_num_array(:,pCo
unt-2) Rand_num_array(:,pCount) Rand_num_array(:,pCount-1)],...
                'LineStyle','-', 'LineWidth',2,...
                'Marker','.', 'MarkerSize', 1);
        end
    end
  else
    if ((pCount == 14) || (pCount==19))
        hold on;
plot(Norm_smoothed_data_array(:,2),Norm_smoothed_data_array(:,pCount+2),'Color',[Rand_num_array(:,pCo
unt-2) Rand_num_array(:,pCount) Rand_num_array(:,pCount-1)],...
            'LineStyle','-', 'LineWidth',2,...
            'Marker','.', 'MarkerSize',1);
    else
        hold on;
plot(Norm_smoothed_data_array(:,2),Norm_smoothed_data_array(:,pCount+2),'Color',[Rand_num_array(:,pCo
unt-2) Rand_num_array(:,pCount) Rand_num_array(:,pCount-1)],...
            'LineStyle','-', 'LineWidth',2,...
            'Marker','.', 'MarkerSize',1);

    end



  end
end

for pCount = 1:reactor_count
  if ((pCount >= 1) && (pCount <= 49)) %if ((p == 1) || (p == 2) || (p == 4) || (p == 5)) % if((p == 1) && (p ==
2) && (p == 4) && (p == 5))
    if ((pCount == 2))% || (pCount ==9))
        hold on; plot(Melt_data_array(:,2),Melt_data_array(:,pCount+2),'Color',[Rand_num_array(:,pCount-1)
Rand_num_array(:,pCount) Rand_num_array(:,pCount-1)],...
            'LineStyle','-', 'LineWidth',2,...
            'Marker','.', 'MarkerSize', 1);
    else
        if (pCount == 1)
            figure( 'Name', 'Normalized 1st Derivative Melt Data' );
            plot(Melt_data_array(:,2),Melt_data_array(:,pCount+2), 'Color',[0 0 0],...
                'LineStyle','-', 'LineWidth',2,...
                'Marker','.', 'MarkerSize', 1);

            xlabel( 'Temperature', 'FontSize', 25 );
            ylabel( 'Ultra Fitted -dRFU/dT', 'FontSize', 25 );
            grid off;
        else
            hold on; plot(Melt_data_array(:,2),Melt_data_array(:,pCount+2),'Color',[Rand_num_array(:,pCount-2)
Rand_num_array(:,pCount) Rand_num_array(:,pCount-1)],...
                'LineStyle','-', 'LineWidth',2,...
                'Marker','.', 'MarkerSize', 1);
        end
    end
  else
    if ((pCount == 14) || (pCount==19))
        hold on; plot(Melt_data_array(:,2),Melt_data_array(:,pCount+2),'Color',[Rand_num_array(:,pCount-2)
Rand_num_array(:,pCount) Rand_num_array(:,pCount-1)],...
```

```
            'LineStyle','-', 'LineWidth',2,...
            'Marker','.', 'MarkerSize',1);
        else
            hold on; plot(Melt_data_array(:,2),Melt_data_array(:,pCount+2),'Color',[Rand_num_array(:,pCount-2)
Rand_num_array(:,pCount) Rand_num_array(:,pCount-1)],...
            'LineStyle','-', 'LineWidth',2,...
            'Marker','.', 'MarkerSize',1);

        end



    end
end
for pCount = 1:reactor_count
    if ((pCount >= 1) && (pCount <= 49)) %if ((p == 1) || (p == 2) || (p == 4) || (p == 5)) % if((p == 1) && (p ==
2) && (p == 4) && (p == 5))
        if ((pCount == 2))% || (pCount ==9))
            hold on;
plot(Smoothed_data_array(:,2),Smoothed_data_array(:,pCount+2),'Color',[Rand_num_array(:,pCount-1)
Rand_num_array(:,pCount) Rand_num_array(:,pCount-1)],...
            'LineStyle','-', 'LineWidth',2,...
            'Marker','.', 'MarkerSize', 1);
        else
            if (pCount == 1)
                figure( 'Name', 'Smoothed data' );
                plot(Smoothed_data_array(:,2),Smoothed_data_array(:,pCount+2), 'Color',[0 0 0],...
                    'LineStyle','-', 'LineWidth',2,...
                    'Marker','.', 'MarkerSize', 1);

                xlabel( 'Temperature', 'FontSize', 25 );
                ylabel( 'RFUs', 'FontSize', 25 );
                grid off;
            else
                hold on;
plot(Smoothed_data_array(:,2),Smoothed_data_array(:,pCount+2),'Color',[Rand_num_array(:,pCount-2)
Rand_num_array(:,pCount) Rand_num_array(:,pCount-1)],...
                    'LineStyle','-', 'LineWidth',2,...
                    'Marker','.', 'MarkerSize', 1);
            end
        end
    else
        if ((pCount == 14) || (pCount==19))
            hold on;
plot(Smoothed_data_array(:,2),Smoothed_data_array(:,pCount+2),'Color',[Rand_num_array(:,pCount-2)
Rand_num_array(:,pCount) Rand_num_array(:,pCount-1)],...
            'LineStyle','-', 'LineWidth',2,...
            'Marker','.', 'MarkerSize',1);
        else
            hold on;
plot(Smoothed_data_array(:,2),Smoothed_data_array(:,pCount+2),'Color',[Rand_num_array(:,pCount-2)
Rand_num_array(:,pCount) Rand_num_array(:,pCount-1)],...
            'LineStyle','-', 'LineWidth',2,...
            'Marker','.', 'MarkerSize',1);

        end

    end
end
```

```
for pCount = 1:reactor_count
   if ((pCount >= 1) && (pCount <= 49)) %if ((p == 1) || (p == 2) || (p == 4) || (p == 5)) % if((p == 1) && (p ==
2) && (p == 4) && (p == 5))
      if ((pCount == 2))% || (pCount ==9))
         hold on; plot(Melt_data_array(:,2),Melt_data_array(:,7)-
Melt_data_array(:,pCount+2),'Color',[Rand_num_array(:,pCount-1) Rand_num_array(:,pCount)
Rand_num_array(:,pCount-1)],...
            'LineStyle','none', 'LineWidth',1,...
            'Marker','.', 'MarkerSize', 1);
      else
         if (pCount == 1)
            figure( 'Name', 'Normalized 1st Derivative Melt H37RV-R35 plot' );
            plot(Melt_data_array(:,2),Melt_data_array(:,7)-Melt_data_array(:,pCount+2), 'Color',[0 0 0],...
               'LineStyle','-', 'LineWidth',2,...
               'Marker','.', 'MarkerSize', 1);

            xlabel( 'Temperature', 'FontSize', 25 );
            ylabel( 'RFUs', 'FontSize', 25 );
            grid off;
         else
            hold on; plot(Melt_data_array(:,2),Melt_data_array(:,7)-
Melt_data_array(:,pCount+2),'Color',[Rand_num_array(:,pCount-2) Rand_num_array(:,pCount)
Rand_num_array(:,pCount-1)],...
               'LineStyle','-', 'LineWidth',2,...
               'Marker','.', 'MarkerSize', 1);
         end
      end
   else
      if ((pCount == 14) || (pCount==19))
         hold on; plot(Melt_data_array(:,2),Melt_data_array(:,7)-
Melt_data_array(:,pCount+2),'Color',[Rand_num_array(:,pCount-2) Rand_num_array(:,pCount)
Rand_num_array(:,pCount-1)],...
            'LineStyle','-', 'LineWidth',2,...
            'Marker','.', 'MarkerSize',1);
      else
         hold on; plot(Melt_data_array(:,2),Melt_data_array(:,7)-
Melt_data_array(:,pCount+2),'Color',[Rand_num_array(:,pCount-2) Rand_num_array(:,pCount)
Rand_num_array(:,pCount-1)],...
            'LineStyle','-', 'LineWidth',2,...
            'Marker','.', 'MarkerSize',1);

      end

   end
end


Melt_peak_index = find(dy2 == max(dy2(:)))
Melt_temp = dt2(Melt_peak_index)
Maximum = max(dy2(:))
%
%
%FWHM calculation-------------------------------------------------------------
for ck = 1:reactor_count
   a = Melt_data_array(:,ck+2);
   c = Melt_data_array(:,2);
   b = max(a);
   hmax = b/2;
   for it2 = 1:size(a)
```

```
        if (a(it2) < hmax)
            digit(it2) = 0;
        else
            digit(it2) = 1;
        end
    end

    for it3 = 1: size(a)-1
        digit2(it3) = digit(it3) - digit(it3+1);
        if(digit2(it3) == 1)
            t1(it3) = c(it3);
        else
            t1(it3) = 0;
        end

    end

    for it4 = 1: size(a)-1
        digit2(it4) = digit(it4) - digit(it4+1);
        if(digit2(it4) == -1)
            t2(it4) = c(it4);
        else
            t2(it4) = 0;
        end

    end
    for m = 1:reactor_count
        T1 = sum(t1);
        T2 = sum(t2);
        if ((T1 > 95) && (T1 < 70))
            T1 = 0;
        else
            T1 = sum(t1);
            if ((T2 > 95) && (T2 < 70))
                T1 = 0;
            else
                T2 = sum(t2);
            end
        end


        fwh_max(ck) = abs(T1-T2);
    end
end
Thresh = 50;

for ink=1:reactor_count
    if(fwh_max(ink)<Thresh)
        Fullw2(ink) = fwh_max(ink);
    else
        Fullw2(ink) = 0;
    end
end

Fullw3 = (Fullw2 - min(Fullw2)) / ( max(Fullw2) - min(Fullw2) );

mksize = 50;
for p = 1:reactor_count
```

```
   if ((p >= 1) && (p <= 49)) %if ((p == 1) || (p == 2) || (p == 4) || (p == 5)) % if((p == 1) && (p == 2) && (p
== 4) && (p == 5))
      if ((p == 2))% || (p==9))
         hold on; plot(MeltDD(p,1),MeltDD(p,2),'Color',[Rand_num_array(:,p-1) Rand_num_array(:,p)
Rand_num_array(:,p-1)],...
            'LineStyle','none', 'LineWidth',1,...
            'Marker','.', 'MarkerSize',mksize*Fullw3(p)+5);
      else
         if (p == 1)
            figure( 'Name', 'Melt Data Display' );
            plot(MeltDD(p,1),MeltDD(p,2),'Color',[0 0 0],...
               'LineStyle','none', 'LineWidth',1,...
               'Marker','.', 'MarkerSize',mksize*Fullw3(p)+5);
            xlabel( 'Reactor Number','FontSize', 25 );
            ylabel( 'Melting Temperature (T_M)', 'FontSize', 25 );
            grid on;
         else
            hold on; plot(MeltDD(p,1),MeltDD(p,2),'Color',[Rand_num_array(:,p-2) Rand_num_array(:,p)
Rand_num_array(:,p-1)],...
               'LineStyle','none', 'LineWidth',1,...
               'Marker','.', 'MarkerSize',mksize*Fullw3(p)+5);
         end
      end
   else
      if ((p == 14) || (p==19))
         hold on; plot(MeltDD(p,1),MeltDD(p,2),'Color',[Rand_num_array(:,p-2) Rand_num_array(:,p)
Rand_num_array(:,p-1)],...
            'LineStyle','none', 'LineWidth',1,...
            'Marker','.', 'MarkerSize',mksize*Fullw3(p)+5);
      else
         hold on; plot(MeltDD(p,1),MeltDD(p,2),'Color',[Rand_num_array(:,p-2) Rand_num_array(:,p)
Rand_num_array(:,p-1)],...
            'LineStyle','none', 'LineWidth',1,...
            'Marker','.', 'MarkerSize',mksize*Fullw3(p)+5);


      end


      %    else    hold on; plot(MeltDD(:,1),MeltDD(:,p),'Color',[0 1 0],...
      %          'LineStyle','none', 'LineWidth',1,...
      %          'Marker','.', 'MarkerSize',40);
   end
end



for p = 1:reactor_count
   if ((p >= 1) && (p <= 49)) %if ((p == 1) || (p == 2) || (p == 4) || (p == 5)) % if((p == 1) && (p == 2) && (p
== 4) && (p == 5))
      if ((p == 4) || (p==9))
         hold on; plot(Fullw2(1:ck),'Color',[1 0 0],...
            'LineStyle','-', 'LineWidth',1,...
            'Marker','.', 'MarkerSize',10);
      else
         if (p == 1)
            figure( 'Name', 'Full width at hmax display' );
            plot(Fullw2(1:ck),'Color',[0 0 0],...
               'LineStyle','-', 'LineWidth',1,...
               'Marker','.', 'MarkerSize',10);
            xlabel( 'Reactor Number','FontSize', 25 );
            ylabel( 'fwhm', 'FontSize', 25 );
```

```
            grid off;
         else
            hold on; plot(Fullw2(1:ck),'Color',[1 0 0],...
               'LineStyle','-', 'LineWidth',1,...
               'Marker','.', 'MarkerSize',10);
         end
      end
   else
      if ((p == 14) || (p==19))
         hold on; plot(Fullw2(1:ck),'Color',[1 0 0],...
            'LineStyle','-', 'LineWidth',1,...
            'Marker','.', 'MarkerSize',10);
      else
         hold on; plot(Fullw2(1:ck),'Color',[1 0 0],...
            'LineStyle','-', 'LineWidth',1,...
            'Marker','.', 'MarkerSize',10);

      end

   end
end
%%%%%%%%%%%%%%%%%%%%%%%%%%%%%%%%%%%%%%%%%%%%%%%%%


for pCount = 1:reactor_count
   if ((pCount >= 1) && (pCount <= 49)) %if ((p == 1) || (p == 2) || (p == 4) || (p == 5)) % if((p == 1) && (p ==
2) && (p == 4) && (p == 5))
      if ((pCount ==2))%|| (pCount ==8))
         hold on; plot(Amplif_Array(:,1),Amplif_Array(:,pCount+4),'Color',[Rand_num_array(:,pCount-1)
Rand_num_array(:,pCount) Rand_num_array(:,pCount-1)],...
            'LineStyle','-', 'LineWidth',2,...
            'Marker','.', 'MarkerSize', 1);
      else
         if (pCount == 1)
            figure( 'Name', 'Real Time Amplification Curves' );
            plot(Amplif_Array(:,1),Amplif_Array(:,pCount+4), 'Color',[0 0 0],...
               'LineStyle','-', 'LineWidth',2,...
               'Marker','.', 'MarkerSize', 1);

            xlabel( 'Cycle Number', 'FontSize', 25 );
            ylabel( 'RFUs', 'FontSize', 25 );
            grid off;
         else
            hold on; plot(Amplif_Array(:,1),Amplif_Array(:,pCount+4),'Color',[Rand_num_array(:,pCount-2)
Rand_num_array(:,pCount) Rand_num_array(:,pCount-1)],...
               'LineStyle','-', 'LineWidth',2,...
               'Marker','.', 'MarkerSize', 1);
         end
      end
   else
      if ((pCount == 13) || (pCount==18))
         hold on; plot(Amplif_Array(:,1),Amplif_Array(:,pCount+4),'Color',[Rand_num_array(:,pCount-2)
Rand_num_array(:,pCount) Rand_num_array(:,pCount-1)],...
            'LineStyle','-', 'LineWidth',2,...
            'Marker','.', 'MarkerSize',1);
      else
         hold on; plot(Amplif_Array(:,1),Amplif_Array(:,pCount+4),'Color',[Rand_num_array(:,pCount-2)
Rand_num_array(:,pCount) Rand_num_array(:,pCount-1)],...
            'LineStyle','-', 'LineWidth',2,...
```

```
            'Marker','.', 'MarkerSize',1);

        end


    end
end

Melt_temps_only(1,1) = 0;

for mk = 1:reactor_count

    Melt_temps_only(:,mk) = MeltDD(mk,2);
end

Melt_temps_map(1,1) = 0;

for tk = 1:reactor_count

    if ((tk >= 2) && (tk <= 12))%(tk <= 11)
        Melt_temps_map(tk-1,1) = MeltDD(tk,2);

    else
        if ((tk >= 13) && (tk <= 23))
            Melt_temps_map(tk-12,2) = MeltDD(tk,2);

        else
            if ((tk >= 24) && (tk <= 34))
                Melt_temps_map(tk-11*2-1,3) = MeltDD(tk,2);

            else
                if ((tk >= 35) && (tk <= 45))
                    Melt_temps_map(tk-11*3-1,4) = MeltDD(tk,2);
                else
                    if ((tk >= 46) && (tk <= 56))
                        Melt_temps_map(tk-11*4-1,5) = MeltDD(tk,2);
                    else
                        if ((tk >= 57) && (tk <= 67))
                            Melt_temps_map(tk-11*5-1,6) = MeltDD(tk,2);
                        else
                            if ((tk >= 68) && (tk <= 78))
                                Melt_temps_map(tk-11*6-1,7) = MeltDD(tk,2);
                            else
                                if ((tk >= 79) && (tk <= 89))
                                    Melt_temps_map(tk-11*7-1,8) = MeltDD(tk,2);
                                else
                                    if ((tk >= 90) && (tk <= 100))
                                        Melt_temps_map(tk-11*8-1,9) = MeltDD(tk,2);
                                    else
                                        if ((tk >= 101) && (tk <= 111))
                                            Melt_temps_map(tk-11*9-1,10) = MeltDD(tk,2);
                                        else
                                            if ((tk >= 112) && (tk <= 122))
                                                Melt_temps_map(tk-11*10-1,11) = MeltDD(tk,2);
                                            else
                                                if ((tk >= 123) && (tk <= 133))
                                                    Melt_temps_map(tk-11*11-1,12) = MeltDD(tk,2);
                                                end
```

```
                    end
                end
            end
        end
    end
end
end
%%%%%%%%%%%Maximum fluorecence vs Melt temp
Range1_fluo_array(1,1) = 0;

for rk = 1:reactor_count

    Range1_fluo_array(:,rk) = max(Amplif_Array(:,rk+4)-min(Amplif_Array(:,rk+4)));
end



Max_fluo_array(1,1) = 0;

for bk = 1:reactor_count

    Max_fluo_array(:,bk) = max(Amplif_Array(:,bk+4));
end

for bk = 1:reactor_count
    if ((bk == 2))% || (bk==3))
        hold on; plot(Max_fluo_array(:,bk),Melt_temps_only(:,bk),'Color',[Rand_num_array(:,bk-1)
Rand_num_array(:,bk) Rand_num_array(:,bk-1)],...
            'LineStyle','none', 'LineWidth',1,...
            'Marker','.', 'MarkerSize',Range1_fluo_array(:,bk)*500);

    else
        if (bk == 1)
            figure( 'Name', 'Max Fluoresence vs Melt temp' );
            plot(Max_fluo_array(:,1),Melt_temps_only(:,1),'Color',[0 0 0],...
                'LineStyle','none', 'LineWidth',1,...
                'Marker','.', 'MarkerSize',Range1_fluo_array(:,bk)*500);
            xlabel( 'Maximum Fluorescence','FontSize', 25 );
            ylabel( 'Melting Temperature (T_M)', 'FontSize', 25 );
            grid on;
            axis([0.3 0.38 74 92]);
        else
            hold on; plot(Max_fluo_array(:,bk),Melt_temps_only(:,bk),'Color',[Rand_num_array(:,bk-2)
Rand_num_array(:,bk) Rand_num_array(:,bk-1)],...
                'LineStyle','none', 'LineWidth',1,...
                'Marker','.', 'MarkerSize',Range1_fluo_array(:,bk)*500);

        end

    end
end
```

```
for pk = 1:reactor_count
   if ((pk == 2))% || (bk==3))
      hold on; plot(Range1_fluo_array(:,pk),Melt_temps_only(:,pk),'Color',[Rand_num_array(:,pk-1)
Rand_num_array(:,pk) Rand_num_array(:,pk-1)],...
         'LineStyle','none', 'LineWidth',1,...
         'Marker','.', 'MarkerSize',20);


   else
      if (pk == 1)
         figure( 'Name', 'Amplification Range vs Melt temp' );
         plot(Range1_fluo_array(:,pk),Melt_temps_only(:,pk),'Color',[0 0 0],...
            'LineStyle','none', 'LineWidth',1,...
            'Marker','.', 'MarkerSize',20);
         xlabel( 'Amplification Range','FontSize', 25 );
         ylabel( 'Melting Temperature (T_M)', 'FontSize', 25 );
         grid on;
         axis([0 0.08 74 92]);
      else
         hold on; plot(Range1_fluo_array(:,pk),Melt_temps_only(:,pk),'Color',[Rand_num_array(:,pk-2)
Rand_num_array(:,pk) Rand_num_array(:,pk-1)],...
            'LineStyle','none', 'LineWidth',1,...
            'Marker','.', 'MarkerSize',20);


      end


   end
end

Cleaned_Norm_smoothed_data_array(10000,129) = 0;
Cleaned_Melt_data_array(9999,129) = 0;

for pk = 1:reactor_count

   if Max_fluo_array(:,pk) > 0.29
      Cleaned_Norm_smoothed_data_array(:,pk) = Norm_smoothed_data_array(:,pk+2);
      Cleaned_Melt_data_array(:,pk) = Melt_data_array(:,pk+2);
   end
end

for zk = 1:reactor_count
   if ((zk >= 1) && (zk <= 49)) %if ((p == 1) || (p == 2) || (p == 4) || (p == 5)) % if((p == 1) && (p == 2) && (p
== 4) && (p == 5))
      if ((zk == 2))% || (pCount ==9))
         hold on;
plot(Norm_smoothed_data_array(:,2),Cleaned_Norm_smoothed_data_array(:,zk),'Color',[Rand_num_array(:,zk-
1) Rand_num_array(:,zk) Rand_num_array(:,zk-1)],...
            'LineStyle','-', 'LineWidth',2,...
            'Marker','.', 'MarkerSize', 1);
      else
         if (zk == 1)
            figure( 'Name', 'Normalized Smoothed Data' );
            plot(Norm_smoothed_data_array(:,2),Cleaned_Norm_smoothed_data_array(:,zk), 'Color',[1 1 1],...
               'LineStyle','-', 'LineWidth',2,...
               'Marker','.', 'MarkerSize', 1);

            xlabel( 'Temperature', 'FontSize', 25 );
            ylabel( 'Ultra Fitted -dRFU/dT', 'FontSize', 25 );
            grid off;
         else
```

```
            hold on;
plot(Norm_smoothed_data_array(:,2),Cleaned_Norm_smoothed_data_array(:,zk),'Color',[Rand_num_array(:,zk-
2) Rand_num_array(:,zk) Rand_num_array(:,zk-1)],...
                'LineStyle','-', 'LineWidth',2,...
                'Marker','.', 'MarkerSize', 1);
        end
    end
  else
    if ((zk == 14) || (zk==19))
        hold on;
plot(Norm_smoothed_data_array(:,2),Cleaned_Norm_smoothed_data_array(:,zk),'Color',[Rand_num_array(:,zk-
2) Rand_num_array(:,zk) Rand_num_array(:,zk-1)],...
            'LineStyle','-', 'LineWidth',2,...
            'Marker','.', 'MarkerSize',1);
    else
        hold on;
plot(Norm_smoothed_data_array(:,2),Cleaned_Norm_smoothed_data_array(:,zk),'Color',[Rand_num_array(:,zk-
2) Rand_num_array(:,zk) Rand_num_array(:,zk-1)],...
            'LineStyle','-', 'LineWidth',2,...
            'Marker','.', 'MarkerSize',1);

    end


  end
end

for zk = 1:reactor_count
  if ((zk >= 1) && (zk <= 49)) %if ((p == 1) || (p == 2) || (p == 4) || (p == 5)) % if((p == 1) && (p == 2) && (p
== 4) && (p == 5))
    if ((zk == 2))% || (pCount ==9))
        hold on; plot(Melt_data_array(:,2),Cleaned_Melt_data_array(:,zk),'Color',[Rand_num_array(:,zk-1)
Rand_num_array(:,zk) Rand_num_array(:,zk-1)],...
            'LineStyle','-', 'LineWidth',2,...
            'Marker','.', 'MarkerSize', 1);
    else
        if (zk == 1)
            figure( 'Name', 'Cleaned 1st Derivative Melt Data' );
            plot(Melt_data_array(:,2),Cleaned_Melt_data_array(:,zk), 'Color',[1 1 1],...
              'LineStyle','-', 'LineWidth',2,...
              'Marker','.', 'MarkerSize', 1);

            xlabel( 'Temperature', 'FontSize', 25 );
            ylabel( 'Ultra Fitted -dRFU/dT', 'FontSize', 25 );
            grid off;
        else
            hold on; plot(Melt_data_array(:,2),Cleaned_Melt_data_array(:,zk),'Color',[Rand_num_array(:,zk-2)
Rand_num_array(:,zk) Rand_num_array(:,zk-1)],...
                'LineStyle','-', 'LineWidth',2,...
                'Marker','.', 'MarkerSize', 1);
        end
    end
  else
    if ((zk == 14) || (zk==19))
        hold on; plot(Melt_data_array(:,2),Cleaned_Melt_data_array(:,zk),'Color',[Rand_num_array(:,zk-2)
Rand_num_array(:,zk) Rand_num_array(:,zk-1)],...
            'LineStyle','-', 'LineWidth',2,...
            'Marker','.', 'MarkerSize',1);
    else
```

```
        hold on; plot(Melt_data_array(:,2),Cleaned_Melt_data_array(:,zk),'Color',[Rand_num_array(:,zk-2)
Rand_num_array(:,zk) Rand_num_array(:,zk-1)],...
            'LineStyle','-', 'LineWidth',2,...
            'Marker','.', 'MarkerSize',1);

        end


    end
end


Melt_temps_map(1,1) = 0;

%%%%%%%Multiplot code%%%%%%%%%%%%%%%%%%%%%%%%%%%%%


fname = 'C:\Users\High_Resolution_MeltRecords.xls'';
fname2 = 'C:\Users\ Real_time_PCR_Records.xls';
nplots = 180;   %number of graphs to plot
nrows = 6;      %number of rows
ncols = 6;      %numer of columns

num = dlmread(fname); %This is just the original dataset
num2 = dlmread(fname2);%Amplification

myx = Norm_smoothed_data_array(:,2); %X values
myx2 = num2(:,1);
myx3 = Melt_data_array(:,2);

plotCount = 0;
for count=25:nplots



    myy = Norm_smoothed_data_array(:,3+count); %Y values melts
    myy2 = num2(:,5+count);
    myy3 = Melt_data_array(:,3+count);

    if (count == 1)
        figure
    end

    %%%%%%%%%%%%%%%%%%%%%%%%%%%%%%%%%%%%%%%%%%%%%%%%%
    if(count<15)
        mcolor = 'ko'; %specify marker color
        mfc = [0 0 0]; %specify marker face color
    else
        mcolor = 'ko';
        mfc = [0 0 0];
    end

    %Optional: For changing the thickness of some graphs. For instance, here we
    %increase the thickness of every 7th reactor

    mksize = 2;
    plotCount = plotCount+1;
    subplot(nrows,ncols,plotCount)   %Here you specify the dumensions of the plot grid
```

```
    plot(myx2,myy2, mcolor,...
        'MarkerFaceColor',mfc,...
        'MarkerSize',mksize);
    grid on
    axis([1 35 0.27 0.9]);
    set(gca,'XGrid','on','YGrid','on', 'GridLineStyle','-');
    title(num2str(count));


     plotCount = plotCount+1;
    subplot(nrows,ncols,plotCount)    %Here you specify the dumensions of the plot grid

    plot(myx,myy, mcolor,...
        'MarkerFaceColor',mfc,...
        'MarkerSize',mksize);
    grid on
    axis([75 90 0 1]);
    set(gca,'XGrid','on','YGrid','on', 'GridLineStyle','-');
    title(num2str(Melt_temps_only(count+1)));

    plotCount = plotCount+1;
    subplot(nrows,ncols,plotCount)    %Here you specify the dumensions of the plot grid

    plot(myx3,myy3, mcolor,...
        'MarkerFaceColor',mfc,...
        'MarkerSize',mksize);
    grid on
    axis([75 90 -0.5E-5 10E-5]);
    set(gca,'XGrid','on','YGrid','on', 'GridLineStyle','-');
    title(num2str(count));
end


toc
```

REFERENCES LIST

1. Murray CJ, Ortblad KF, Guinovart C, Lim SS, Wolock TM, Roberts DA, Dansereau EA, Graetz N, Barber RM, Brown JC: **Global, regional, and national incidence and mortality for HIV, tuberculosis, and malaria during 1990–2013: a systematic analysis for the Global Burden of Disease Study 2013**. *The Lancet* 2014, **384**(9947):1005-1070.

2. Zumla A, Petersen E, Nyirenda T, Chakaya J: **Tackling the Tuberculosis Epidemic in sub-Saharan Africa–unique opportunities arising from the second European Developing Countries Clinical Trials Partnership (EDCTP) programme 2015-2024**. *International Journal of Infectious Diseases* 2015, **32**:46-49.

3. WHO.: **Global Tuberculosis Report 2014**: World Health Organization; 2014.

4. Sharma SK, Mohanan S, Sharma A: **Relevance of latent TB infection in areas of high TB prevalence**. *CHEST Journal* 2012, **142**(3):761-773.

5. Patra J, Jha P, Rehm J, Suraweera W: **Tobacco smoking, alcohol drinking, diabetes, low body mass index and the risk of self-reported symptoms of active tuberculosis: individual participant data (IPD) meta-analyses of 72,684 individuals in 14 high tuberculosis burden countries**. *PloS one* 2014, **9**(5):e96433.

6. Churchyard G, Mametja L, Mvusi L, Ndjeka N, Hesseling A, Reid A, Babatunde S, Pillay Y: **Tuberculosis control in South Africa: Successes, challenges and recommendations**. *SAMJ: South African Medical Journal* 2014, **104**(3):234-248.

7. Health SADo: **National Tuberculosis Management Guidelines 2014**: Department of Health; 2014.

8. Zhang Y, Yew W: **Mechanisms of drug resistance in Mycobacterium tuberculosis [State of the art series. Drug-resistant tuberculosis. Edited by CY. Chiang. Number 1 in the series]**. *The International Journal of Tuberculosis and Lung Disease* 2009, **13**(11):1320-1330.

9. Hillemann D, Rüsch-Gerdes S, Boehme C, Richter E: **Rapid molecular detection of extrapulmonary tuberculosis by the automated GeneXpert MTB/RIF system**. *Journal of clinical microbiology* 2011, **49**(4):1202-1205.

10. Vogelstein B, Kinzler KW: **Digital Pcr**. *Proceedings of the National Academy of Sciences* 1999, **96**(16):9236-9241.

11. Cohen T, van Helden PD, Wilson D, Colijn C, McLaughlin MM, Abubakar I, Warren RM: **Mixed-strain Mycobacterium tuberculosis infections and the implications for tuberculosis treatment and control**. *Clinical microbiology reviews* 2012, **25**(4):708-719.

12. Rüsch-Gerdes S, Pfyffer GE, Casal M, Chadwick M, Siddiqi S: **Multicenter laboratory validation of the BACTEC MGIT 960 technique for testing susceptibilities of Mycobacterium tuberculosis to classical second-line drugs and newer antimicrobials**. *Journal of clinical microbiology* 2006, **44**(3):688-692.

13. Tortoli E, Benedetti M, Fontanelli A, Simonetti MT: **Evaluation of automated BACTEC MGIT 960 system for testing susceptibility of Mycobacterium tuberculosis to four major antituberculous drugs: comparison with the radiometric BACTEC 460TB method and the agar plate method of proportion**. *Journal of clinical microbiology* 2002, **40**(2):607-610.

14. Shamputa IC, Jugheli L, Sadradze N, Willery E, Portaels F, Supply P, Rigouts L: **Mixed infection and clonal representativeness of a single sputum sample in tuberculosis patients from a penitentiary hospital in Georgia**. *Respir Res* 2006, **7**(99):10.1186.

15. Bergmann JS, Woods GL: **Clinical evaluation of the Roche AMPLICOR PCR Mycobacterium tuberculosis test for detection of M. tuberculosis in respiratory specimens**. *Journal of clinical microbiology* 1996, **34**(5):1083-1085.

16. McHugh T, Pope C, Ling C, Patel S, Billington O, Gosling R, Lipman M, Gillespie S: **Prospective evaluation of BDProbeTec strand displacement amplification (SDA) system for diagnosis of tuberculosis in non-respiratory and respiratory samples**. *Journal of medical microbiology* 2004, **53**(12):1215-1219.

17. O'Sullivan CE, Miller DR, Schneider PS, Roberts GD: **Evaluation of Gen-Probe amplified Mycobacterium tuberculosis direct test by using respiratory and nonrespiratory specimens in a tertiary care center laboratory**. *Journal of clinical microbiology* 2002, **40**(5):1723-1727.

18. Sarrazin C, Teuber G, Kokka R, Rabenau H, Zeuzem S: **Detection of Residual Hepatitis C Virus RNA by Transcription-Mediated Amplification in Patients With Complete Virologic Response According to Polymerase Chain Reaction–Based Assays**. *Hepatology* 2000, **32**(4):818-823.

19. Barnard M, Albert H, Coetzee G, O'Brien R, Bosman ME: **Rapid molecular screening for multidrug-resistant tuberculosis in a high-volume public health laboratory in South Africa**. *American journal of respiratory and critical care medicine* 2008, **177**(7):787-792.

20. de Luna FF-A, Ruiz P, Gutiérrez J, Casal M: **Evaluation of the GenoType Mycobacteria Direct assay for detection of Mycobacterium tuberculosis complex and four atypical mycobacterial species in clinical samples**. *Journal of clinical microbiology* 2006, **44**(8):3025-3027.

21. Rie AV, Page-Shipp L, Scott L, Sanne I, Stevens W: **Xpert® MTB/RIF for point-of-care diagnosis of TB in high-HIV burden, resource-limited countries: hype or hope?** 2010.

22. Sanders R, Huggett JF, Bushell CA, Cowen S, Scott DJ, Foy CA: **Evaluation of digital PCR for absolute DNA quantification**. *Analytical chemistry* 2011, **83**(17):6474-6484.

23. Baker M: **Digital PCR hits its stride**. *nature methods* 2012, **9**(6):541-544.

24. Small PM, Pai M: **Tuberculosis Diagnosis—Time for a Game Change**. *Curr Opin Pulm Med* 2010, **16**:271-284.

25. Boehme CC, Nabeta P, Hillemann D, Nicol MP, Shenai S, Krapp F, Allen J, Tech B, Tahirli R, Blakemore R: **Rapid Molecular Detection of Tuberculosis and Rifampin Resistance**. 2010.

26. http://www.moleculartb.org/gb/pdf/ppt/13_SYMP_ISoundiram_GeneXperttech_2902.pdf: (Accessed on 09 October 2015).

27. Evans CA: **Genexpert-a game-changer for tuberculosis control?** *PLoS medicine* 2011, **8**(7):882.

28. Schnippel K, Meyer-Rath G, Long L, MacLeod W, Sanne I, Stevens WS, Rosen S: **Scaling up Xpert MTB/RIF technology: the costs of laboratory-vs. clinic-based roll-out in South Africa**. *Tropical Medicine & International Health* 2012, **17**(9):1142-1151.

29. Zhang B, Salieb-Beugelaar GB, Nigo MM, Weidmann M, Hunziker P: **Diagnosing dengue virus infection—rapid tests and the role of micro/nanotechnologies**. *Nanomedicine: Nanotechnology, Biology and Medicine* 2015.

30. CLAYDEN P: **HIV Point of Care Diagnostics Pipeline**. *2011 Pipeline Report* 2011:53.

31. Whitesides GM: **The origins and the future of microfluidics**. *Nature* 2006, **442**(7101):368-373.

32. Le HP: **Progress and Trends in Ink-jet Printing Technology Part**. *Journal of Imaging Science and Technology* 1998, **42**:49-62.

33. MANZ A, MIYAHARA Y, MIURA J, WATANABE Y, MIYAGI H, SATO K: **Design of an Open~ tubular Column Liquid Chromatograph Using Silicon Chip Technology**. *Sensors and Actuators, B* 1990, **249**:255.

34. Shoji S, Esashi M, Matsuo T: **Prototype miniature blood gas analyser fabricated on a silicon wafer**. *Sensors and Actuators* 1988, **14**(2):101-107.

35. Van Lintel H, Van de Pol F, Bouwstra S: **A piezoelectric micropump based on micromachining of silicon**. *Sensors and actuators* 1988, **15**(2):153-167.

36. Zengerle R, Ulrich J, Kluge S, Richter M, Richter A: **A bidirectional silicon micropump**. *Sensors and Actuators A: Physical* 1995, **50**(1):81-86.

37. Haeberle S, Zengerle R: **Microfluidic platforms for lab-on-a-chip applications**. *Lab on a Chip* 2007, **7**(9):1094-1110.

38. Mark D, Haeberle S, Roth G, von Stetten F, Zengerle R: **Microfluidic lab-on-a-chip platforms: requirements, characteristics and applications**. *Chemical Society Reviews* 2010, **39**(3):1153-1182.

39. Brody JP, Yager P, Goldstein RE, Austin RH: **Biotechnology at low Reynolds numbers**. *Biophysical journal* 1996, **71**(6):3430-3441.

40. Whitesides G, Stroock A: **Flexible methods for microfluidics [J]**. *Phys Today* 2001, **54**(6):42-48.

41. Beebe DJ, Mensing GA, Walker GM: **Physics and applications of microfluidics in biology**. *Annual review of biomedical engineering* 2002, **4**(1):261-286.

42. White FM, Corfield I: **Viscous fluid flow**, vol. 3: McGraw-Hill New York; 2006.

43. Stroock AD, Whitesides GM: **Controlling flows in microchannels with patterned surface charge and topography**. *Accounts of chemical research* 2003, **36**(8):597-604.

44. Ismagilov RF, Stroock AD, Kenis PJ, Whitesides G, Stone HA: **Experimental and theoretical scaling laws for transverse diffusive broadening in two-phase laminar flows in microchannels**. *Applied Physics Letters* 2000, **76**(17):2376-2378.

45. Brody JP, Yager P: **Diffusion-based extraction in a microfabricated device**. *Sensors and Actuators A: Physical* 1997, **58**(1):13-18.

46. Kamholz AE, Yager P: **Theoretical analysis of molecular diffusion in pressure-driven laminar flow in microfluidic channels**. *Biophysical journal* 2001, **80**(1):155-160.

47. Lin B, Levchenko A: **Spatial manipulation with microfluidics**. *Frontiers in bioengineering and biotechnology* 2015, **3**.

48. Rim S-J, Leong-Poi H, Lindner JR, Wei K, Fisher NG, Kaul S: **Decrease in coronary blood flow reserve during hyperlipidemia is secondary to an increase in blood viscosity**. *Circulation* 2001, **104**(22):2704-2709.

49. Dodds S, Phillips P: **The haemodynamics of multiple sequential stenoses and the criteria for a critical stenosis**. *European journal of vascular and endovascular surgery* 2003, **26**(4):348-353.

50. Snakenborg D, Perozziello G, Geschke O, Kutter JP: **A fast and reliable way to establish fluidic connections to planar microchips**. *Journal of Micromechanics and Microengineering* 2007, **17**(1):98.

51. Pennathur S, Meinhart C, Soh H: **How to exploit the features of microfluidics technology**. *Lab on a chip* 2008, **8**(1):20.

52. Trefethen L: **SURFACE TENSION LUID MECHANICS**. *Lubricating oil* 1969, **25**:35.

53. Levich V, Krylov V: **Surface-tension-driven phenomena**. *Annual Review of Fluid Mechanics* 1969, **1**(1):293-316.

54. Zhao C-X, Middelberg AP: **Two-phase microfluidic flows**. *Chemical Engineering Science* 2011, **66**(7):1394-1411.

55. Tian W-C, Finehout E: **Microfluidics for biological applications**, vol. 16: Springer Science & Business Media; 2009.

56. Cheng X, Irimia D, Dixon M, Sekine K, Demirci U, Zamir L, Tompkins RG, Rodriguez W, Toner M: **A microfluidic device for practical label-free CD4+ T cell counting of HIV-infected subjects**. *Lab on a Chip* 2007, **7**(2):170-178.

57. Minteer SD: **Microfluidic techniques: reviews and protocols**, vol. 321: Springer Science & Business Media; 2006.

58. Dhar R, Ahuja S, Narender D: **THE ADVANCEMENT IN PHOTONICS MAKES OPTICAL LITHOGRAPHY REINVIGORATE AND FUTURE SEEMS AS BRIGHT AS EVER**.

59. Psaltis D, Quake SR, Yang C: **Developing optofluidic technology through the fusion of microfluidics and optics**. *Nature* 2006, **442**(7101):381-386.

60. Thorsen T, Maerkl SJ, Quake SR: **Microfluidic large-scale integration**. *Science* 2002, **298**(5593):580-584.

61. Tang SK, Whitesides GM: **Basic microfluidic and soft lithographic techniques**.

62. Janasek D, Franzke J, Manz A: **Scaling and the design of miniaturized chemical-analysis systems**. *Nature* 2006, **442**(7101):374-380.

63. Vargas-Bernal R, Rodríguez-Miranda E, Herrera-Pérez G: **Evolution and Expectations of Enzymatic Biosensors for Pesticides**: INTECH Open Access Publisher; 2012.

64. Wang X, Uchiyama S: **Polymers for Biosensors Construction**: INTECH Open Access Publisher; 2013.

65. Kuswandi B, Huskens J, Verboom W: **Optical sensing systems for microfluidic devices: a review**. *Analytica chimica acta* 2007, **601**(2):141-155.

66. Baker CA, Duong CT, Grimley A, Roper MG: **Recent advances in microfluidic detection systems**. *Bioanalysis* 2009, **1**(5):967-975.

67. Swinehart D: **The Beer-Lambert Law**. *Journal of Chemical Education* 1962, **39**:333.

68. Vykoukal DM, Stone GP, Gascoyne PR, Alt EU, Vykoukal J: **Quantitative Detection of Bioassays with a Low-Cost Image-Sensor Array for Integrated Microsystems**. *Angewandte Chemie* 2009, **121**(41):7785-7790.

69. Wang S, Zhao X, Khimji I, Akbas R, Qiu W, Edwards D, Cramer DW, Ye B, Demirci U: **Integration of cell phone imaging with microchip ELISA to detect ovarian cancer HE4 biomarker in urine at the point-of-care**. *Lab on a chip* 2011, **11**(20):3411-3418.

70. Jokerst JC, Adkins JA, Bisha B, Mentele MM, Goodridge LD, Henry CS: **Development of a paper-based analytical device for colorimetric detection of select foodborne pathogens**. *Analytical chemistry* 2012, **84**(6):2900-2907.

71. Valeur B, Berberan-Santos MN: **Molecular fluorescence: principles and applications**: John Wiley & Sons; 2012.

72. Lakowicz JR: **Principles of fluorescence spectroscopy**: Springer Science & Business Media; 2013.

73. Jamieson T, Bakhshi R, Petrova D, Pocock R, Imani M, Seifalian AM: **Biological applications of quantum dots**. *Biomaterials* 2007, **28**(31):4717-4732.

74. Roy R, Hohng S, Ha T: **A practical guide to single-molecule FRET**. *Nature methods* 2008, **5**(6):507-516.

75. Giepmans BN, Adams SR, Ellisman MH, Tsien RY: **The fluorescent toolbox for assessing protein location and function**. *Science* 2006, **312**(5771):217-224.

76. Ha T: **Single-molecule fluorescence methods for the study of nucleic acids**. *Current opinion in structural biology* 2001, **11**(3):287-292.

77. Myers FB, Lee LP: **Innovations in optical microfluidic technologies for point-of-care diagnostics**. *Lab on a Chip* 2008, **8**(12):2015-2031.

78. Lee LM, Cui X, Yang C: **The application of on-chip optofluidic microscopy for imaging Giardia lamblia trophozoites and cysts**. *Biomedical microdevices* 2009, **11**(5):951-958.

79. Ramalingam N, Rui Z, Liu H-B, Dai C-C, Kaushik R, Ratnaharika B, Gong H-Q: **Real-time PCR-based microfluidic array chip for simultaneous detection of multiple waterborne pathogens**. *Sensors and Actuators B: Chemical* 2010, **145**(1):543-552.

80. Yildirim N, Long F, Gao C, He M, Shi H-C, Gu AZ: **Aptamer-based optical biosensor for rapid and sensitive detection of 17β-Estradiol in water samples**. *Environmental science & technology* 2012, **46**(6):3288-3294.

81. Ishimatsu R, Naruse A, Liu R, Nakano K, Yahiro M, Adachi C, Imato T: **An organic thin film photodiode as a portable photodetector for the detection of alkylphenol polyethoxylates by a flow fluorescence-immunoassay on magnetic microbeads in a microchannel**. *Talanta* 2013, **117**:139-145.

82. Dodeigne C, Thunus L, Lejeune R: **Chemiluminescence as diagnostic tool. A review**. *Talanta* 2000, **51**(3):415-439.

83. Xiang A, Wei F, Lei X, Liu Y, Guo Y: **A simple and rapid capillary chemiluminescence immunoassay for quantitatively detecting human serum HBsAg**. *European journal of clinical microbiology & infectious diseases* 2013, **32**(12):1557-1564.

84. Hao M, Ma Z: **An ultrasensitive chemiluminescence biosensor for carcinoembryonic antigen based on autocatalytic enlargement of immunogold nanoprobes**. *Sensors* 2012, **12**(12):17320-17329.

85. Yang M, Sun S, Kostov Y, Rasooly A: **An automated point-of-care system for immunodetection of staphylococcal enterotoxin B**. *Analytical biochemistry* 2011, **416**(1):74-81.

86. Caputo D, de Cesare G, Dolci LS, Mirasoli M, Nascetti A, Roda A, Scipinotti R: **Microfluidic chip with integrated a-Si: H photodiodes for chemiluminescence-based bioassays**. *Sensors Journal, IEEE* 2013, **13**(7):2595-2602.

87. Lin CC, Ko FH, Chen CC, Yang YS, Chang FC, Wu CS: **Miniaturized metal semiconductor metal photocurrent system for biomolecular sensing via chemiluminescence**. *Electrophoresis* 2009, **30**(18):3189-3197.

88. Wojciechowski JR, Shriver-Lake LC, Yamaguchi MY, Füreder E, Pieler R, Schamesberger M, Winder C, Prall HJr, Sonnleitner M, Ligler FS: **Organic photodiodes for biosensor miniaturization**. *Analytical chemistry* 2009, **81**(9):3455-3461.

89. Sabban S: **Development of an in vitro model system for studying the interaction of Equus caballus IgE with its high-affinity FcεRI receptor**. University of Sheffield; 2011.

90. Kurita R, Yokota Y, Sato Y, Mizutani F, Niwa O: **On-chip enzyme immunoassay of a cardiac marker using a microfluidic device combined with a portable surface plasmon resonance system**. *Analytical chemistry* 2006, **78**(15):5525-5531.

91. Ouellet E, Lausted C, Lin T, Yang CWT, Hood L, Lagally ET: **Parallel microfluidic surface plasmon resonance imaging arrays**. *Lab on a Chip* 2010, **10**(5):581-588.

92. Krupin O, Asiri H, Wang C, Tait RN, Berini P: **Biosensing using straight long-range surface plasmon waveguides**. *Optics express* 2013, **21**(1):698-709.

93. Foudeh AM, Daoud JT, Faucher SP, Veres T, Tabrizian M: **Sub-femtomole detection of 16s rRNA from Legionella pneumophila using surface plasmon resonance imaging**. *Biosensors and Bioelectronics* 2014, **52**:129-135.

94. Wu J, Gu M: **Microfluidic sensing: state of the art fabrication and detection techniques**. *Journal of biomedical optics* 2011, **16**(8):080901-080901-080912.

95. Thévenot DR, Toth K, Durst RA, Wilson GS: **Electrochemical biosensors: recommended definitions and classification**. *Biosensors and Bioelectronics* 2001, **16**(1):121-131.

96. Wang J: **Analytical electrochemistry**: John Wiley & Sons; 2006.

97. Wang J: **Electrochemical detection for microscale analytical systems: a review**. *Talanta* 2002, **56**(2):223-231.

98. Koncki R: **Recent developments in potentiometric biosensors for biomedical analysis**. *Analytica chimica acta* 2007, **599**(1):7-15.

99. Liao W-Y, Weng C-H, Leeb G-B, Chou T-C: **Development and characterization of an all-solid-state potentiometric biosensor array microfluidic device for multiple ion analysis**. *Lab Chip* 2006, **6**:1362-1368.

100. Chou J-C, Tsai Y-L, Cheng T-Y, Liao Y-H, Lin J-W, Chen J-T, Chou H-T: **A novel and high performance potentiometric arrayed flexible glucose biosensor based on microfluidic device**. In: *Nanotechnology (IEEE-NANO), 2013 13th IEEE Conference on: 2013*. IEEE: 561-565.

101. Lobo MJ, Miranda AJ, Tuñón P: **Amperometric biosensors based on NAD (P)-dependent dehydrogenase enzymes**. *Electroanalysis* 1997, **9**(3):191-202.

102. Wang J: **Amperometric biosensors for clinical and therapeutic drug monitoring: a review**. *Journal of pharmaceutical and biomedical analysis* 1999, **19**(1):47-53.

103. Habermüller K, Mosbach M, Schuhmann W: **Electron-transfer mechanisms in amperometric biosensors**. *Fresenius' journal of analytical chemistry* 2000, **366**(6-7):560-568.

104. Gau J-J, Lan EH, Dunn B, Ho C-M, Woo JC: **A MEMS based amperometric detector for E. coli bacteria using self-assembled monolayers**. *Biosensors and Bioelectronics* 2001, **16**(9):745-755.

105. Abdel-Hamid I, Ivnitski D, Atanasov P, Wilkins E: **Flow-through immunofiltration assay system for rapid detection of E. coli O157: H7**. *Biosensors & Bioelectronics* 1999, **14**:309-316.

106. Tang D, Yuan R, Chai Y, Fu Y, Dai J, Liu Y, Zhong X: **New amperometric and potentiometric immunosensors based on gold nanoparticles/tris (2, 2′-bipyridyl) cobalt (III) multilayer films for hepatitis B surface antigen determinations**. *Biosensors and Bioelectronics* 2005, **21**(4):539-548.

107. Jaffrezic-Renault N, Dzyadevych SV: **Conductometric microbiosensors for environmental monitoring**. *Sensors* 2008, **8**(4):2569-2588.

108. Bonanni A, Esplandiu MJ, del Valle M: **Impedimetric genosensing of DNA polymorphism correlated to cystic fibrosis: a comparison among different protocols and electrode surfaces**. *Biosensors and Bioelectronics* 2010, **26**(4):1245-1251.

109. Bonanni A, Fernández-Cuesta I, Borrisé X, Pérez-Murano F, Alegret S, del Valle M: **DNA hybridization detection by electrochemical impedance spectroscopy using interdigitated gold nanoelectrodes**. *Microchimica Acta* 2010, **170**(3-4):275-281.

110. Bonanni A, Pividori M, Del Valle M: **Impedimetric detection of influenza A (H1N1) DNA sequence using carbon nanotubes platform and gold nanoparticles amplification**. *Analyst* 2010, **135**(7):1765-1772.

111. Bonanni A, Pividori MI, Campoy S, Barbé J, Del Valle M: **Impedimetric detection of double-tagged PCR products using novel amplification procedures based on gold nanoparticles and Protein G**. *Analyst* 2009, **134**(3):602-608.

112. Rasooly A, Herold KE: **Biosensors and biodetection**: Springer; 2009.

113. Kumar A: **Biosensors based on piezoelectric crystal detectors: theory and application**. *JOM-e* 2000, **52**(10):1-6.

114. Mao X, Yang L, Su X-L, Li Y: **A nanoparticle amplification based quartz crystal microbalance DNA sensor for detection of Escherichia coli O157: H7**. *Biosensors and Bioelectronics* 2006, **21**(7):1178-1185.

115. Su M, Li S, Dravid VP: **Microcantilever resonance-based DNA detection with nanoparticle probes**. *Applied Physics Letters* 2003, **82**(20):3562-3564.

116. O'sullivan C, Guilbault G: **Commercial quartz crystal microbalances–theory and applications**. *Biosensors and bioelectronics* 1999, **14**(8):663-670.

117. Uludag Y, Tothill IE: **Cancer Biomarker Detection in Serum Samples Using Surface Plasmon Resonance and Quartz Crystal Microbalance Sensors with Nanoparticle Signal Amplification**. 2012.

118. García-Martinez G, Bustabad EA, Perrot H, Gabrielli C, Bucur B, Lazerges M, Rose D, Rodriguez-Pardo L, Fariña J, Compère C: **Development of a mass sensitive quartz crystal microbalance (QCM)-based DNA biosensor using a 50 MHz electronic oscillator circuit**. *Sensors* 2011, **11**(8):7656-7664.

119. Xia H, Wang F, Huang Q, Huang J, Chen M, Wang J, Yao C, Chen Q, Cai G, Fu W: **Detection of Staphylococcus epidermidis by a quartz crystal microbalance nucleic acid biosensor array using Au nanoparticle signal amplification**. *Sensors* 2008, **8**(10):6453-6470.

120. Raiteri R, Grattarola M, Butt H-J, Skládal P: **Micromechanical cantilever-based biosensors**. *Sensors and Actuators B: Chemical* 2001, **79**(2):115-126.

121. Zhou Y, Wang Z, Yue W, Tang K, Ruan W, Zhang Q, Liu L: **Label-Free detection of p53 antibody using a microcantilever biosensor with piezoresistive readout**. In: *Sensors, 2009 IEEE: 2009*. IEEE: 819-822.

122. Hansen KM, Ji H-F, Wu G, Datar R, Cote R, Majumdar A, Thundat T: **Cantilever-based optical deflection assay for discrimination of DNA single-nucleotide mismatches**. *Analytical Chemistry* 2001, **73**(7):1567-1571.

123. Haines PJ: **Thermal methods of analysis: principles, applications and problems**: Springer Science & Business Media; 2012.

124. Davaji B, Lee CH: **Thermal Measurement Techniques in Analytical Microfluidic Devices**. *JoVE (Journal of Visualized Experiments)* 2015(100):e52828-e52828.

125. Zhang H, Chon CH, Pan X, Li D: **Methods for counting particles in microfluidic applications**. *Microfluidics and nanofluidics* 2009, **7**(6):739-749.

126. Vutha AK, Davaji B, Lee CH, Walker GM: **A microfluidic device for thermal particle detection**. *Microfluidics and Nanofluidics* 2014, **17**(5):871-878.

127. Esfandyarpour H, Davis R: **An Integrated Differential Nanocalimeter with On-Chip Microfluidic Multiplexing for High Throughput Genomics and Proteomics**. In: *14th Int'l Conf on Miniaturized Systems for Chem And Life Sciences*. 3-7.

128. Lenaerts A, Barry CE, Dartois V: **Heterogeneity in tuberculosis pathology, microenvironments and therapeutic responses**. *Immunological reviews* 2015, **264**(1):288-307.

129. Onstott S: **AutoCAD 2015 and AutoCAD LT 2015 Essentials: Autodesk Official Press**: John Wiley & Sons; 2014.

130. Chen X, Kong F, Wang Q, Li C, Zhang J, Gilbert GL: **Rapid detection of isoniazid, rifampin, and ofloxacin resistance in Mycobacterium tuberculosis clinical isolates using high-resolution melting analysis**. *Journal of clinical microbiology* 2011, **49**(10):3450-3457.

131. Bustin SA, Kessler HH: **5 Amplification and detection methods**. *Molecular Diagnostics of Infectious Diseases*.

132. Matsubara Y, Kerman K, Kobayashi M, Yamamura S, Morita Y, Tamiya E: **Microchamber array based DNA quantification and specific sequence detection from a single copy via PCR in nanoliter volumes**. *Biosensors and Bioelectronics* 2005, **20**(8):1482-1490.

133. Gulliksen A, Solli L, Karlsen F, Rogne H, Hovig E, Nordstrøm T, Sirevåg R: **Real-Time Nucleic Acid Sequence-Based Amplification in Nanoliter Volumes**. *Analytical Chemistry* 2004, **76**(1):9-14.

134. Belgrader P, Elkin CJ, Brown SB, Nasarabadi SN, Langlois RG, Milanovich FP, Colston BW, Marshall GD: **A reusable flow-through polymerase chain reaction instrument for the continuous monitoring of infectious biological agents**. *Analytical chemistry* 2003, **75**(14):3446-3450.

135. Braun D: **PCR by thermal convection**. *Modern Physics Letters B* 2004, **18**(16):775-784.

136. Cao W, Bean B, Corey S, Coursey JS, Hasson KC, Inoue H, Isano T, Kanderian S, Lane B, Liang H: **Automated Microfluidic Platform for Serial Polymerase Chain Reaction and High-Resolution Melting Analysis**. *Journal of laboratory automation* 2015:2211068215579015.

137. http://www.bioline.com/us/sensifast-hrm-kit.html.

138. El-Ali J, Perch-Nielsen I, Poulsen C, Bang D, Telleman P, Wolff A: **Simulation and experimental validation of a SU-8 based PCR thermocycler chip with integrated heaters and temperature sensor**. *Sensors and Actuators A* 2004, **110**:3-10.

139. Krishnan M, Agrawal N, Burns MA, Ugaz VM: **Reactions and fluidics in miniaturized natural convection systems**. *Analytical Chemistry* 2004, **76**(21):6254-6265.

140. Rodriguez I, Lesaicherre M, Tie Y, Zou Q, Yu C, Singh J, Meng LT, Uppili S, Li SF, Gopalakrishnakone P: **Practical integration of polymerase chain reaction amplification and electrophoretic analysis in microfluidic devices for genetic analysis**. *Electrophoresis* 2003, **24**(1-2):172-178.

141. Zhao Z, Cui Z, Cui D, Xia S: **Monolithically integrated PCR biochip for DNA amplification**. *Sensors and Actuators A: Physical* 2003, **108**(1):162-167.

142. Zhang C, Xu J, Ma W, Zheng W: **PCR microfluidic devices for DNA amplification**. *Biotechnology advances* 2006, **24**(3):243-284.

143. Kopp MU, de Mello AJ, Manz A: **Chemical Amplification: Continuous-Flow PCR on a Chip**. *SCIENCE* 1998, **280**:15.

144. Stevens MP, Garland SM, Tabrizi SN: **Development and validation of a real-time PCR assay specifically detecting human papillomavirus 52 using the Roche LightCycler® 480 system**. *Journal of virological methods* 2008, **147**(2):290-296.

145. Zhao Z, Cui D, Xia S, Cui Z: **An integrated biochip design and fabrication**. In: *SPIE's International Symposium on Smart Materials, Nano-, and Micro-Smart Systems: 2002*. International Society for Optics and Photonics: 321-326.

146. Lee D-S, Park SH, Yang H, Chung K-H, Yoon TH, Kim S-J, Kim K, Kim YT: **Bulk-micromachined submicroliter-volume PCR chip with very rapid thermal response and low power consumption**. *Lab on a Chip* 2004, **4**(4):401-407.

147. Kalinina O, Lebedeva I, Brown J, Silver J: **Nanoliter scale PCR with TaqMan detection**. *Nucleic Acids Research* 1997, **25**(10):2000.

148. Venturini E, Turkova A, Chiappini E, Galli L, de Martino M, Thorne C: **Tuberculosis and HIV co-infection in children**. *BMC Infectious Diseases* 2014, **14**.

149. Johnson GL, Bibby DF, Wong S, Agrawal SG, Bustin SA: **A MIQE-Compliant Real-Time PCR Assay for Aspergillus Detection**. 2012.

150. Yang J, Liu Y, Rauch CB, Stevens RL, Liu RH, Lenigk R, Grodzinski P: **High sensitivity PCR assay in plastic micro reactors**. *Lab Chip* 2002, **2**:179-187.

151. Schütz E, von Ahsen N: **Influencing factors of dsDNA dye (high-resolution) melting curves and improved genotype call based on thermodynamic considerations**. *Analytical biochemistry* 2009, **385**(1):143.

152. Bustin S, Benes V, Nolan T, Pfaffl M: **Quantitative real-time RT-PCR–a perspective**. *Journal of molecular endocrinology* 2005, **34**(3):597-601.

153. Zimmermann BG, Grill S, Holzgreve W, Zhong XY, Jackson LG, Hahn S: **Digital PCR: a powerful new tool for noninvasive prenatal diagnosis?** *Prenatal diagnosis* 2008, **28**(12):1087-1093.

154. White III RA, Quake SR, Curr K: **Digital PCR provides absolute quantitation of viral load for an occult RNA virus**. *Journal of Virological Methods* 2012, **179**:45-50.

155. Pekin D, Skhiri Y, Baret J-C, Le Corre D, Mazutis L, Ben C, Laurent-Puig P, Griffiths AD, Taly V: **Quantitative and sensitive detection of rare mutations using droplet-based microfluidics**. *Lab Chip* 2011, **11**:2156-2166.

156. White III RA, Blainey P, Fan HC, Quake SR: **Digital PCR provides sensitive and absolute calibration for high throughput sequencing**.

157. Didelot A, Kotsopoulos SK, Lupo A, Pekin D, Li X, Atochin I, Hutchison JB, Taly V: **Multiplex Picoliter-Droplet Digital PCR for Quantitative Assessment of DNA Integrity in Clinical Samples**. *Clinical Chemistry* 2013, **59**(5):815-823.

158. Whale AS, Huggett JF, Cowen S, Speirs V, Shaw J, Ellison S, Foy CA, Scott DJ: **Comparison of microfluidic digital PCR and conventional quantitative PCR for measuring copy number variation**. *Nucleic Acids Research* 2012, **1**:9.

159. Fukuba T, Naganuma T, Fujii T: **Microfabricated flow-through PCR device for underwater microbiological study**. In: *Underwater Technology, 2002 Proceedings of the 2002 International Symposium on: 2002*. IEEE: 101-105.

160. Erill I, Campoy S, Rus J, Fonseca L, Ivorra A, Navarro Z, Plaza JA, Aguiló J, Barbé J: **Development of a CMOS-compatible PCR chip: comparison of design and system strategies**. *J Micromech Microeng* 2004, **14**:1-11.

161. West J, Karamata B, Lillis B, Gleeson JP, Alderman J, Collins JK, Lane W, Mathewsona A, Berneya H: **Application of magnetohydrodynamic actuation to continuous flow chemistry**. *Lab Chip* 2002, **2**:224-230.

162. Anderson RC, Su X, Bogdan GJ, Fenton J: **A miniature integrated device for automated multistep genetic assays**. *Nucleic Acids Research* 2000, **28**(12):e60.

163. Lin Y-C, Huang M-Y, Young K-C, Chang T-T, Wu C-Y: **A rapid micro-polymerase chain reaction system for hepatitis C virus amplification**. *Sensors and Actuators B: Chemical* 2000, **71**(1):2-8.

164. Gascoyne P, Satayavivad J, Ruchirawat M: **Microfluidic approaches to malaria detection**. *Acta tropica* 2004, **89**(3):357.

165. Ingelman-Sundberg M: **Genetic polymorphisms of cytochrome P450 2D6 (CYP2D6): clinical consequences, evolutionary aspects and functional diversity**. *The pharmacogenomics journal* 2005, **5**(1):6-13.

166. Cai L, Kong F, Jelfs P, Gilbert GL, Sintchenko V: **Rolling circle amplification and multiplex allele-specific PCR for rapid detection of katG and inhA gene mutations in Mycobacterium tuberculosis**. *International Journal of Medical Microbiology* 2009, **299**(8):574-581.

[i] This system was jointly developed with Ian Mbano, with whom I worked with on some aspects of the project.
[ii] This data was jointly obtained with Ian Mbano, with whom I worked with on some aspects of the project
[iii] This data was jointly obtained with Ian Mbano, with whom I worked with on some aspects of the project
[iv] This data was jointly obtained with Ian Mbano, with whom I worked with on some aspects of the project
[v] This data was jointly obtained with Ian Mbano, with whom I worked with on some aspects of the project